Application of Ion Electrospray Propulsion to Lunar and Interplanetary Missions

by

Caleb W. Whitlock

B.S., Astronautical Engineering, U.S. Air Force Academy (2012)

Submitted to the Department of Aeronautics and Astronautics
in partial fulfillment of the requirements for the degree of

Master of Science in Aeronautics and Astronautics

at the

MASSACHUSETTS INSTITUTE OF TECHNOLOGY

June 2014

Signature redacted

Author .....
Department of Aeronautics and Astronautics
May 22, 2014

Signature redacted

Certified by .....
Paulo Lozano
Associate Professor
Thesis Supervisor

Signature redacted

Certified by ...
Leena Singh
Principal Member of Technical Staff, CSDL
Thesis Supervisor

Signature redacted

Accepted by ....
Paulo Lozano
Chair, Graduate Program Committee

Application of Ion Electrospray Propulsion to Lunar and Interplanetary Missions

by

Caleb W. Whitlock

Submitted to the Department of Aeronautics and Astronautics
on May 22, 2014, in partial fulfillment of the
requirements for the degree of
Master of Science in Aeronautics and Astronautics

Abstract

High specific impulse electric propulsion systems enable ambitious lunar and interplanetary missions that return a wealth of scientific data. Many of these technologies are difficult to scale down, meaning the spacecraft are relatively massive and expensive. The Space Propulsion Lab (SPL) at the Massachusetts Institute of Technology (MIT) is developing compact, high specific impulse ion electrospray thrusters which do not suffer from the same sizing limitations. The Ion Electrospray Propulsion System (iEPS) is tailored for small spacecraft and can perform high ΔV maneuvers. This enables a plethora of lunar and interplanetary missions using nanosatellites, which can lead to substantial cost reductions.

The main objective of the research presented in this thesis is to develop a guidance and control (GC) architecture for small spacecraft using iEPS modules for main propulsion and attitude control actuation and to evaluate its performance through simulation. The Lunar Impactor mission serves as the primary case study, and the results offer valuable insight into the design of the propulsion system while validating the functionality of the GC algorithm. These methods are extended in a second case study focusing on exploration of a near-earth asteroid.

Thesis Supervisor: Paulo Lozano
Title: Associate Professor

Thesis Supervisor: Leena Singh
Title: Principal Member of Technical Staff, CSDL

Disclaimer

The views expressed in this document are those of the author and do not reflect the official policy or position of the United States Air Force, Department of Defense, or the U.S. Government.

Acknowledgments

Studying engineering has deepened my faith and broadened my understanding of God's manifold wisdom. I've had the privilege of spending many years learning about the natural world and how to explore it through science and engineering, and I'm continually awed as I discover how complex and beautiful it really is. The universe resounds with His glory.

"The heavens declare the glory of God;
the skies proclaim the work of his hands.
Day after day they pour forth speech;
night after night they reveal knowledge.
They have no speech, they use no words;
no sound is heard from them.
Yet their voice goes out into all the earth,
their words to the ends of the world."
(Psalm 19:1-4, NIV)

It has been a privilege to study at MIT as a Draper Lab Fellow and have the opportunity to author this thesis. For this and all future work I may accomplish, *Soli Deo Gloria.*

Thank you to my sweet wife for loving me so wholeheartedly. Your soul shines with the light of the Spirit, and I continually learn from your faith. What a blessing it is to be married to you and grow every day in our love for one another. I would not have made it through this without your support and encouragement, and life would not have been nearly as full or fun. I can't wait to continue our adventure together!

Thank you to all my family for loving me so much. Without you, I would not have such a strong desire to be a man of faith and live a life of service. Thank you for supporting me in following my calling and inspiring me each and every day. Thank you to all my dear friends near and far who so richly bless me, and hopefully we'll see each other soon.

Thank you, Prof. Lozano, for teaching and advising me so well throughout my time at MIT. You are a gifted technical expert, but more importantly, you're a talented leader and mentor. Your passion for research has helped me remain excited about my studies, and I look forward to keeping up with you and the SPL in the years to come.

Thank you, Dr. Singh, for advising me throughout my time at Draper. You are a very skilled engineer and a good teacher. You've taught me a great deal about how to be technically precise, understandable, and confident in my work. This is going to help me throughout my career and my life.

Contents

1 Introduction **17**

1.1 Motivation 17

1.2 Space Propulsion Fundamentals 18

1.3 Goals 20

1.4 Requirements 21

1.4.1 Main Propulsion 23

1.4.2 Attitude Control 25

1.4.3 Mission Analysis 26

2 Ion Electrospray Propulsion **27**

2.1 Review of Electric Propulsion Technologies 27

2.1.1 Hall Effect Thrusters and Ion Engines 27

2.1.2 Field-Effect Electric Propulsion and Pulsed Plasma Thrusters 29

2.1.3 Magnetoplasmadynamic Thrusters 30

2.2 Basic Principles 31

2.3 Thrusters 33

2.3.1 iEPS 33

2.3.2 Fabrication and Assembly 34

2.3.3 Power Processing Unit 36

2.3.4 Performance 36

2.4 Implementation 37

3 Guidance and Control **39**

3.1 Architecture 40

3.2 Navigation 41

3.2.1 Attitude Knowledge 42

3.2.2 Translational State Knowledge 42

3.3 Guidance 42

3.3.1 Guidance Logic 43

3.4 Control 48

3.4.1 Error Calculation 49

3.4.2 Control Law 49

3.4.3 Control Allocation 50

3.5 Summary 50

4 Lunar Missions **52**

4.1 Lunar Impactor 52

4.1.1 Background 53

4.1.2 Mission Requirements 55

4.2 Mission Architecture 57

4.2.1 Concept of Operations 59

4.3 Spacecraft Architecture 61

4.3.1 Instrumentation 61

4.3.2 Communication 62

4.3.3 Physical Configuration 62

4.4 Simulation 64

4.4.1 Methodology 65

4.4.2 Architecture 66

4.5 Trajectory Design, Guidance, Navigation, and Control 68

4.5.1 Trajectory Design 68

4.5.2 Guidance 72

4.5.3 Navigation 74

4.5.4 Control . . . 76
4.6 Results and Analysis . . . 77
4.6.1 De-tumble and Sun-tracking . . . 77
4.6.2 Check-out Phase . . . 77
4.6.3 Transit Phase . . . 78
4.6.4 Science Phase . . . 88
4.6.5 Extension to Other Missions . . . 89
4.7 Concluding Remarks . . . 89
4.7.1 Concerns . . . 90

5 Interplanetary Missions **93**
5.1 NEO Surveyor . . . 93
5.1.1 Background . . . 94
5.1.2 Mission Requirements . . . 95
5.2 Mission Architecture . . . 95
5.2.1 Concept of Operations . . . 97
5.3 Spacecraft Architecture . . . 99
5.3.1 Instrumentation . . . 99
5.3.2 Communication . . . 100
5.3.3 Physical Configuration . . . 101
5.4 Trajectory Design, Guidance, Navigation, and Control . . . 103
5.4.1 TrajectoryDesign . . . 104
5.4.2 Guidance . . . 108
5.4.3 Navigation . . . 108
5.4.4 Control . . . 110
5.5 Results and Analysis . . . 111
5.5.1 Transit Phase . . . 111
5.5.2 Science Phase . . . 112
5.6 Concluding Remarks . . . 113
5.6.1 Concerns . . . 114

6 Conclusion **116**

6.1 Future Work 117

6.1.1 GC Algorithm 118

6.1.2 Lunar Impactor 119

6.1.3 NEO Surveyor 119

6.1.4 Further Exploration 119

List of Figures

1-1 Rocket diagram 18
1-2 Electric propulsion technology comparison 24

2-1 NSTAR ion engine 28
2-2 Hall effect thruster 29
2-3 FEEP thruster 30
2-4 PPT 30
2-5 MPD thruster 31
2-6 Electrospray thruster diagram 32
2-7 Electrospray thruster beam neutrality 33
2-8 iEPS diagram 34
2-9 iEPS CAD drawing 34
2-10 iEPS thruster and emitter tips 35
2-11 iEPS small propellant tank 35
2-12 PETA PPU 36

3-1 Mission phases 40
3-2 Guidance and control algorithm diagram 41
3-3 Guidance routine diagram 43
3-4 LVLH frame definition 44
3-5 LVLH frame illustration 45
3-6 Impulsive maneuver 47
3-7 Series of impulsive maneuvers 48
3-8 Control routine diagram 49

3-9 PD controller 50
3-10 Control allocation 50

4-1 Low angle impact trajectory 53
4-2 Lunar magnetism map 54
4-3 Reiner Gamma horizontal magnetic field 56
4-4 Reiner Gamma impact trajectories 57
4-5 Impact geometry 57
4-6 Lunar Impactor mission profile 58
4-7 Lunar Impactor CONOPS diagram 59
4-8 Doppler shift ranging 63
4-9 Lunar Impactor CAD drawing 64
4-10 Lunar Impactor internal layout 65
4-11 Lunar Impactor body frame 65
4-12 Simulation diagram 66
4-13 Spacecraft model diagram 68
4-14 Direct impact trajectory 70
4-15 Direct impact trajectory terminal phase 71
4-16 Back propagation from Reiner Gamma 72
4-17 Lunar swing-by trajectory 73
4-18 Spacecraft trajectory following 75
4-19 Lunar Impactor de-tumble results 78
4-20 Lunar Impactor slew and hold maneuver 79
4-21 Direct impact trajectory 80
4-22 Direct impact trajectory following results 81
4-23 Direct impact trajectory following results 82
4-24 Direct impact trajectory following results 83
4-25 Lunar swing-by trajectory 84
4-26 Lunar swing-by trajectory following results 85
4-27 Lunar swing-by trajectory following results 87

4-28 Lunar swing-by trajectory following results 88
4-29 Direct impact trajectory following results 90
4-30 Direct impact trajectory following results 91

5-1 NEO Surveyor mission architecture 97
5-2 Imaging the NEO 98
5-3 Imaging camera 99
5-4 ISARA antenna 100
5-5 Inflatable CubeSat high-gain antenna 101
5-6 NEO Surveyor propulsion subsystem CAD drawing 102
5-7 NEO Surveyor propellant tank structure 103
5-8 NEO Surveyor CAD drawing 104
5-9 NEO Surveyor CAD drawing 105
5-10 NEO Surveyor propulsion system CAD drawing 106
5-11 NEO Surveyor earth escape trajectories 108
5-12 NEO Surveyor interplanetary trajectory 109
5-13 NEO Surveyor earth escape with lunar swing-by 110
5-14 NEO Surveyor transit phase 111
5-15 NEO Surveyor transit phase close-up 112
5-16 NEO Surveyor results 113

List of Tables

1.1 General Spacecraft Design Considerations 22
1.2 General Programmatic Considerations 23
1.3 Propulsive Requirements 24
1.4 ADCS Requirements 26

2.1 Ionic Liquid Properties 31
2.2 iEPS Performance 37

4.1 Impact Angle Requirements 57
4.2 CONOPS 60
4.3 Simulation Paramcters 67
4.4 Trajectory Design Assumptions 69
4.5 Direct Ascent Trajectory Data 71
4.6 Lunar Swing-by Trajectory Data 72
4.7 Required Accuracy 74
4.8 Trajectory Design 89

5.1 1991 VG Orbital Elements 95
5.2 NEO Surveyor Assumptions and Design Considerations 96
5.3 NEO Surveyor Trajectory Design 107
5.4 NEO Surveyor Propulsion System Performance 107
5.5 NEO Surveyor Propulsion System Performance 108
5.6 NEO Surveyor Propulsion System Performance 110

List of Acronyms

1U 1-unit. 61

6-DOF six degrees of freedom. 65

ADCS Attitude Determination and Control Subsystem. 21, 24, 25, 26, 36, 40, 42, 48, 60, 62, 63, 64, 67, 76, 77, 79, 81, 82, 83, 86, 87, 88, 89, 90, 91, 98, 109, 110, 114, 117, 118

AMR Anisotropic magneto-resistive. 61

ARC Austrian Research Centers. 29

CAD computer-aided design. 33, 34, 63, 101, 102, 103

CDH Command and Data Handling. 66

CMOS complementary metal-oxide semiconductor. 99

CoM center of mass. 67

CONOPS concept of operations. 58, 59, 61

COTS commercial off-the-shelf. 117

CSDL Charles Stark Draper Laboratory. 65

DM deployment module. 40

DoD Department of Defense. 37

DSN Deep Space Network. 62, 99, 109

ECI earth-centered inertial. 43

FEEP Field-effect electric propulsion. 29

FSW flight software. 66

GC guidance and control. 2, 50, 53, 65, 66, 67, 68, 77, 78, 89, 113, 119

GEO geostationary earth orbit. 52, 57, 58, 68, 69, 73, 91, 95, 106, 111, 114

GNC Guidance, Navigation, and Control. 21, 39, 55, 59, 103, 117

GRC Glenn Research Center. 29

GTO geostationary transfer orbit. 95

HCI heliocentric inertial. 111

HCW Hill-Clohessy-Wiltshire. 42, 43, 44, 43

HET Hall effect thruster. 21, 28

HGA high-gain antenna. 100, 101

iEPS Ion Electrospray Propulsion System. 2, 17, 33, 34, 35, 36, 37, 62, 77, 82, 89, 93, 95, 107, 117

IMU Inertial Measurement Unit. 59, 74, 91, 109, 114

ISARA Integrated Solar Array and Reflectarray Antenna. 100

LEO low-earth orbit. 20, 52, 88, 91, 114

LGA low-gain antenna. 101

LVLH local vertical, local horizontal. 42, 43, 44, 43, 48, 49, 63, 68, 79, 85, 89

MATLAB MATrix LABoratory. 66

MEMS microelectromechanical systems. 32, 36

MIT Massachusetts Institute of Technology. 2, 32, 100

MoI moment of inertia. 67

MPC Model Predictive Control. 40

MPD Magnetoplasmadynamic thruster. 30

NASA National Aeronautics and Space Administration. 19, 28, 29, 37, 62, 93, 99, 104

NEO near-earth object. 12, 93, 94, 95, 97, 98, 102, 103, 107, 109, 110, 111, 113, 119

PCB printed circuit board. 100

PD proportional-derivative. 49

PETA Precision Electrospray Thruster Assembly. 36, 95

PPT Pulsed plasma thruster. 29

PPU power processing unit. 29, 35, 36, 60, 64, 82, 88, 95, 101, 103, 113, 119

RK4 Runge-Kutta 4. 66, 67, 68

RWA Reaction Wheel Assembly. 62, 101, 103, 109, 114, 119

SA solar array. 101

SoI sphere of influence. 86, 95

SPICE Spacecraft Planet Instrument C-matrix Events. 66

SPL Space Propulsion Lab. 2, 32

SRP Solar radiation pressure. 86

STK Systems Tool Kit. 68

SWIFT Solar Wind Ion Flux Tracer. 61

TRL Technology Readiness Level. 116

VNC velocity, normal, co-normal. 68

WSB weak stability boundary. 119

Chapter 1

Introduction

Robotic lunar and interplanetary missions are vital in paving the way for mankind to increase its presence in space. Not only is the scientific knowledge invaluable to understanding our place in the cosmos, but it is a necessary precursor to manned exploration and colonization. Recent decades have seen tremendous returns on investment; ambitious ventures have yielded high-fidelity gravity measurements, stunning images of celestial bodies, knowledge of planetary climates and resources, and even clear evidence of extra-solar planets. The surveyor landers and other lunar spacecraft lit the path for the Apollo program, and the Martian landers, rovers, and exploratory orbiters have provided the data necessary for a manned mission [1]. Probes have been sent to comets, asteroids, and all of the outer planets and have revolutionized our understanding of the solar system [2].

1.1 Motivation

Reaching these destinations is very difficult and extraordinarily expensive, limiting admittance to all but the most substantial entities. Space propulsion and launch are two challenges that if properly addressed will lead to the most considerable improvements in cost and accessibility. This research focuses on the design, use, and performance of spacecraft equipped with a new class of electric propulsion technology, iEPS, which has the potential to revolutionize space exploration.

1.2 Space Propulsion Fundamentals

To gain a better understanding of the key drivers of cost as well as the underlying challenges in such missions, it is useful to review some fundamental space propulsion concepts. In order to maneuver, a spacecraft must be able to accelerate. This is accomplished by mass reaction, meaning the spacecraft expels part of its own mass. Figure 1-1 shows a simple diagram of this process.

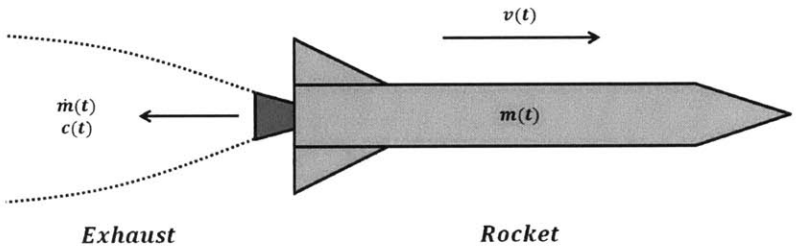

Figure 1-1: Diagram of a rocket expelling exhaust at velocity $c(t)$ with a mass flow rate $\dot{m}(t)$.

According to Newton's third law, the force that the vehicle imparts on the expelled mass has an equal and opposite reaction on the vehicle itself. Expressed analytically, the force exerted on the spacecraft is

$$F(t) = \dot{m}(t)c(t) \tag{1.1}$$

If the mass flow rate $\dot{m}$ and exhaust velocity c are held constant, the expression becomes

$$F = \dot{m}c = ma \tag{1.2}$$

Required force depends on the mission type. Planetary launch and rapid maneuvering demand high thrust, which is achieved using high mass flow rates albeit lower exhaust velocities. This is not very efficient, however, and requires a large amount of propellant. It is more advantageous for deep space missions, which do not require high thrust, to operate with a higher exhaust velocity. This is more efficient and results in a lower propellant mass fraction, which is defined as

$$\zeta = \frac{m_p}{m_0} \tag{1.3}$$

The propellant mass fraction can be related to the initial and final spacecraft mass.

$$m_0 = m_f + m_p \tag{1.4}$$

$$\zeta = \frac{m_p}{m_p + m_f} = 1 - \frac{m_f}{m_0} \tag{1.5}$$

Substituting the relationship into the rocket equation yields the total change in velocity the spacecraft can achieve assuming a fixed exhaust velocity.

$$\Delta V = -c \ln(\frac{m_f}{m_0}) = -c \ln(1 - \zeta) \tag{1.6}$$

Expressing the equation in terms of the propellant mass fraction, one has the identity

$$\zeta = 1 - e^{-\frac{\Delta V}{c}} \tag{1.7}$$

Therefore, for a fixed mission ΔV, increasing the exhaust velocity decreases the propellant mass fraction. If the dry mass is held constant, the spacecraft using a propulsion system with a higher exhaust velocity will be less massive. Specific impulse is a commonly used measure of propellant use efficiency.

$$I_{sp} = \frac{c}{g_0} \tag{1.8}$$

High specific impulse is advantageous in lunar and interplanetary missions requiring high ΔV. Chemical engines are limited to about 500 seconds I_{sp} since the kinetic energy of the rocket exhaust is limited by the energy released in the reaction. Electric thrusters, on the other hand, can achieve much higher I_{sp} since they rely on the acceleration of charged particles using electric and magnetic fields. Implementation of such technology enables a substantial leap in performance.

To illustrate the dramatic mass savings possible, one can perform a few simple calculations. The Dawn spacecraft, part of a National Aeronautics and Space Ad-

ministration (NASA) mission to the protoplanet Vesta and the dwarf planet Ceres, has a dry mass of 815 kg and carries 425 kg of propellant; its main engine operates with a specific impulse of 3100 sec [3]. According to Equation 1.6, it is theoretically capable of 12.76 km/sec ΔV. If Dawn employed a chemical bi-propellant system with a specific impulse of 310 sec and had an equivalent dry mass, its initial mass would be 54,175 kg. The figure balloons further with necessary structural additions to contain, pressurize, and transport the voluminous propellant, resulting in an unwieldy, monolithic, and excessively expensive spacecraft.

Launch is also a key driver of cost. Delivering spacecraft to low-earth orbit (LEO) costs $3,000-30,000 per kilogram, but most deep space missions require insertion into escape trajectories, which is far more expensive [16]. This usually requires the full capability of a reliable rocket such as the Atlas V, which carries a price tag of $223 million [4]. A more economical alternative is launching in a ride-share configuration, where the spacecraft is carried as secondary cargo. Extra propulsive capability may be necessary to escape from Earth's gravitational influence or change its course, but spacecraft equipped with high specific impulse engines can provide it with a small to modest increase in propellant mass fraction.

Ride-share is a very attractive prospect because of the low price, but there are stringent mass and volume constraints for hosted spacecraft. Smaller vehicles have a lower payload capacity and may not be able to carry instruments with the same capability as larger platforms. Such designs are not meant to replace flagship missions but to provide an inexpensive alternative at the low end of the spectrum. Downsizing the spacecraft and using high specific impulse engines may translate to greater scientific return per dollar spent.

1.3 Goals

The primary goal of this research is to formulate an architecture for lunar and interplanetary missions centered around small satellites, particularly the CubeSat form factor, that use high performance electric propulsion systems. The main focus is the

guidance and control architecture; the tight constraints and new technology require unique consideration. The strategy for achieving this is as follows:

1. Develop a guidance and control algorithm for lunar and interplanetary CubeSat missions using low thrust, high specific impulse propulsion systems.
2. Test and refine this algorithm in an appropriate simulation environment.
3. Perform case studies and analyze the results to back out key considerations for the missions, particularly concerning the propulsion system.

A secondary goal is creating algorithms that can be easily modified and building a flexible simulation. Constraining it to a particular subset of missions is undesirable as potential applications and extensions are very diverse.

1.4 Requirements

The level of difficulty necessitates deliberate, meticulous examination of the design considerations for low thrust, high ΔV missions to the moon and beyond. The spacecraft must be able to survive high radiation doses and return data from extreme distances after traveling long periods with substantial maneuvering. Table 1.1 summarizes several of the most important considerations, which are critical in generating the requirements. The list is by no means exhaustive, but it is intended to highlight key encumbrances.

Spacecraft design presents extraordinary challenges, but it is also a significant undertaking on the programmatic front. Development efforts are typically very lengthy and the missions highly unique. Table 1.2 summarizes some of the important considerations.

Lunar and interplanetary missions are a substantial undertaking, demanding excellence in engineering to overcome myriad challenges. Of particular concern is the propulsion system since it is a key driver of cost and capability.

Table 1.1: General Spacecraft Design Considerations

Subsystem	**Design Consideration**
Propulsion	The propulsion subsystem must provide the necessary thrust and total impulse. Electric thrusters often fire for weeks or months, and total ΔV is often substantial. The engines must be reliable. Any changes must be thoroughly understood, and compensation for off-nominal performance must be made.
Guidance, Navigation, and Control	It is crucial that the Guidance, Navigation, and Control (GNC) algorithms function properly. They must be able to determine the path of travel, interpret all incoming sensor data, and compute commands for the actuators.
Attitude Determination and Control	The Attitude Determination and Control Subsystem (ADCS) must maintain knowledge and control of spacecraft orientation and rates, requiring reliable sensors and actuators. Precise pointing is required for thrusting and communication.
Command and Data Handling	The command and data handling subsystem, particularly the flight processor, must be capable of operating in the radiation environment of interplanetary space and running computationally intensive algorithms. Autonomy is greatly valued as it reduces the need for expensive communication and lessens dependence on the communication subsystem.
Power	The power subsystem must collect sufficient solar power (or produce it by other means) to operate the spacecraft at its farthest point from the sun. Reliable power conversion is also critical, particularly for electric thrusters.
Communications	Proper antenna pointing, particularly for high-gain antennas, is crucial. The communications subsystem must be able to send back relevant telemetry and scientific data with sufficient signal strength to be received at earth.
Structure	The structure must be lightweight and well-balanced. The most strenuous loading typically occurs at launch.
Thermal	Spacecraft must be able to maintain a reasonable temperature throughout its flight. Thermal conditions often vary drastically depending on spacecraft location relative to the sun and other celestial bodies.
Payload	The payload must be radiation tolerant and able to survive long periods of inactivity.

Table 1.2: General Programmatic Considerations

Item	Comments
Program Management and Systems Engineering	Missions usually have very lengthy development timelines, requiring continuity in management and systems engineering. Cost estimation and budgeting are difficult yet tremendously important.
Software Development	Software is customized for each mission and requires substantial development effort. Development timelines are typically lengthy.
Assembly and Test	Each spacecraft must be carefully assembled, and testing must be completed at many levels. Reliability and survivability must be ensured.
Launch	Most missions require a dedicated launch vehicle or a substantial portion of its propulsive capability. It must be very reliable and perform precise trajectory insertion.
Operations	Spacecraft operations are often very involved and can continue years past the design lifetime. Low thrust missions in particular demand frequent communication with the spacecraft.

1.4.1 Main Propulsion

Main engines for lunar and interplanetary spacecraft must be reliable and efficient. The Kaufman ion engine and the Hall effect thruster (HET) in particular have a reputation for dependability and longevity. They enable missions that could not be executed using conventional technologies, but even with these advances, the spacecraft usually have a mass >500 kg. One of the primary reasons they cannot be downsized further is that they do not scale down well. Efficiency plummets as their physical dimensions decrease beyond a certain point. Plasmas require higher density to keep similar levels of ionization at smaller dimensions, and higher plasma density leads to a more aggressive environment that decreases efficiency and device lifetime.

A comparison of high specific impulse electric thrusters is given in Figure 1-2 and illustrates the scarcity of technologies that exist for small, low-power missions [5].

The one technology that scales well to low power levels is ion electrospray propulsion. Rather than relying on confinement of electrons to ionize propellant, these thrusters electrostatically extract and accelerate charged particles from ionic liq-

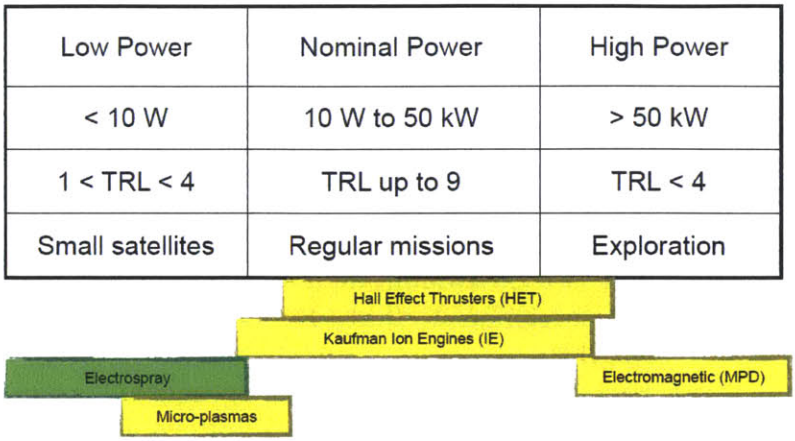

Figure 1-2: Comparison of several electric propulsion technologies.

uids [25]. They require no pressurant, valves, or complex feeding systems because the fuel is driven by capillary forces induced by the ion evaporation process. Chapter 2 describes this technology and the thrusters in greater detail; in short, it can be used to provide unparalleled high specific impulse propulsion for small spacecraft.

Closer examination of the requirements and concerns for the propulsion system is necessary. Table 1.3 lists those that are most critical.

Table 1.3: Propulsive Requirements

Requirement	**Comments**
Total ΔV	Highly dependent on mission; 2-10 km/sec expected. Long, low-thrust maneuvers usually require higher ΔV than impulsive, high-thrust maneuvers.
Thrust	Expected thrust to weight ratio between 1e-5 and 1e-4. Thrust scales linearly with power.
Thrusting time	1,000-10,000 hours
Mission duration	2-60 months
Environment	High radiation environment beyond magnetosphere; solar flux dependent on distance from sun.
Physical configuration	Main engine likely a body-fixed cluster of smaller electrospray thrusters; ADCS thrusters placed as far as possible from spacecraft center of mass.

Duration is not expected to be as long as that of larger spacecraft because of the radiation environment. The mass penalty for shielding and the lack of radiation hardened or tolerant components for small spacecraft means that for the near future

lifetime is expected to be relatively short. Further research and investment in such technology is necessary, but this does not preclude ambitious missions within the next few years.

It is important to note that power generation is a key driver of performance. The thrusters are electric rather than chemical, and higher power means a higher mass flow rate and higher thrust (for a constant I_{sp}). The advantages gained by increasing power to the thrusters must be balanced with the mass increases in power generation, processing, and propulsion system hardware; thrust to weight ratio is the important quantity. Spacecraft with greater acceleration can accomplish maneuvers faster (lower total ΔV), particularly spiraling out of a gravity well. The relationship between thrust and power is governed by the equation

$$F = \frac{2\eta P}{c} \tag{1.9}$$

where η is the overall efficiency of the propulsion system. Careful trade studies are required to assure the power subsystem is properly scaled for the mission.

1.4.2 Attitude Control

Electrospray thrusters can also be used as actuators for the ADCS and are suitable for de-saturating reaction wheels. High-rate attitude maneuvers cannot be accomplished with thrusters alone because the torques are so low, but rapid slewing is usually not necessary for interplanetary missions. Projections of the requirements and important considerations are given in Table 1.4.

It is important to locate the actuators far from the center of mass to maximize torque, and it must be determined what thrust levels are sufficient to provide those torques. The propellant reservoirs must be large enough to contain the fuel necessary to deliver the total impulse required for the entire journey. This is particularly important for an all-thruster architecture.

Table 1.4: ADCS Requirements

Requirement	Comments
On/off cycles	If used as the primary ADCS actuators, the thrusters are expected to cycle hundreds of thousands to millions of times. The thruster control module and power processing unit (particularly the switches) must be capable of supporting such operation.
On time	Total on time varies from mission to mission, but it is expected to range from 10-500 hours.
Thrust	Thrust depends on required torque. Each thruster will likely operate from 1-50 μN.
Propellant consumption	Propellant consumption depends on thrust and total on time.
Pulse width	Pulse width depends on required torque and thrust level.
Physical configuration	Placing the thrusters far from the center of mass is advantageous. Symmetric arrangements are favored to simplify dynamics.
Disturbance torque rejection	The thrusters must compensate for disturbance torques, most notably thrust misalignment and solar radiation pressure.

1.4.3 Mission Analysis

To this point, simulation and analysis have been conducted without regard for the guidance, navigation, and control architecture. While this is permissible for preliminary estimates, it is critical to develop the algorithms to understand the specific demands on the propulsion system. This serves two purposes:

1. Develop algorithms for eventual adaptation and implementation on lunar and interplanetary missions using ion electrospray propulsion.

2. Identify key considerations for the propulsion and ADCS subsystems, highlight concerns, and discuss mitigation strategies for anticipated difficulties.

Addressing these items contributes to the advancement of technologies and methods for lunar and interplanetary missions. Of particular significance is lowering the threshold for fielding spacecraft capable of reaching these destinations.

Chapter 2

Ion Electrospray Propulsion

To better engineer the guidance and control algorithm as well as the spacecraft, it is necessary to have a thorough understanding of ion electrospray propulsion. This includes the fundamental operating principles and the design of practical thrusters, but more importantly, it encompasses the rationale behind selecting this novel technology.

2.1 Review of Electric Propulsion Technologies

Before diving headlong into the details, one must ascertain whether or not ion electrospray propulsion is the optimal choice for this mission class. It lacks the maturity of other technologies, and employing it in the near future directly controverts the conservative philosophy typical of the organizations that fly such spacecraft.

Much of the justification comes from reviewing various electric propulsion technologies and ascertaining whether or not they can be adapted for implementation on nanosatellites. Flexibility, simplicity, and ease of production are as important as performance for a low-cost spacecraft.

2.1.1 Hall Effect Thrusters and Ion Engines

Ion engines are the workhorse of high ΔV interplanetary voyages, and they have performed superbly in several medium power missions in recent years. They have a

high specific impulse (2500-4000 sec) and a reasonable lifetime and efficiency. The major problems are that they are bulky, heavy, and have a very complex power processing unit [5, 29].

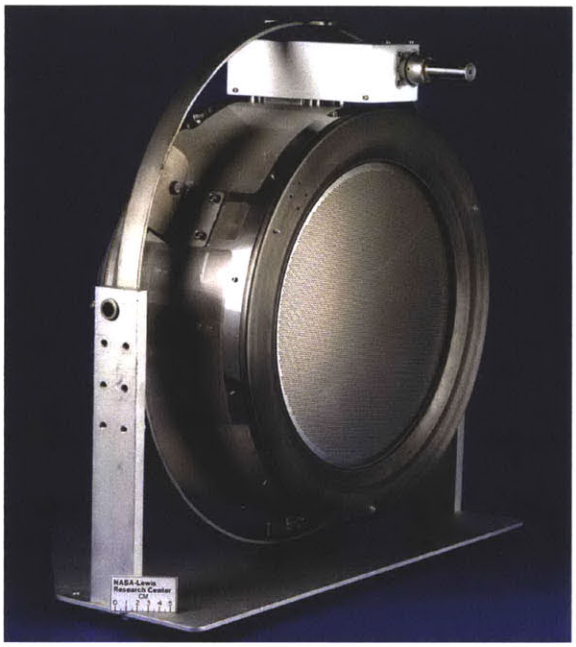

Figure 2-1: NASA NSTAR ion engine (1 kW power, 3900 sec I_{sp}, 50% efficiency) [6].

Scaling these thrusters down to fit aboard a small satellite, particularly a CubeSat, is possible, but issues arise. Plasmas require higher density to keep similar levels of ionization at smaller dimensions, and higher plasma density leads to a harsher environment that decreases efficiency and device lifetime. Longevity and efficiency are requisites for high ΔV interplanetary voyages.

Hall effect thrusters are favorable for medium-power missions and have seen increased use on large commercial spacecraft. Their reasonable lifetime, efficiency, and specific impulse (1500-1800 sec) combined with flight heritage make them an appealing option for high ΔV missions. They have complex power processing units though, and they are bulky and heavy. HETs do not scale down well for the same reason as ion engines; efforts to address these issues have yielded little fruit.

Both ion engines and HETs operate best between 0.05-10 kW, which is a substantial amount of power for a CubeSat to devote to the propulsion subsystem alone.

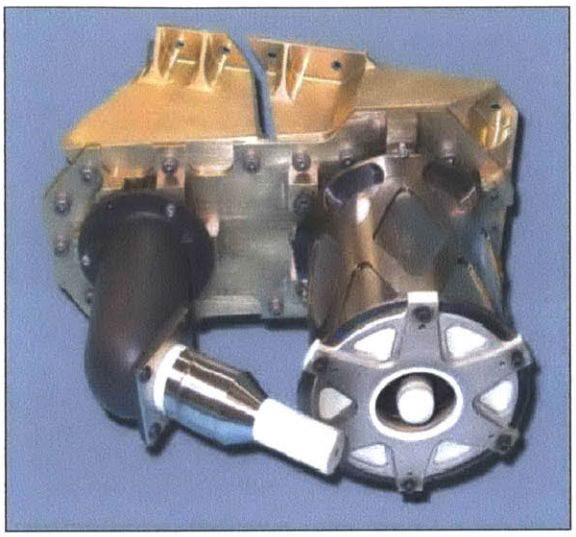

Figure 2-2: Busek BHT-200 (200 W power, 1390 sec I_{sp}, 44% efficiency) [7].

Furthermore, the propellant is usually a noble gas, which requires pressurization and a plumbing system with valves. Generating the magnetic and electric fields that confine the electrons and accelerate the ions requires heavy magnets and complex power processing units. Despite a rich flight heritage, their technological maturity for the low power regime is lacking, and they are not ideal for implementation in CubeSats.

2.1.2 Field-Effect Electric Propulsion and Pulsed Plasma Thrusters

Field-effect electric propulsion (FEEP) thrusters are well-suited for fine pointing control as they have very low thrust, and they can be configured in a relatively compact arrangement. Since field evaporation is the driving mechanism, it can be scaled down easier than the aforementioned thrusters. There are a number of limitations, though. Heat is required to melt the liquid metal propellant, lifetime is limited by erosion, and an electron-neutralizing cathode is required [5, 29].

Pulsed plasma thrusters (PPTs) were the first electric propulsion devices flown in space, and they are relatively simple. They are suitable for precision maneuvering since they operate with short pulses. The largest limitation is their low efficiency, which means a large power processing unit (PPU) is required. For a spacecraft with such stringent mass and power constraints, this is a poor option for main propulsion.

Figure 2-3: FEEP thruster (ARC, 5 W power, 6000 sec I_{sp}) [34].

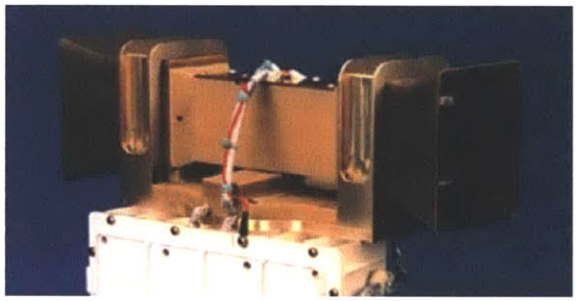

Figure 2-4: Pulsed plasma thruster (NASA GRC, 0.86 mN thrust, 1300 sec I_{sp}, 8.4% efficiency) [8].

The scalability issues of ion engines and Hall-effect thrusters are solved in part by FEEP and PPT, but they do not have the propulsive capability or maturity to fly on lunar and interplanetary nanosatellite missions. The hurdles that remain are too substantial to ensure a reasonable probability of success in the near term.

2.1.3 Magnetoplasmadynamic Thrusters

Magnetoplasmadynamic thrusters (MPDs) cover the high end of the power spectrum ($\sim$1 MW). They have poor efficiency at low and medium power and require further development before being flown [5].

These thrusters are difficult to test on the ground and have major heat dissipation issues. While promising for future high-power missions, this technology offers little for small spacecraft.

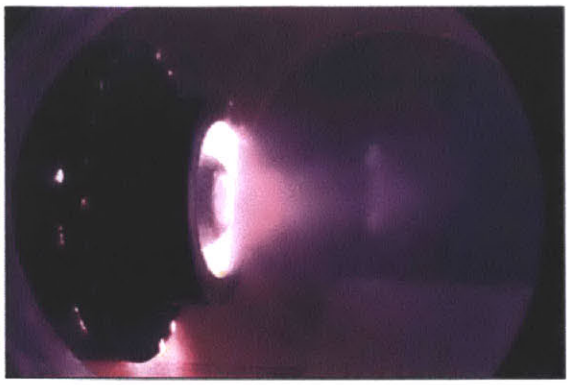

Figure 2-5: Argon MPD thruster.

2.2 Basic Principles

Electrospraying was originally developed for mass spectrometry of macromolecules; very little fragmentation occurs compared to other ionizing techniques [22]. Little time transpired before engineers adapted this ion source for use in electric thrusters. Electrospray propulsion is based on the electrostatic extraction and acceleration of positive and negative ions from an ionic liquid, a zero-vapor pressure conductive salt that remains in the liquid phase at room temperature. Table 2.1 summarizes important properties of two common ionic liquids.

Table 2.1: Ionic Liquid Properties

Ionic liquid	**EMI-Im**	**EMI-BF_4**
Conductivity (si/m, 25 C)	0.84	1.3
Viscosity (cP, 25 C)	28	34.1
Surface Tension (dyn/cm^3)	41.6	52
Density (g/cm^3)	1.52	1.24
+ ion mass	111.2	111.2
- ion mass	280.1	86.8
Melting Point (C)	-15	12
Decomposition temperature (C)	450	412

Electric fields on the order of 1 V/nm are required to extract charged species. Such intense fields are routinely achieved at the tip of electrically stressed liquid menisci called Taylor cones [35], which form most readily at the end of sharp emitter structures where the electric field intensity is magnified. Emission occurs from the tip

of the Taylor cone; the ions are accelerated and pass through a downstream extractor aperture. Figure 2-6 depicts this process.

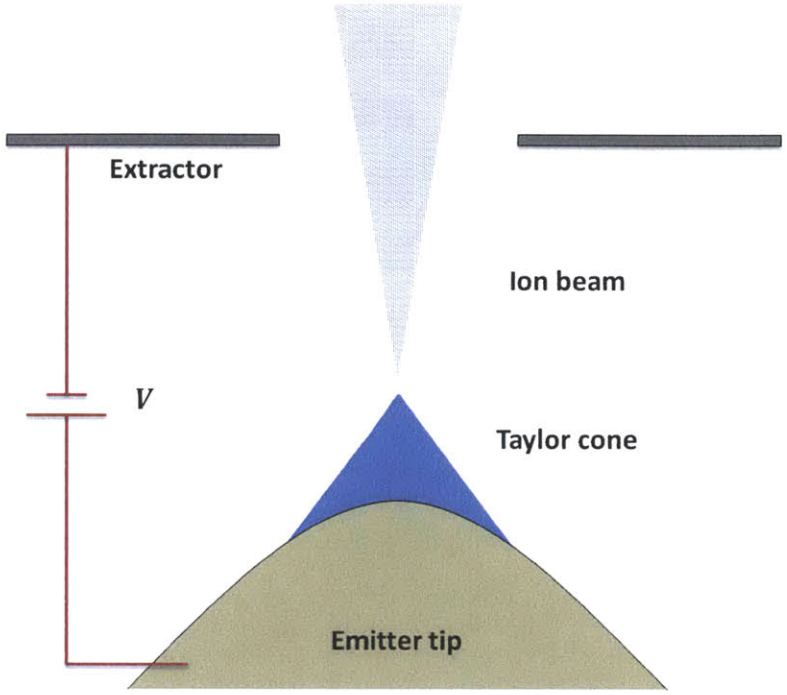

Figure 2-6: Diagram of an electrospray thruster firing. In its basic configuration, it consists of a power supply, an emitter tip wetted with ionic fluid, and a perforated extractor.

An important characteristic of electrosprays is that both positive and negative species can be emitted. In consequence, there is no need for an electron-neutralizing cathode. In a practical configuration, the thruster includes two separate head modules emitting oppositely charged ions of comparable mass and producing similar thrust as seen in Figure 2-7.

Each emitter is capable of generating up to 1 μA of ionic current, corresponding to about 0.1 μN of thrust. The MIT SPL has demonstrated emitters that achieve high specific impulse ($I_{sp} > 2000$ sec) at high efficiency ($\eta > 0.8$). Another significant advantage of this technology is the ease with which the specific impulse can be modulated. Simply changing the electric field (by adjusting the voltage applied between the emitter tip and the extractor) can change the operating regime, which affects specific impulse [18].

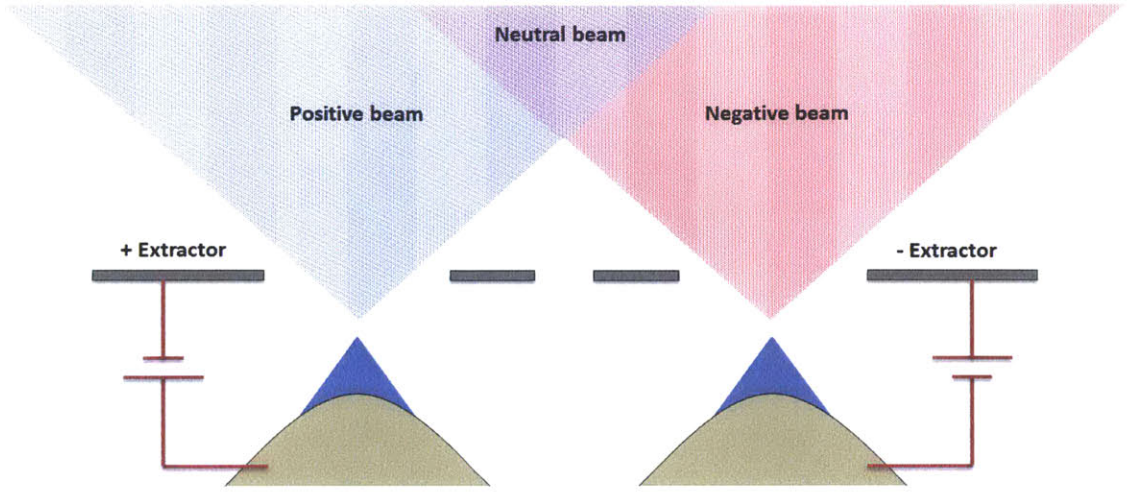

Figure 2-7: Two thrusters firing at opposite polarity yield a net neutral ion beam.

2.3 Thrusters

The excellent scalability of ion electrospray propulsion makes it ideal for implementation in thrusters designed for nanosatellites. The thrust from single emitters is too small for most practical applications. Because of this, there is a need to build dense arrays of emitters that fire in parallel. This is achieved by merging the fundamental working principles behind ion electrospray thrusters with recent developments in microelectromechanical systems (MEMS) materials and processes.

2.3.1 iEPS

The iEPS is the manifestation of these concepts. Emitters are fabricated on porous materials so that propellant can flow via capillarity through the bulk of the material, driven by the ion evaporation process. Therefore, no pressurization is required for pumping (or storing) the propellant [25]. Figure 2-8 shows this configuration.

Chemical stability of the propellant is achieved by periodically alternating the polarity of modules or groups of modules, each having its own ionic liquid reservoir. This strategy was identified early in the development of ionic liquid ion sources to avoid electrochemical degradation [27].

iEPS is designed for small spacecraft, particularly CubeSats. Figure 2-9 shows a

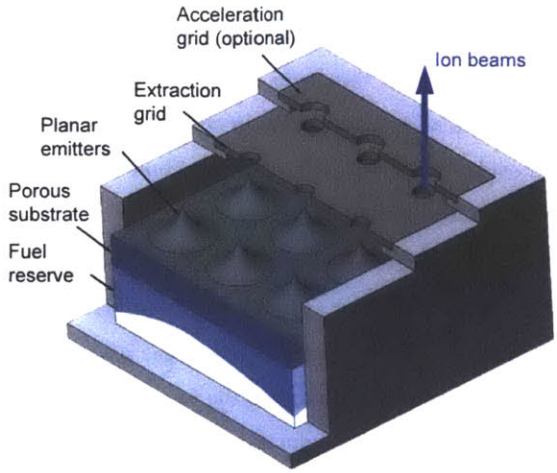

Figure 2-8: Diagram of the major components of ion electrospray thrusters [20].

computer-aided design (CAD) drawing of the thruster, which measures approximately a centimeter in length and width.

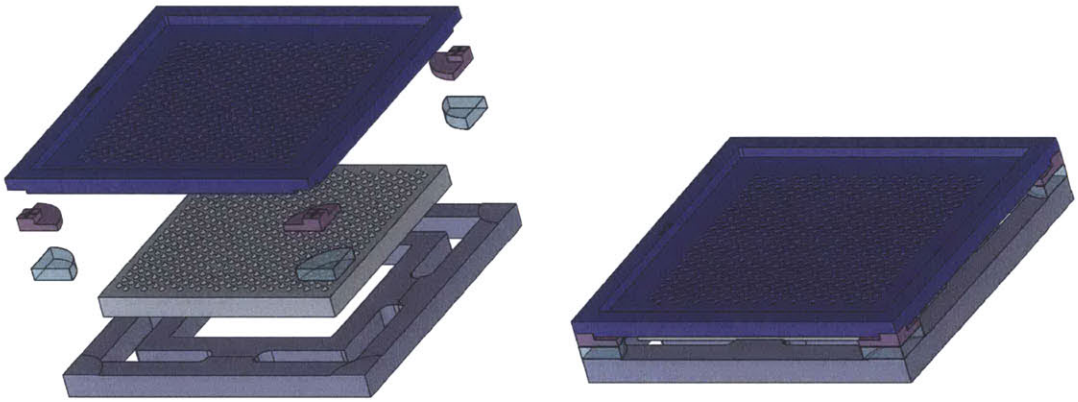

Figure 2-9: CAD drawing of iEPS showing structure, emitter array with 480 tips, and extractor grid.

2.3.2 Fabrication and Assembly

Fabricating a thruster with such small dimensions and components is no trivial task. The features must be uniform and the process repeatable. Figure 2-10 shows a substrate with micromachined emitter tips as well as the completed package.

The propellant reservoir can be scaled to any size. The walls are lined with porous

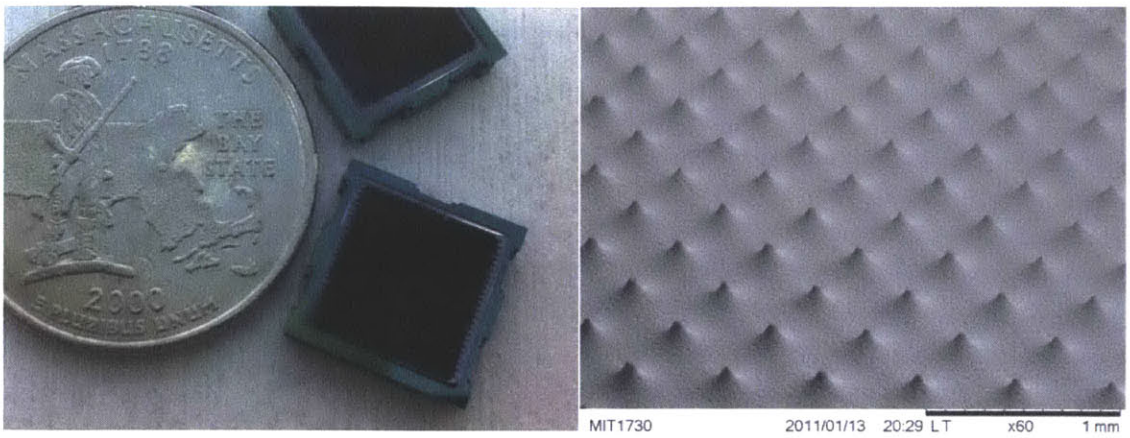

Figure 2-10: Image of iEPS thruster without propellant reservoir (left) and micromachined emitter tips (right).

material that acts like a wick, allowing propellant to travel to the back side of the porous substrate in which the tips are machined.

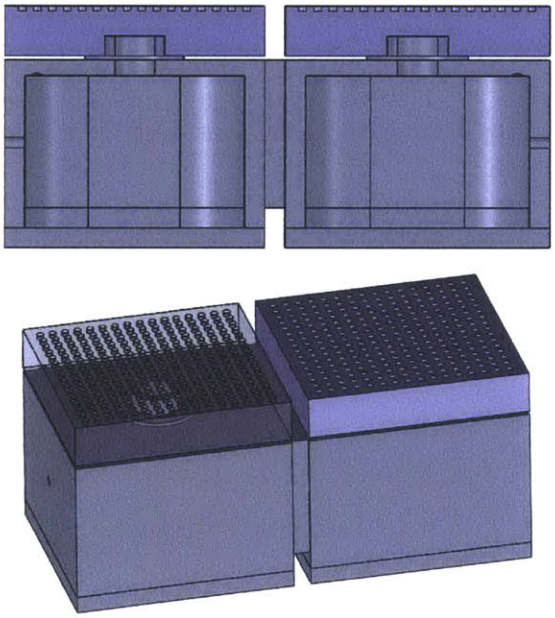

Figure 2-11: Small propellant tank cut-away view (top) and isometric view (bottom).

Assembling the thrusters requires diligence and ingenuity. Alignment of the tips and extractor grid is critical, and it is achieved by including special alignment features. The ultimate result is a product that can be quickly fabricated in large quantities.

2.3.3 Power Processing Unit

PPUs are a key component in every electric propulsion system. Simplicity and low mass are highly desirable, and iEPS lends itself to a PPU with such characteristics. Work on the PPU is progressing steadily, promising high efficiency and low mass and volume. Its development progresses in parallel to the thrusters, and it can easily be scaled up to meet any power requirement. Figure 2-12 shows one such PPU, which has eight channels [28].

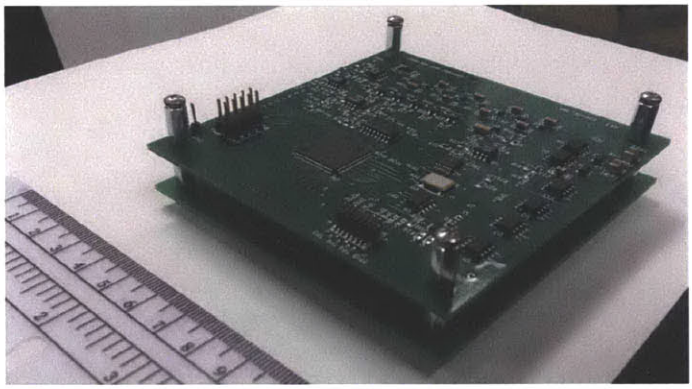

Figure 2-12: Precision Electrospray Thruster Assembly (PETA) PPU for iEPS.

This unit is radiation tolerant, and future iterations can be designed to withstand higher doses. The design is simple and the components robust.

2.3.4 Performance

iEPS performs very well, particularly for its mass and size. Table 2.2 details several important performance metrics, listing typical ranges as well as the results from iEPS v1 testing [19].

Continuing research and development promises a tremendous increase in performance. Thrust density can be multiplied by increasing the number of emission sites per unit area, which can be done by densifying the emitter tips or fabricating each such that multiple Taylor cones form. Present limitations are due to fabrication and assembly, not physics, and rapid advancements in MEMS capabilities are sure to push the boundaries further.

Table 2.2: iEPS Performance

Metric	Approximate Range	iEPS v1
Efficiency	0.3-0.8	~0.7-0.8
Specific impulse (sec)	200-4000	2000-3000
Thrust (μN)	20-60	~40
Mass (g)	0.5-1	~0.7
Peak power	0.1 mW - 1 W	~0.65 W
Dimensions (mm)	~10×10×2	12×12×2

Rapid start-up time and ability to withstand nearly unlimited on/off cycles makes the thrusters well-suited for ADCS actuators should the spacecraft not need to accomplish high-rate maneuvers. iEPS has a favorable start-up profile; there are few transients since ion emission starts at a discrete voltage. Furthermore, thrust can be adjusted easily (from 1-60 μN per module according to the most recent estimates). This allows for more flexibility, precision, and fuel savings; higher thrust can be used for aggressive slew maneuvers while lower thrust can be used for precision pointing.

Propellant slosh is an important consideration in spacecraft design, and its adverse effects can be mitigated by segmenting the propellant tank. This configuration lends itself to producing a main engine with independently controlled sectors, which offers greater controllability.

2.4 Implementation

Because of its scalability and simplicity, iEPS can be used to provide or augment propulsive capability for a broad range of missions. Even massive spacecraft can use large panels of thrusters to provide actuation; station-keeping and even substantial orbital maneuvers can be performed as long as enough time, power, and propellant are budgeted. They have the greatest potential for small, low-power spacecraft and offer game-changing performance.

The development timeframe for iEPS is very favorable. Thrusters are slated to fly as soon as 2014 or 2015, and research continues under NASA and Department of Defense (DoD) contracts. Lifetime testing is planned and is the primary hurdle

that remains before designing, fabricating, and testing scaled-up propulsion systems. At the current pace, launching lunar and interplanetary missions as early as 2017 or 2018 is feasible.

Chapter 3

Guidance and Control

To accomplish its mission, a spacecraft must be able to determine a course of travel to its destination and follow it. It must maintain attitude knowledge, estimate its state, and control its pointing and flight path. This requires an ensemble of sensors to collect information about its environment, software to process this information and compute commands, and actuators to apply forces and torques. These functions are collectively known as guidance, navigation, and control (GNC).

GNC architecture depends on the mission and the capabilities of the spacecraft. Low-thrust propulsion systems require special consideration, particularly regarding the modeling of maneuvers. Fortunately, a great deal of effort has been devoted to developing suitable algorithms, and they have been demonstrated in a series of highly successful missions.

GNC for small satellite missions does not require a total overhaul of traditional architectures; many of the basic methods remain unchanged. What must be addressed, however, are the specific operating characteristics of the propulsion system, the tight constraints of the CubeSat standard, and using ion electrospray thrusters as attitude control subsystem actuators. Navigation is not anticipated to differ from typical deep space missions, so it is not addressed in detail.

3.1 Architecture

Each lunar and interplanetary mission consists of several phases after launch, and the GNC algorithm must function properly and transition smoothly between each. Figure 3-1 shows a progression of the basic phases.

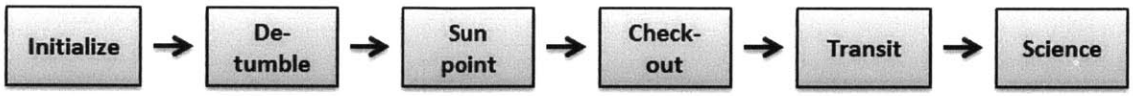

Figure 3-1: Typical phases for lunar and interplanetary missions.

After release from the deployment module (DM), the spacecraft initializes, powering up the necessary subsystems for de-tumbling. Once the rates are sufficiently low, the solar panels are pointed toward the sun to fully charge the batteries. The spacecraft holds this orientation until entering the check-out phase, in which all of the subsystems are activated and nominal performance is verified. After this, the spacecraft begins its transit, using the main engine to perform the required orbital maneuvers while the ADCS controls pointing. After arriving at its destination, the spacecraft enters the science phase, in which it collects data and transmits it back to earth.

From de-tumble through check-out, only pointing must be controlled. The spacecraft must be able to slew and hold a particular attitude. During transit, the main engine is activated, and the algorithm must produce commands to control the attitude and the thrust vector. The algorithm is ordered as follows. First, the navigation routine computes an estimate of the spacecraft's rotational and translational state using on-board sensors and a model of the spacecraft dynamics. The state estimate is passed to the guidance routine, which calculates the maneuvers required to maintain the proper flight path. Finally, the maneuvers are passed to the controller, which calculates the commands for each actuator. The focus of this research is on guidance and control, and Figure 3-2 shows a diagram of the architecture at the highest level.

Model Predictive Control (MPC) lends itself to this mission class. This method-

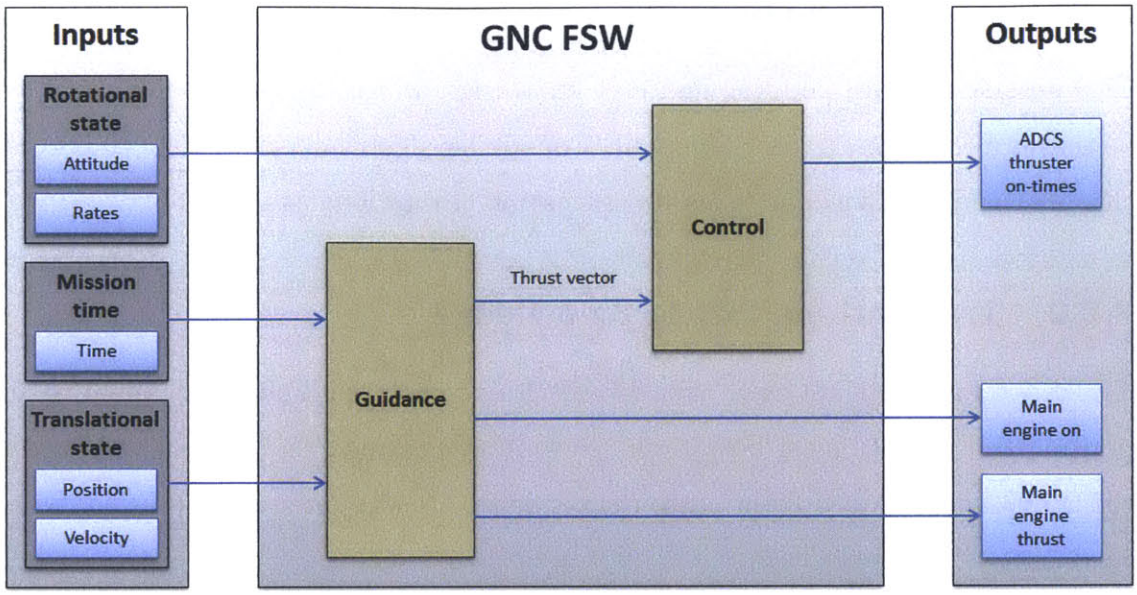

Figure 3-2: Diagram of the guidance and control algorithm.

ology entails a model of the system dynamics built into the controller; the commands are computed using the predicted behavior of the spacecraft. This is advantageous for calculating and continually updating a lengthy series of maneuvers approximating continuous thrust.

3.2 Navigation

"Navigation is defined as the science behind transporting ships, aircraft, or spacecraft from place to place; particularly, the method of determining position, course, and distance traveled as well as the determination of the time reference [31]."

Although it is not explicitly included in the algorithm, navigation is indispensable. Attitude and rate measurements must be made continuously, and periodic updates of position and velocity are required. There is no need to re-invent the wheel; flight-tested legacy techniques are to be used where possible.

3.2.1 Attitude Knowledge

This mission requires pointing and rate knowledge, which can be determined based on sensor measurements. A Kalman filter or similar algorithm can be used to process this information to yield an accurate estimation of rotational state.

3.2.2 Translational State Knowledge

The spacecraft state estimate will diverge from the actual state over time, so its position and velocity must be determined from the ground. The differences between the actual and intended flight path, the residuals, are computed and uplinked to the spacecraft.

3.3 Guidance

"Guidance is defined to be the on-board determination of the desired path of travel from the vehicle's current location to a designated target [31]."

Guidance routines typically include targeters that periodically re-compute the trajectory to the destination, but this is not included as targeting is not the primary focus of the research. A trajectory is designed using a separate software package, and a table is produced that lists the spacecraft position and velocity in an inertial frame at a uniform time interval. The spacecraft effectively leapfrogs from point to point until it reaches its destination. It is more technically correct to call this portion the trajectory-following routine than the guidance routine. Figure 3-3 shows a diagram representing this portion of the flight software.

The routine computes the burns necessary to achieve the desired state and continuously updates them. After this, it selects whether the main engine or the ADCS thrusters are to provide the actuation.

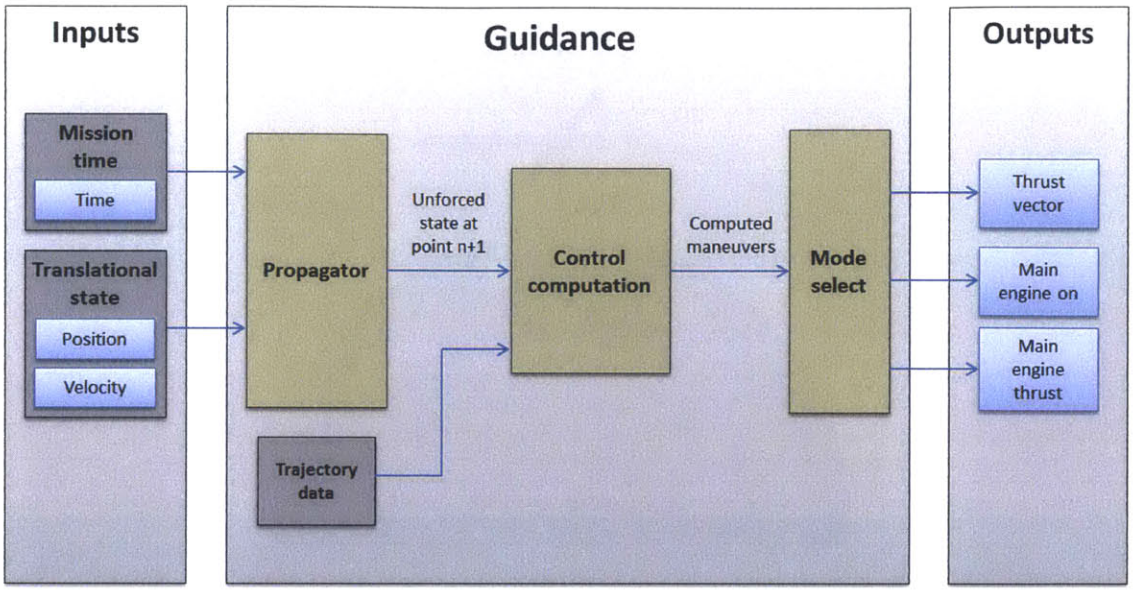

Figure 3-3: Diagram of the guidance routine.

3.3.1 Guidance Logic

The guidance algorithm approximates a continuous thrust arc with a set of impulsive maneuvers. These maneuvers are computed using the Hill-Clohessy-Wiltshire (HCW) relative motion model, which gives a first-order approximation of a spacecraft's motion (in a circular or elliptical orbit) relative to that of another in a circular orbit about a central body considered a point mass. The reference spacecraft (or waypoint) is typically called the 'target' while the other spacecraft is denoted the 'chaser.' The terminology comes from the primary application of this formulation, which is planning a rendezvous. Leapfrogging from waypoint to waypoint is effectively like performing a series of rendezvous; the objective is to achieve a particular state rather than meeting up with a target vehicle. The relative position and velocity vectors are expressed in the local vertical, local horizontal (LVLH) coordinate frame, which is illustrated in Figure 3-4.

Figure 3-5 depicts the position of the chaser spacecraft relative to the target spacecraft. If the target and chaser are co-orbital, meaning the only difference is in their true anomaly, the relative state will not change.

The spacecraft of interest is the chaser, which is to maneuver such that it attains

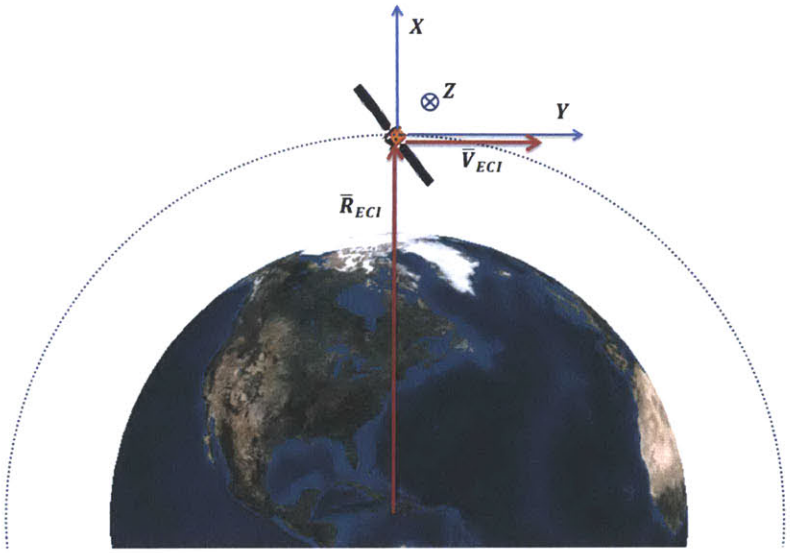

Figure 3-4: LVLH frame. The X-axis is directed along the position vector (radial), the Y-axis is directed along the velocity vector but parallel to the surface of the central body (along-track), and the Z-axis completes the set (cross-track). $\bar{R}_{ECI}$ is the position vector in the ECI frame, and $\bar{V}_{ECI}$ is the velocity vector.

the desired state X_{n+1} at the desired time t_{n+1}. If X_{n+1} is expressed in the relative coordinate frame, the HCW model can be used. The question is what to use as the target (meaning the reference point; the term target is misleading in this discussion).

The solution is using the estimated state of the spacecraft assuming no maneuvering is performed. At time t_n, the spacecraft state is propagated forward without thrust to t_{n+1} (in the inertial frame), resulting in $\hat{X}_{n+1}$. The difference $X_{n+1} - \hat{X}_{n+1}$ is then expressed in the LVLH frame relative to $\hat{X}_{n+1}$. Finally, the maneuvers required to achieve this desired relative state are computed.

Assuming $R_{LVLH} \ll R_{ECI}$, the HCW equations of motion are expressed as

$$\begin{aligned} \ddot{x} - 3n^2 x - 2n\dot{y} &= \frac{F_x}{m_{s/c}} \\ \ddot{y} + 2n\dot{x} &= \frac{F_y}{m_{s/c}} \\ \ddot{z} + n^2 z &= \frac{F_z}{m_{s/c}} \end{aligned} \tag{3.1}$$

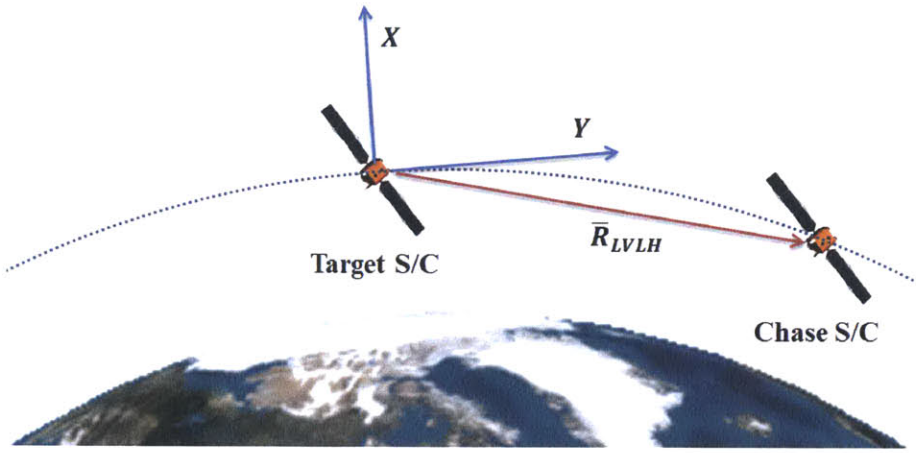

Figure 3-5: The HCW model describes the motion of a chaser spacecraft relative to a target spacecraft, and this relative state is expressed in the LVLH frame of the target spacecraft.

where F_x, F_y, and F_z are components of the external force vector excluding central body gravity and $m_{s/c}$ is the mass of the spacecraft. Cross-track motion is de-coupled from in-plane motion. The angular rate n is equal to

$$n = \sqrt{\frac{\mu}{a^3}} \tag{3.2}$$

where μ represents the gravitational parameter of the central body and a represents the semi-major axis of the orbit.

The continuous time system realization given in Equation 3.3.1 can be represented in state space form as

$$\dot{X}(t) = A(t)X(t) + B(t)u(t) \tag{3.3}$$

where $X(t) = \begin{bmatrix} x(t) & y(t) & z(t) & \dot{x}(t) & \dot{y}(t) & \dot{z}(t) \end{bmatrix}'$ is the state vector and $u(t) = \begin{bmatrix} F_x(t) & F_y(t) & F_z(t) \end{bmatrix}'$ is the control vector of thrust forces. $A(t)$ is the state matrix and $B(t)$ is the input matrix.

Assuming a time step of $t_{k+1} - t_k$ seconds, the model can be converted to a discrete-time form.

$$X_{k+1} = \phi X_k + \Gamma u_k \tag{3.4}$$

where the state transition matrix ϕ is given by

$$\phi = \int_{t_k}^{t_{k+1}} e^{A\tau}\, d\tau = \tag{3.5}$$

$$\begin{bmatrix}
4 - 3\cos(nt_{k+1}) & 0 & 0 & \frac{1}{n}\sin(nt_{k+1}) & \frac{2}{n}(1 - \cos(nt_{k+1})) & 0 \\
6(\sin(nt_{k+1}) - nt_{k+1}) & 1 & 0 & -\frac{2}{n}(1 - \cos(nt_{k+1})) & \frac{1}{n}(4\sin(nt_{k+1}) - 3nt_{k+1}) & 0 \\
0 & 0 & \cos(nt_{k+1}) & 0 & 0 & \frac{1}{n}\sin(nt_{k+1}) \\
3n\sin(nt_{k+1}) & 0 & 0 & \cos(nt_{k+1}) & 2\sin(nt_{k+1}) & 0 \\
-6n(1 - \cos(nt_{k+1})) & 0 & 0 & -2\sin(nt_{k+1}) & 4\cos(nt_{k+1}) - 3 & 0 \\
0 & 0 & -n\sin(nt_{k+1}) & 0 & 0 & \cos(nt_{k+1})
\end{bmatrix}$$

The input matrix is discretized using the formula

$$\Gamma = \int_{t_k}^{t_{k+1}} e^{A(t_{k+1}-\tau)} B\, d\tau \tag{3.6}$$

and re-defined such that the control vector u represents an instantaneous change in velocity at t_k.

$$\Gamma = \int_{t_k}^{t_{k+1}} e^{A(t_{k+1}-\tau)}\, d\tau \begin{bmatrix} 0 & 0 & 0 & 1 & 0 & 0 \\ 0 & 0 & 0 & 0 & 1 & 0 \\ 0 & 0 & 0 & 0 & 0 & 1 \end{bmatrix}' \tag{3.7}$$

The objective is to solve for the controls required to attain the goal state. Re-arrange Equation 3.4 to solve for u_k.

$$u_k = \Gamma^{-1}(X_{k+1} - \phi_k X_k) \tag{3.8}$$

When u_k is executed at time t_k (assuming the chaser and target begin at the same location), the relative position of the chaser X_{k+1} at time t_{k+1} is as illustrated in Figure 3-6.

This formulation can be extended to compute i intermediate maneuvers in the following manner.

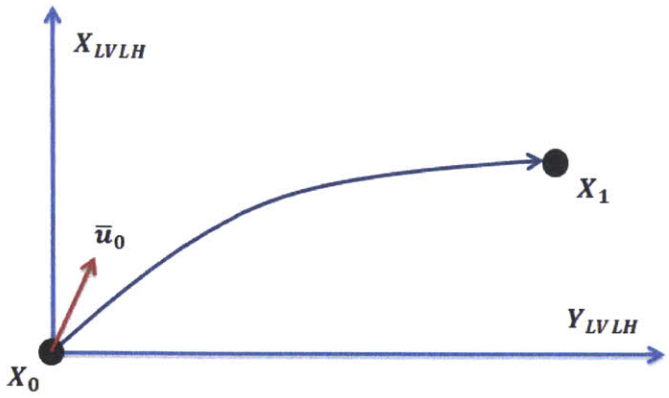

Figure 3-6: Maneuver $\bar{u}_0$ is executed at t_0, resulting in state X_1 at time t_1.

$$
\begin{aligned}
&X_0 \\
&X_1 = \phi_0 X_0 + \Gamma u_0 \\
&X_2 = \phi_1 X_1 + \Gamma u_1 \\
&\quad = \phi_1(\phi_0 X_0 + \Gamma u_0) + \Gamma u_1 \\
&\quad = \phi_1\phi_0 X_0 + \phi_1\Gamma u_0 + \Gamma u_1 \\
&X_i = \prod_{k=i}^{0} \phi_k X_0 + \begin{bmatrix} \prod_{k=i}^{1}\phi_k\Gamma & \prod_{k=i}^{2}\phi_k\Gamma & \cdots & \Gamma \end{bmatrix} \begin{bmatrix} u_0 & u_1 & \cdots & u_k \end{bmatrix}' \\
&\quad = \mathbf{A}X_0 + \mathbf{B}U
\end{aligned}
\tag{3.9}
$$

In the same way, this equation can be re-arranged to solve for U, which is the matrix of maneuvers between X_0 and X_i.

$$U = \mathbf{B}^{-1}(X_i - \mathbf{A}X_0) \tag{3.10}$$

Figure 3-7 illustrates a series of maneuvers executed to achieve the desired final state.

It is important to note that the trajectory is not always circular; the resulting inaccuracies can be kept low by ensuring $t_{n+1} - t_n \ll period$. Furthermore, since the change in semi-major axis is small over this interval, all ϕ_k are approximated as ϕ_0.

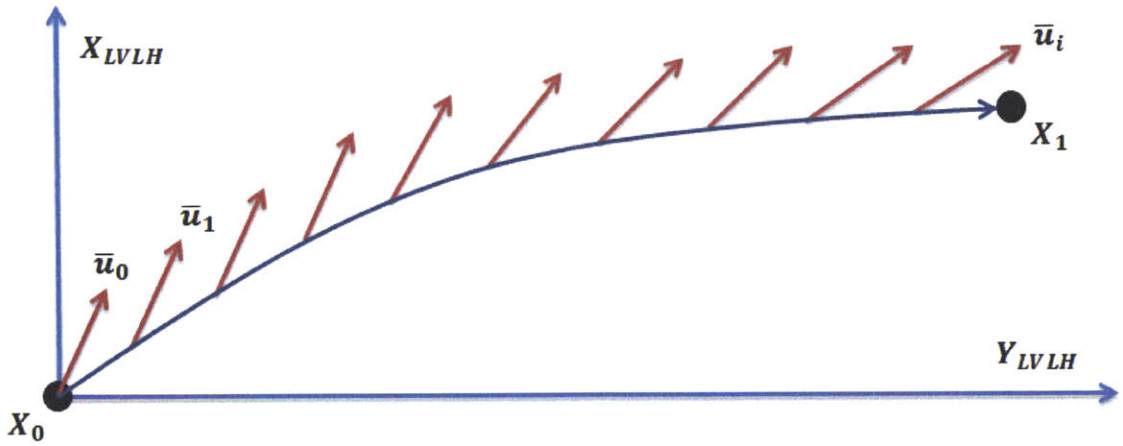

Figure 3-7: Maneuvers u_0 through u_i are executed at a uniform interval, resulting in state X_1 at time t_1.

The controls U are re-computed until the prediction horizon falls below a reasonable value, at which point the solution is held and executed through completion. Failure to do so results in erratic behavior as the spacecraft approaches its goal state.

These controls are computed in a rotating frame and applied in an inertial frame, meaning that fictitious accelerations must be considered. Because the rotation rate of the LVLH frame is low at the altitudes considered, it is not necessary to correct the controls. If the algorithm is re-designed, it is prudent to consider computing the controls in an inertial frame to avoid this complication.

3.4 Control

"Control is defined as the on-board manipulation of vehicle steering controls to track guidance commands while maintaining vehicle pointing with the required precision [31]."

The control system is responsible for calculating the thrust magnitude for the main engine and the commands for the ADCS actuators. If the main engine does not gimbal, the attitude must be adjusted to achieve the commanded thrust vector. Figure 3-8 shows a block diagram of the control portion of the flight software.

The control routine consists of three primary components: error calculation, the

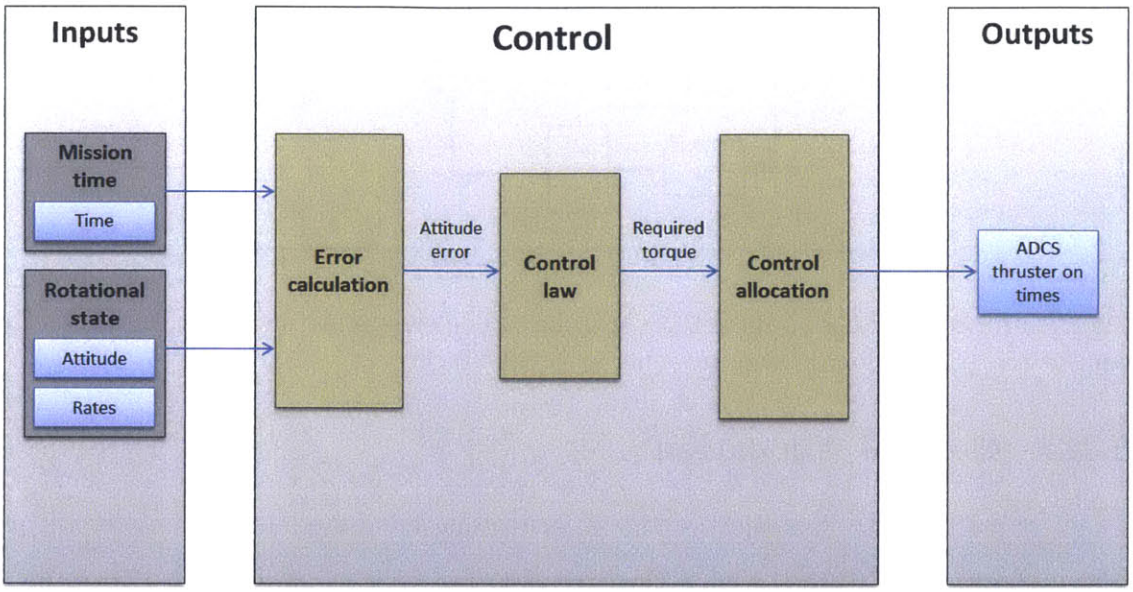

Figure 3-8: Diagram of the control routine.

control law, and the control allocation logic. This sequence transforms the desired maneuvers into commands for the actuators.

3.4.1 Error Calculation

The error calculation block computes the difference between the LVLH frame and the spacecraft body frame. If this angular difference is larger than the deadband magnitude, a slew maneuver about the eigenaxis is commanded.

3.4.2 Control Law

If an eigenaxis slew is commanded, a simple proportional-derivative (PD) control law computes the required torque in the body frame. There is no need for an intricate or more computationally expensive controller as the spacecraft is expected to be simple. Figure 3-9 shows a diagram of the controller.

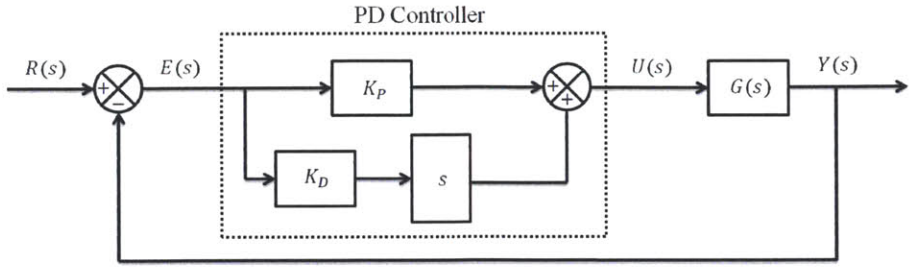

Figure 3-9: Feedback loop with PD controller. The error E is the input, and U is the sum of the proportional term and the derivative term.

3.4.3 Control Allocation

The control allocator transforms the given torque command into an array of on-times denoting the duration each thruster is to fire. For example, if a +Z torque is commanded, the arrays shown in Figure 3-10 fire.

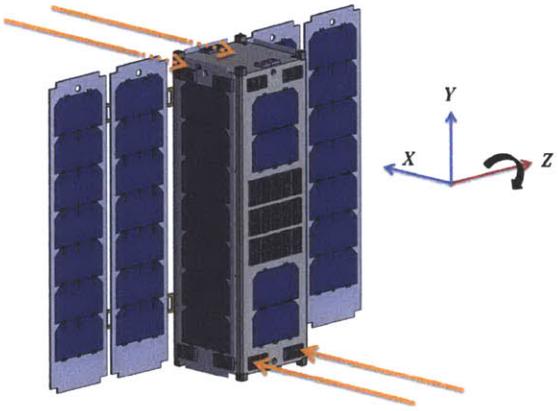

Figure 3-10: The control allocation logic governs which thrusters are activated. The thrusters are oriented such that particular sets can provide a pure torque and a pure force in each axis.

3.5 Summary

Together, these routines allow the spacecraft to follow a reasonably designed trajectory about any central body. Choosing values for the various parameters is critical, and it is addressed in more detail in the next section.

The design and implementation of the GC algorithm is an integral part in the

effort to evaluate nanosatellite missions to the moon and beyond. The algorithm is easy to implement and allows for simulation of a wide variety of missions.

Chapter 4

Lunar Missions

Lunar science is a very active field, particularly with the resurgence of interest in manned spaceflight beyond LEO. A recent series of high-profile missions have greatly deepened our understanding of the moon and are indicators of a growing desire to return to it. Establishing a permanent outpost, setting up scientific observatories, exploiting its vast natural resources, and a host of other opportunities beckon humanity, but there are still many studies and prerequisites to be accomplished [2].

4.1 Lunar Impactor

The Space Propulsion Laboratory is actively participating in a nanosatellite mission called Lunar Impactor. The overarching goal is to obtain high fidelity measurements of localized magnetic regions in the moon's crust [23]. Landing on the surface is an ideal solution to this problem, but the cost is prohibitive. This leaner concept calls for flying CubeSats on unbraked impact trajectories into the features as shown in Figure 4-1.

The mission commences upon spacecraft separation from its carrier in geostationary earth orbit (GEO), after which it stabilizes and charges its batteries. Ground controllers then perform a full check-out of all the subsystems to identify and fix any issues. The spacecraft then initiates the cis-lunar transfer, controls the spiral ascent to the moon, and maintains the proper entry trajectory. In the final seconds

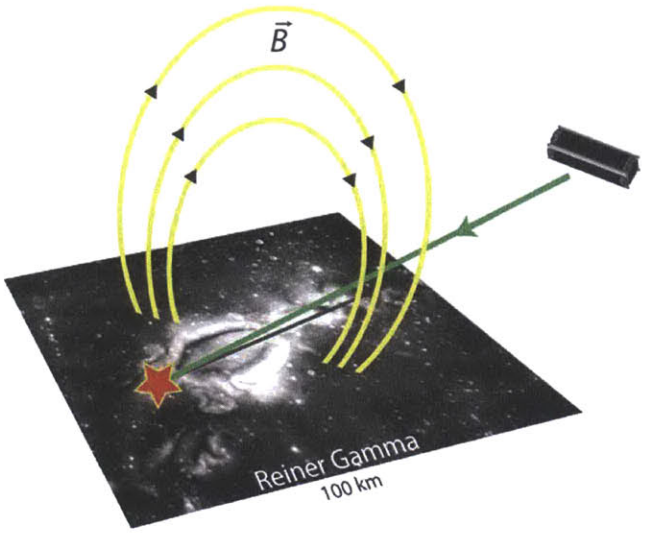

Figure 4-1: CubeSat on a low angle impact trajectory.

before impact, Lunar Impactor takes the measurements and transmits the data back to earth.

Mission analysis through numerical simulation is the preferred method of demonstrating the feasibility of the GC architecture, and it yields valuable insight into the propulsive requirements as well. This examination serves as the centerpiece of the research detailed in this thesis.

4.1.1 Background

The origin of lunar magnetism has remained a mystery since its discovery when subsatellites deployed during Apollo 15 and 16 detected small magnetic regions throughout the moon's crust (~100 km) [14, 15].

"The dominant hypotheses for the formation of these magnetic 'anomalies' suggest they are from either the magnetic field of an ancient lunar dynamo or processes related to the formation of plasmas produced during meteoroid impacts [23]." Some are co-located with brightly-colored features called 'swirls,' which are often attributed to solar wind proton deflection or lunar dust lofting.

Since Apollo, Lunar Propspector and Kaguya have obtained lunar magnetic field data. The spatial resolution is poor, however, as the average sampling altitude was

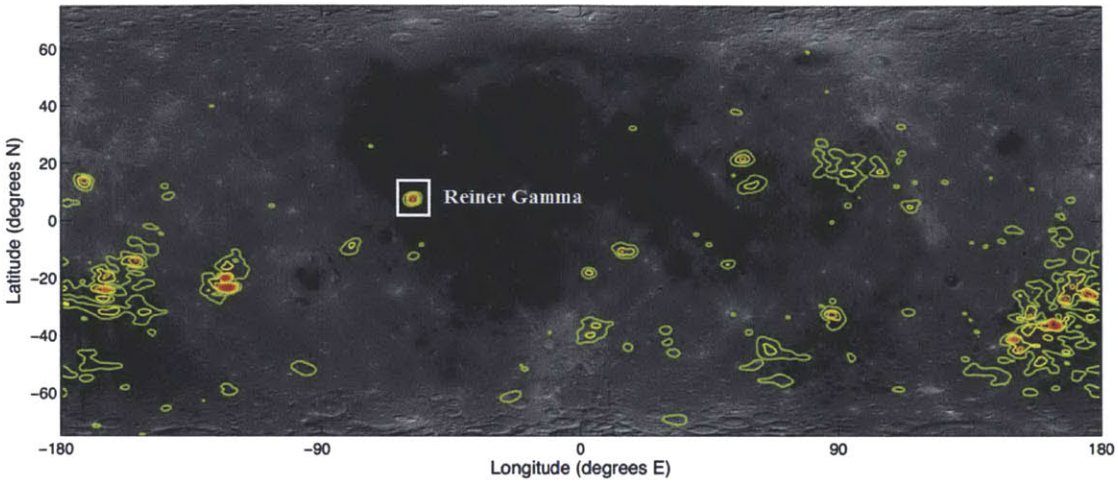

Figure 4-2: Map of lunar magnetism [30].

about 20 km. Scientists posit that a thorough understanding of the magnetic field coherence may shed light on the formation of these unusual abnormalities; verifying or disproving some of the key conjectures requires detailed measurements as close to the surface as possible [23].

Scientific Objectives

1. Constrain the process(es) responsible for magnetizing the underlying material by measuring the structure of near-surface magnetic fields. How complex are the magnetic sources? Is the field structure and direction consistent with material magnetized in a uniform field?

2. Test the hypothesis for formation of the swirl pattern by measuring the correlation of near-surface fields, surface markings, and solar wind flux. Does the magnetic field structure and solar wind flux correlate with the surface pattern? Are vertical near-surface fields associated with the darkest parts of swirls, while horizontal, near-surface fields are associated with the brightest regions, as predicted by the solar wind stand-off model?

3. Use magnetic field and solar wind flux measurements to better understand additional phenomena such as proton reflection and electric fields at swirls.

4. Test the hypothesis of lunar dust lofting and its possible role in swirl formation by measuring near-surface lofted dust. What is the distribution of lofted dust grains near the surface (< 1 km altitude)?

Technical Objectives

The technical objectives stem directly from the scientific objectives and outline the major development efforts required to field a system capable of accomplishing the mission.

1. Develop a 3-axis magnetometer capable of measuring the magnetic field at a frequency of 200 measurements/second, a solar wind ion detector capable of measuring energy and angle distribution at a frequency of 20 measurements/second, and a dust sensor capable of measuring dust flux and size distribution at a frequency of 20 measurements/second.

2. Develop a spacecraft bus capable of housing and deploying the instruments, powering them throughout descent, and sending the data back to earth real-time.

3. Develop a GNC system to bring the spacecraft from its initial orbit to the proper impact point.

4. Develop a compact, high-capability electric propulsion system to perform the desired maneuvers.

The bulk of the research conducted centers around objectives 3 and 4, but forays into spacecraft bus design are required to establish a baseline configuration for simulation and analysis. The preliminary requirements flow from the objectives and narrow the design space.

4.1.2 Mission Requirements

The initial study focuses on the Reiner Gamma anomaly as it exhibits a complex surface pattern and strong magnetic field. Figure 4-3 shows an image of this feature

with an overlay of the magnetic field.

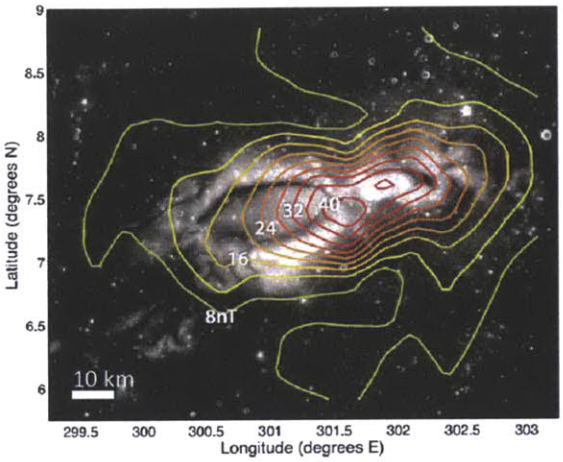

Figure 4-3: Horizontal component of Reiner Gamma magnetic field (~18 km altitude) measured by Lunar Prospector [24].

The impact angle must be shallow to ensure that low altitude measurements cover sufficient horizontal distance to address the objectives. Important information is expected to emerge below ~10 km, but the source model of Hemingway and Garrick-Bethell predicts that the magnetic field structure will be particularly complex below ~3 km [23]. The central cusp features (where the field lines become vertical) predicted by this model are very important as they may be correlated with the prominent dark lanes; the spacecraft must pass below ~3 km as it crosses the center of Reiner Gamma. An ideal trajectory traverses the four cusps and three peaks predicted by the model, but at minimum, it must cross two peaks and three cusps. These profiles are shown in Figure 4-4.

The aim point must reside within the anomaly to allow for very low altitude measurements, and the spacecraft must hit relatively near it to assure success. The maximum allowable miss distance is 2 km; this requirement is driven by the dimensions of Reiner Gamma. Table 4.1 summarizes the required incidence angles given impact position uncertainty as illustrated in Figure 4-5.

In addition to the impact angle requirement, there is an attitude knowledge requirement during the science phase. This is necessary to rotate the magnetic field measurements into the proper frame of reference. The goal objective is attitude

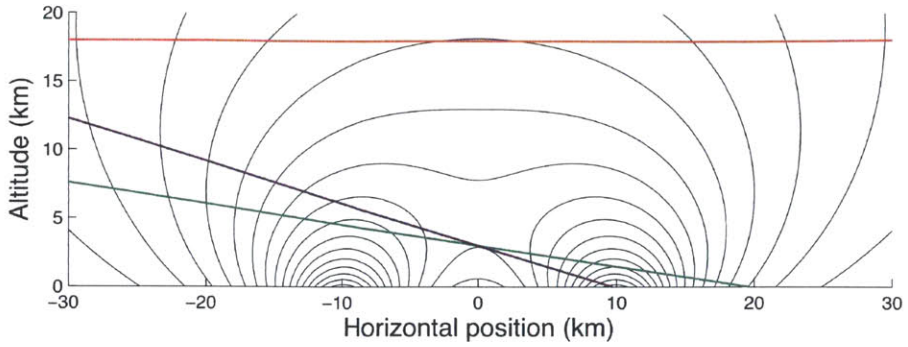

Figure 4-4: Reiner Gamma vertical magnetic field model with trajectories representing goal (green) and floor (purple) objectives. Red represents the lowest altitude reached by Lunar Propspector.

knowledge < 1 deg while the floor objective is knowledge < 5 deg.

Table 4.1: Impact Angle Requirements

Objective	**Description**	d_{min}	$\theta_{max}(\Delta d = 0\ km)$	$\theta_{max}(\Delta d = 2\ km)$
Goal	Traverse 4 cusps	17.6 km	9.7 deg	8.7 deg
Floor	Traverse 3 cusps	7.7 km	21.3 deg	17.2 deg

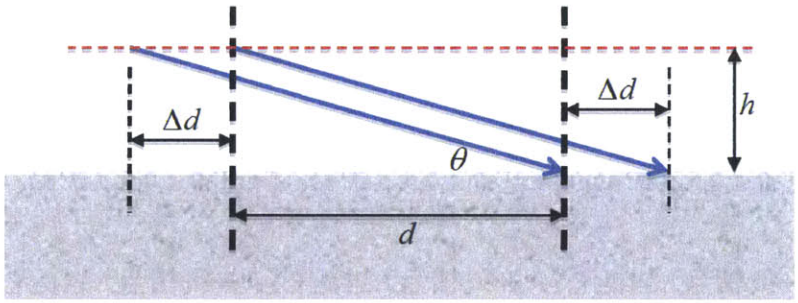

Figure 4-5: Relationship of landing ellipse length Δd, impact angle θ, and ground track distance d. Flight path angle is -θ.

4.2 Mission Architecture

There are many ways to accomplish this mission, but the most cost-effective is to use CubeSats equipped with high-capability ion electrospray propulsion systems. This

eliminates the need to inject the spacecraft in a trans-lunar trajectory; instead, it can travel to orbit in a ride-share configuration aboard a commercial launch vehicle. GEO is a reasonable departure point as CubeSats cannot tolerate the high radiation levels encountered in the Van Allen belts. Figure 4-6 illustrates this profile.

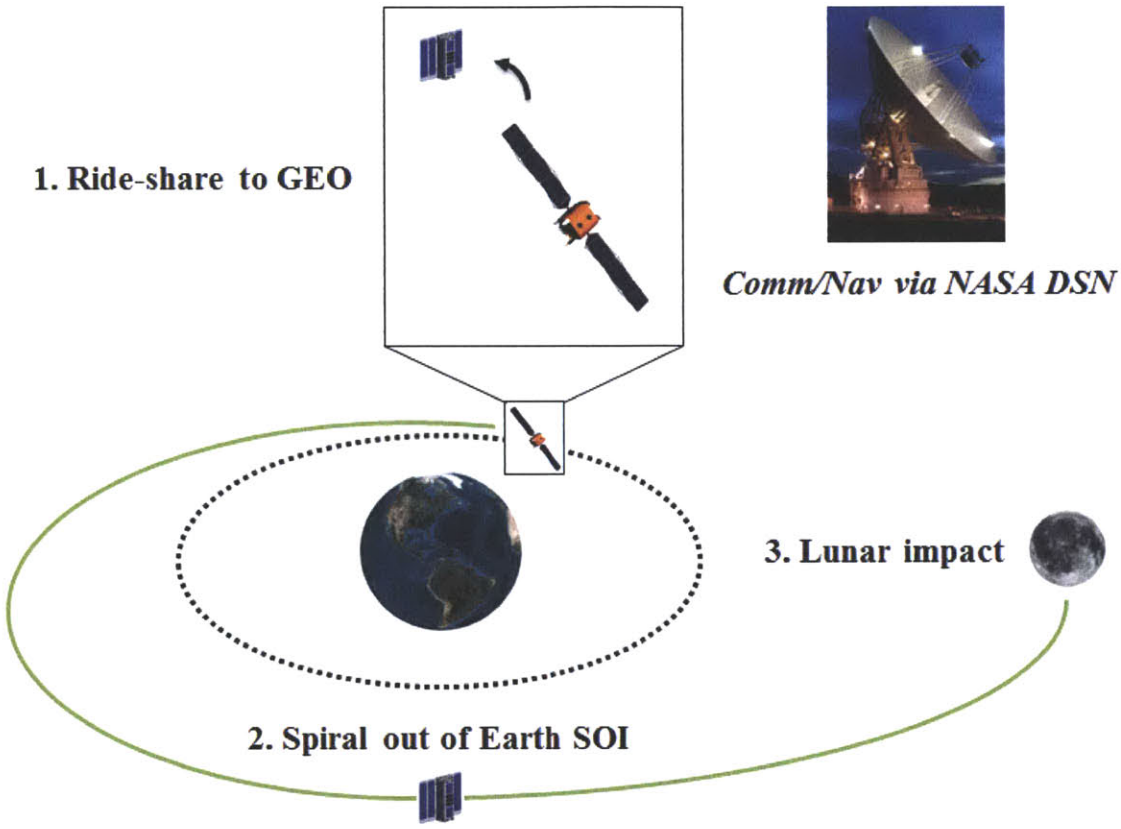

Figure 4-6: CubeSat travels from GEO to Reiner Gamma under its own power.

After deployment from its host, the spacecraft must initialize, de-tumble, and point the solar arrays toward the sun to fully charge the batteries. When this is complete, it enters the check-out phase to verify that all subsystems are performing nominally. Once the spacecraft is cleared, the transit to Reiner Gamma begins; total duration varies based on a number of factors but is on the order of ~2-4 months. When it nears the impact point, the instruments are activated to collect the required data. Particular emphasis is placed on the transit and science phases as they demand the most of the spacecraft.

4.2.1 Concept of Operations

The concept of operations describes how the spacecraft is employed to achieve the scientific objectives. The first step is to identify the various mission phases, describe what must occur in each, and understand the transitions. The command and data handling system must be designed with the necessary modes and capabilities to bring the spacecraft through each. Figure 4-7 shows the concept of operations (CONOPS) diagram, which provides a visual representation of this information.

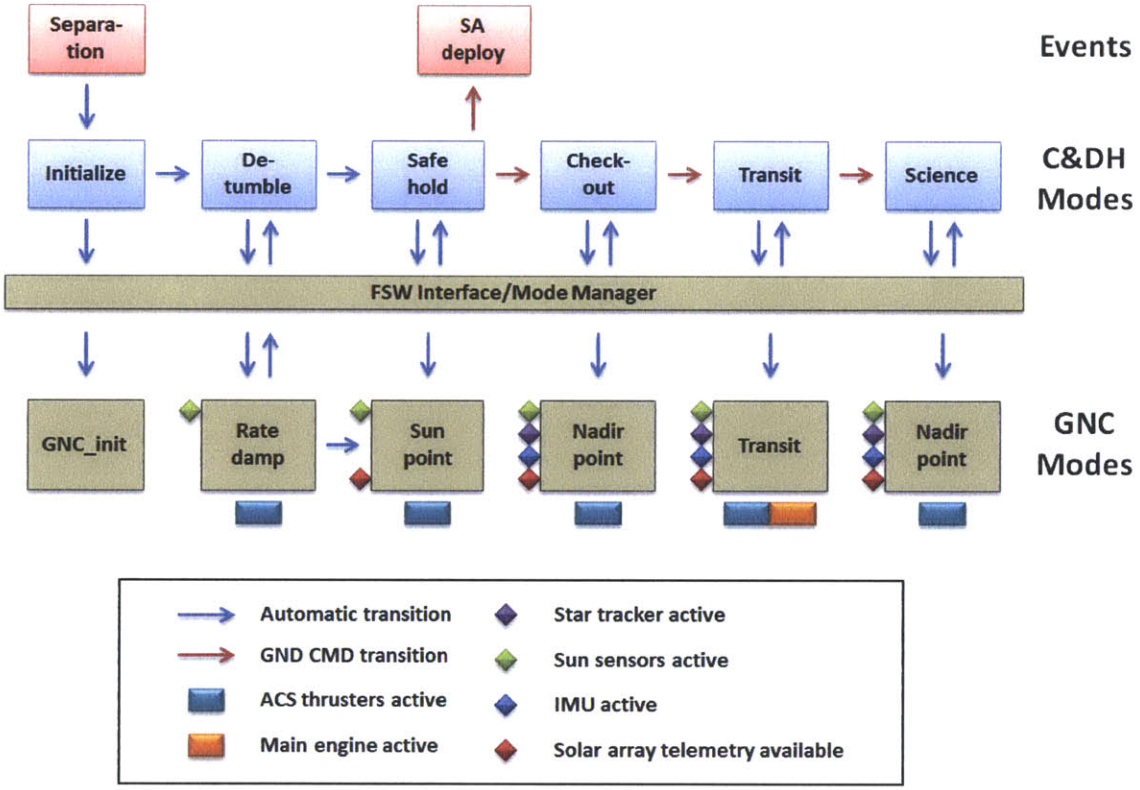

Figure 4-7: Lunar Impactor CONOPS diagram.

This diagram also shows when the various sensors and actuators are active, which gives some idea as to what each transition entails. Table 4.2 explains each phase in greater detail.

Table 4.2: CONOPS

Mission phase	Duration	Entry criteria	GNC modes	GNC operations	Exit criteria
Launch	~12-15 hours	Pre-launch systems nominal and navigation initialized	N/A	N/A	Deployment module releases spacecraft
Deployment (stabilize spacecraft)	~10 minutes	Separation switch triggered	De-tumble Safe hold, deploy solar array	-Null rates -Sun point and hold	Ground command
Check-out	~5-7 days	Ground command	Engineering mode	-Transition between sun-pointing and nadir hold -Star tracker and Inertial Measurement Unit (IMU) activated -Main engine power-up and testing	Check-out complete
Transit (Follow trajectory to desired state)	~2-4 months	Ground command	Transit mode	-GNC algorithm commands attitude and main engine	Desired state reached
Science (Transmit data)	~10 minutes	Ground command	Science mode	-Power down main engine -Transition to nadir hold -Activate instruments	Lunar impact
Disposal (lunar impact)	N/A	N/A	N/A	N/A	Lunar impact

Science Operations

The science phase of the mission is very short. The spacecraft impacts the lunar surface at high velocity, meaning it is only in the region of interest for a matter of seconds. The instruments must be active and properly deployed, and the spacecraft must maintain attitude knowledge.

ADCS

The ADCS must function properly during each mission phase, particularly lunar transit. Since the main engine has no gimbal mechanism, the ADCS must precisely orient the spacecraft to achieve the commanded thrust vector. The spacecraft must be able to slew and hold any commanded attitude.

Propulsion

The main engine must fire with the commanded thrust to remain on the proper trajectory. Besides test firing during the check-out phase, transit demands the most of the propulsion subsystem. Not only must the engine withstand thousands of hours of firing, but the PPU must also operate reliably.

4.3 Spacecraft Architecture

The requirements and CONOPS drive the spacecraft architecture. Key considerations include low cost, ease of manufacture, and compliance with existing techniques and protocol. The CubeSat standard conforms very well with each. CalPoly and Stanford laid out the original specifications to increase university involvement in space science and exploration [9]. The simple infrastructure and standardization of internal components drastically reduces price and complexity as does the self-contained deployment module. Many CubeSats to date have been successfully launched and operated, and their proliferation is accelerating.

A standard CubeSat is a 10×10×10 cm , which is designated 1-unit (1U). The size of the payload and key bus components necessitate a larger platform, so 3U is the form factor of choice (30×10×10 cm). Off-the-shelf deployment modules exist for 3U CubeSats, simplifying integration and launch.

4.3.1 Instrumentation

A 3-axis magnetometer is the primary instrument and must operate between 0-200 Hz. Anisotropic magneto-resistive (AMR) sensing is the preferred technique as it allows for more compact arrangements than fluxgate magnetometers, which are typically flown on such missions. AMR magnetometers have flight heritage, though, and can be designed to fit aboard Lunar Impactor [26]. One set of AMR sensors is to be mounted on an electronics board in the spacecraft while another is to be deployed on a boom (~15 cm) to keep it away from field sources aboard the spacecraft. The

second instrument is the Solar Wind Ion Flux Tracer (SWIFT), which is designed to track deflection and deceleration of ions within the lunar magnetic fields. It uses a hemispherical electrostatic analyzer with two crossed apertures, covering all angles in a 120 deg $\times$ 120 deg field of view for ions with energies ranging from 100 eV to 2 keV. The third instrument is a dust analyzer, which is to measure flux and particle size distribution for all granules <1 μm. It must also sense the original $\pm$ charge state. In total, the payload is expected to occupy $\sim$0.5U.

4.3.2 Communication

The communications subsystem must receive commands and data set from the ground and be able to transmit scientific data and telemetry back to earth. This is particularly crucial during the science phase, in which the data collected by the instruments must be sent back real-time. The link margin must be sufficient for the desired data rate, which is driven by the measurement frequency.

The communications subsystem is also required for Doppler shift ranging, which allows operators to track the spacecraft. "Measurement of the Doppler shift on a spacecraft's coherent downlink carrier allows determination of the line-of-sight component of the spacecraft's velocity. Routine measurement precision is on the order of fractions of a millimeter per second. Ranging tones uplinked and transponded by a spacecraft enable navigators to determine an average distance to and from the spacecraft, with a routine precision of about one meter [10]." Figure 4-8 shows a simple diagram of this technique.

The 34 m subnet of the NASA Deep Space Network (DSN) is to be used with a compact X-band ranging transponder designed to fit aboard a CubeSat.

4.3.3 Physical Configuration

The physical configuration is largely driven by the constraints of the 3U form factor. Although the propulsion system is extraordinarily compact for the performance it delivers, it occupies $\sim$0.5-0.75U. After budgeting for the transponder, payload, and

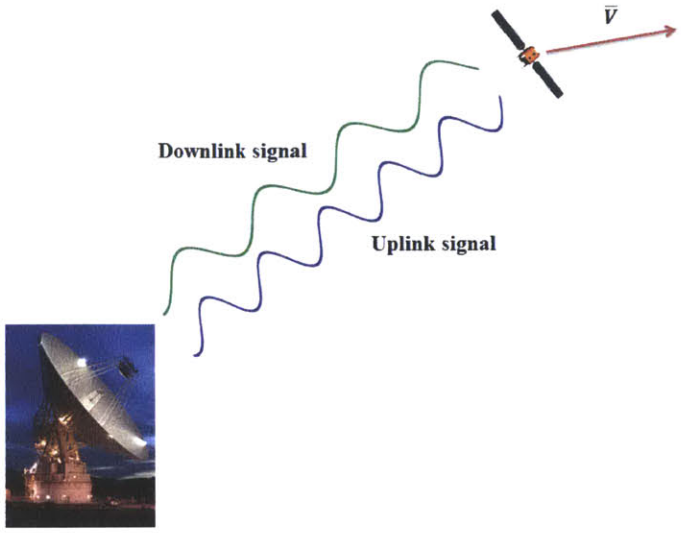

Figure 4-8: Simple diagram showing Doppler shift in the coherent downlink carrier. Making multiple measurements allows for accurate determination of position and velocity.

the rest of the avionics, there is insufficient volume remaining for a 3-axis Reaction Wheel Assembly (RWA). For this reason, the design calls for a thruster-only architecture, where the same type of iEPS thrusters that compose the main engine are used as ADCS actuators.

The main thruster array is located in the center of the spacecraft to ensure that the thrust vector passes through the center of mass, and there is no gimbal mechanism. The attitude control subsystem actuators are placed such that a pure torque about each axis and a pure force along each axis can be achieved. Maximizing the moment arm is also a key consideration. Figure 4-9 shows a CAD drawing of this configuration, which includes double-deployed, body-fixed solar arrays.

The configuration of the flight model may vary, but this provides an excellent starting point for simulation. The bus is designed around the propulsion and ADCS subsystems, which constitute a substantial proportion of the spacecraft mass and volume. Figure 4-10 shows the approximate allocation of resources.

Figure 4-11 shows the body frame of the spacecraft as well as its relationship to the LVLH frame while nadir pointing. The body X-axis is always aligned with the thrust vector.

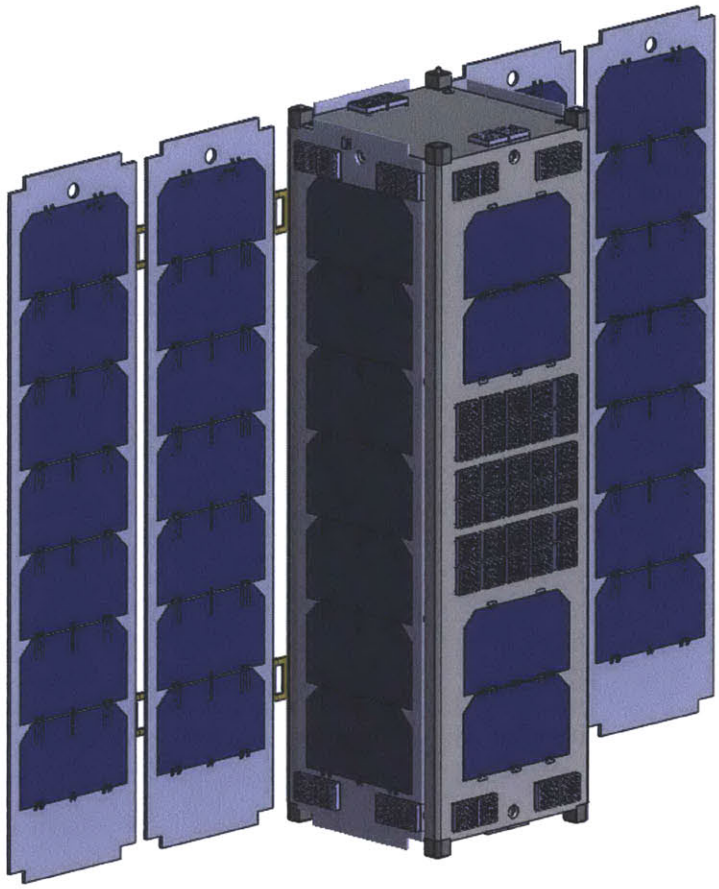

Figure 4-9: CAD drawing of Lunar Impactor.

Because the thrust is so low, the spacecraft spirals out toward the moon. The majority of the thrusting is along the velocity vector to maximize orbital energy gain, meaning the body X-axis is not always directed along the LVLH Y-axis. This is acceptable as long as it does not compromise communications.

4.4 Simulation

Detailed simulation is required to determine whether or not this propulsion architecture is feasible. One of the key concerns is ensuring the ADCS thrusters do not run out of fuel and that they can compensate for disturbances. It is also desirable to give estimates of on/off cycles to aid PPU designers. The simulation must include a model of the spacecraft as well as the model of the flight software containing the GC

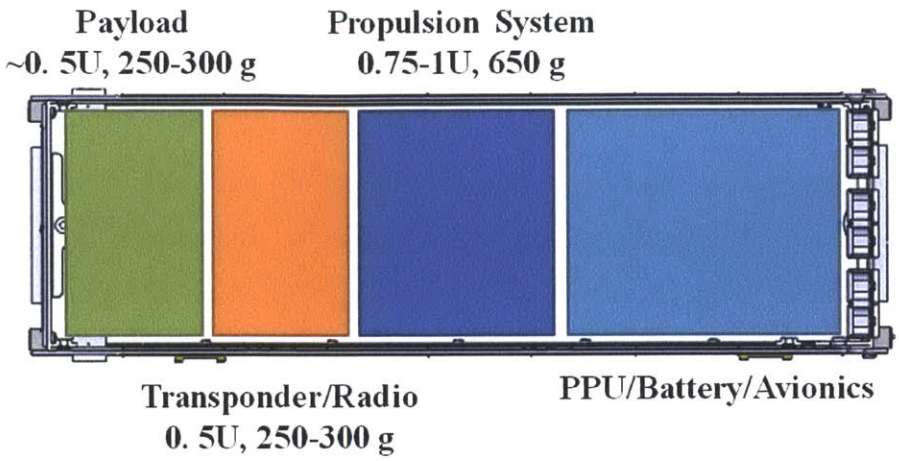

Figure 4-10: Internal layout of Lunar Impactor.

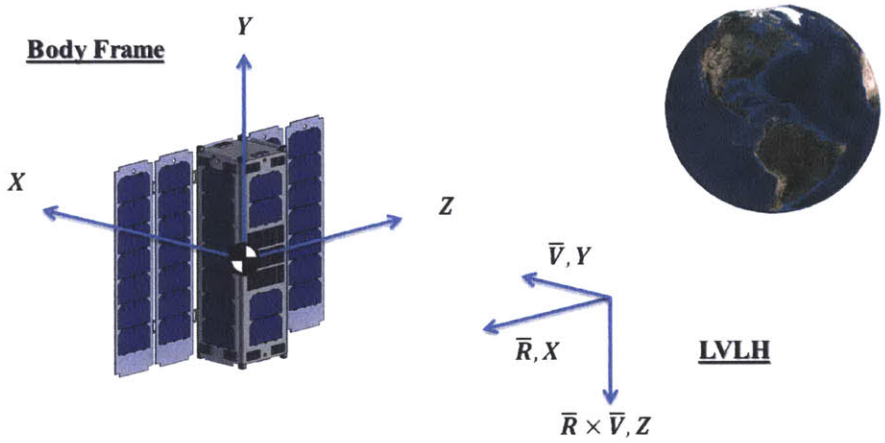

Figure 4-11: The Lunar Impactor body frame and its relationship to the LVLH frame while nadir pointing. This is the orientation during the check-out and science phases.

algorithm discussed in the previous chapter.

4.4.1 Methodology

Thorough testing of the GC algorithm and characterization of the propulsion system requires a six degrees of freedom (6-DOF) simulation incorporating key perturbative forces. Anything less gives an incomplete picture and leaves many important questions unanswered. The computational power of modern processors makes numerical simulation an attractive prospect, particularly considering the duration of low-thrust

lunar missions. The simulation was developed by leveraging and customizing the framework available at Charles Stark Draper Laboratory (CSDL).

Choice of simulation environment and architecture is critical. It must be flexible, and it is preferred that the source code is visible and editable. Systems Tool Kit includes very capable analysis packages, but the underlying code is hidden. Furthermore, it is difficult to inter-operate with MATrix LABoratory (MATLAB) and other tools.

Given the ubiquity of MATLAB and SimuLink as well as the extensive code libraries available, this is the preferred choice. The lunar spacecraft simulation (LunarSim) used for the Orion program incorporates the key elements required of this task, including a reaction control subsystem model, a main engine model, and the option to include third body gravitational forces as well as higher-order Earth gravity models. It is constructed in SimuLink and re-worked to model Lunar Impactor.

4.4.2 Architecture

Figure 4-12 shows a diagram of the simulation architecture. The spacecraft model includes each actuator and the dynamics of the simulated environment, and the flight software (FSW) computes the commands. The FSW does not encompass all Command and Data Handling (CDH) modes; it only includes the GC algorithm.

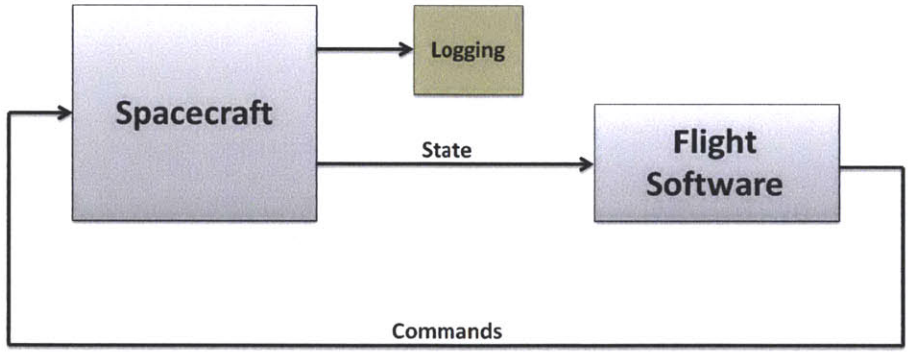

Figure 4-12: Diagram of the simulation.

It is important to select reasonable simulation parameters; this allows for an accurate representation of the actual dynamics and behavior of the spacecraft. Table

4.3 describes several of the most important quantities.

Table 4.3: Simulation Parameters

Item	Description
Propagation	Runge-Kutta 4 (RK4) numerical integration
Simulation step size	0.025 sec
Control cycle	5 Hz
Ephemerides	Tables generated by Spacecraft Planet Instrument C-matrix Events (SPICE); 600 second interval
Epoch	J2000

Synchronizing ephemerides is very important (especially accounting for leap seconds), and LunarSim uses the J2000 epoch. Trajectories must be designed with the same standard.

Spacecraft

The physical configuration displayed in Figure 4-9 is modeled in the simulation. The location and thrust direction for all 20 ADCS jets and the main engine, the mass properties, the propellant properties, start-up and shut-down transients, and the rest of the relevant parameters are specified [32]. Figure 4-13 shows a diagram of the spacecraft model.

The model sums the forces and torques due to the environment (gravity and other perturbations) and those exerted by the actuators and uses an RK4 numerical integrator to propagate the rotational and translational state forward one time step. The sensor models simply pass the state through (perfect navigation), but this is where realistic models can be included. There is no mass decrementing, center of mass (CoM) translation, or moment of inertia (MoI) changes in the simulation, but this capability can be built in.

Flight Software

The flight software is the implementation of the GC algorithm discussed in Chapter 3 and is represented in Figure 3-2.

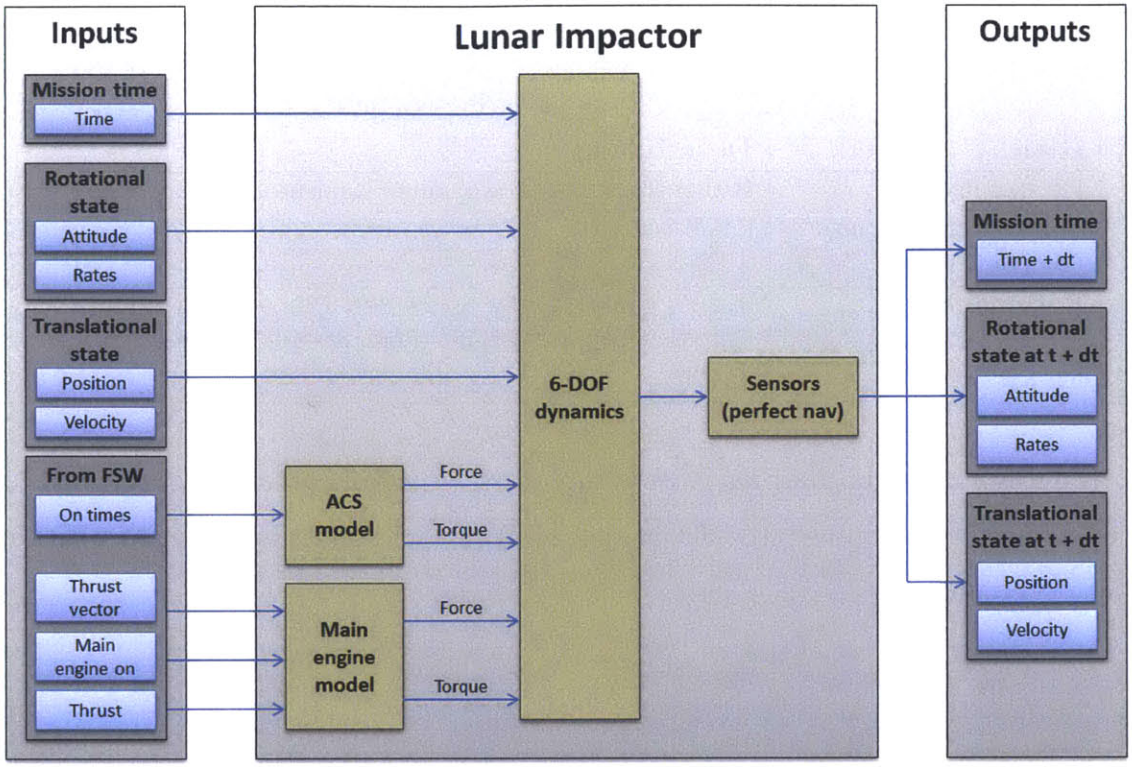

Figure 4-13: Diagram of the spacecraft model.

4.5 Trajectory Design, Guidance, Navigation, and Control

The GC algorithm is transformed into a practical piece of software and tested in the simulation to assure full functionality; many of the relevant considerations are described and the components not explicitly included in the simulation are discussed.

4.5.1 Trajectory Design

To test and evaluate the GC algorithm, trajectories from GEO to Reiner Gamma must be designed. Several low-thrust trajectory design programs exist, but the package of choice is the Astrogator module of Systems Tool Kit (STK) v10.0. Some of the most important assumptions used are listed in Table 4.4.

In the design process, two primary strategies emerge. The first is a direct ascent,

Table 4.4: Trajectory Design Assumptions

Spacecraft	Total mass	5 kg
	Fuel	EMI-BF_4 with 1.24 g/cc density
	Mass decrementing	None
	Main engine	Thrust = 0.0016 N and I_{sp} = 2500 sec
Attitude	Coast	LVLH hold
	Primary thrust	Velocity direction of Earth velocity, normal, co-normal (VNC) frame
	Correction burns	Thrust vector in Earth VNC frame
Propagator	Integrator	RK4
	Step size	100 sec
	Perturbations	Sun, moon, and J_2

which consists of a low-thrust spiral along the equatorial plane that is timed to intersect the moon. It is the fastest option and an excellent alternative if propulsive capability is lost en-route, but the incidence angle is very poor. The second strategy is executing a lunar swing-by to change the plane and increase the orbital energy of the spacecraft before it makes its final approach. This results in a longer mission duration but favorable incidence angles.

Direct Ascent

The direct ascent is designed to be simple. The spacecraft starts in GEO and executes a long primary burn continuously aligned with the orbital velocity vector. There is no plane change maneuver; the timing is chosen such that the spacecraft arrives as the moon passes its ascending node. A shorter correction burn after the primary orbit-raising maneuver is used to put the spacecraft on the proper course to Reiner Gamma. Figure 4-14 shows these phases.

The parameters for the second burn are altered by the differential corrector algorithm until the terminal position is the intended impact point. The final approach is coasting; this leaves margin for unanticipated correction burns or an extended science phase. This is depicted in Figure 4-15.

Table 4.5 summarizes important data for this trajectory. Of particular importance are the total mission time and the terminal flight path angle.

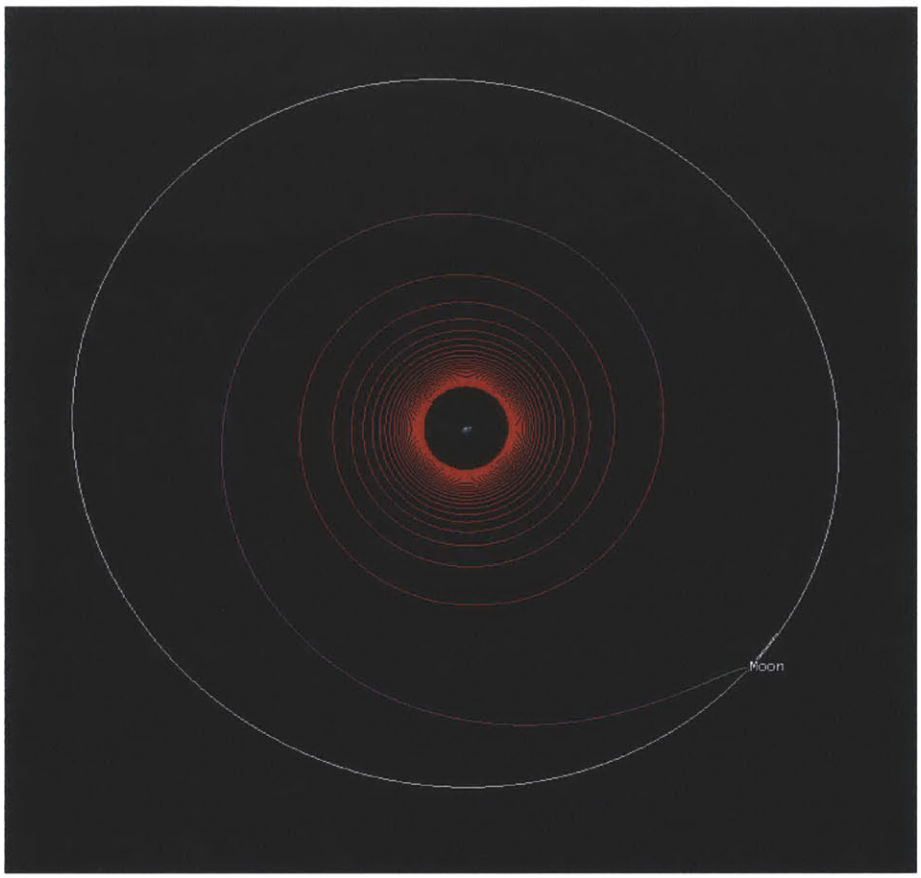

Figure 4-14: Direct impact trajectory. Red and purple denote thrust arcs and green denotes coasting.

The total mission time is low, which is a major benefit considering the harsh radiation environment outside the magnetosphere. Radiation hardening and shielding is not a possibility for every component, so minimizing total time to target is perhaps the best means to ensure maximum probability of success. The terminal flight path angle is not very favorable; it is far lower than the floor value of -21.3 deg, meaning it would not yield the desired scientific return. It is very difficult to design direct ascent trajectories with final conditions that fall within requirements; the approach velocity is not high enough to come in with a low angle.

Lunar Swing-by

Back propagation is an excellent strategy to determine the geometric setup and intervening propulsive maneuvers required to achieve a viable approach. Beginning with

Figure 4-15: Final approach and impact at Reiner Gamma.

Table 4.5: Direct Ascent Trajectory Data

Item	**Value**
ΔV (km/sec)	1.977
Total mission time (days)	72.132
Total thrusting time (days)	71.5
Terminal flight path angle (deg)	-49.240
Propellant used (g, I_{sp} = 2500 sec)	387

the desired impact point, the incoming flight path angle, terminal velocity magnitude, and azimuth are varied. The spacecraft is propagated backward to determine the feasibility of each option, most of which result in the spacecraft descending from lunar orbit or coming in from interplanetary space as seen in Figure 4-16.

Back propagation yields important information, namely that the spacecraft must have a higher incoming velocity than is usual for a direct impact trajectory. An excellent way to attain this energy is performing a lunar swing-by. The spacecraft can achieve the proper setup with approximately the same time and propellant as the direct ascent, and after that point only small correction maneuvers are required to tailor the flight path. Figure 4-17 depicts one such trajectory, which is designed to exceed the floor value of -21.3 deg. Table 4.6 summarizes the important data for

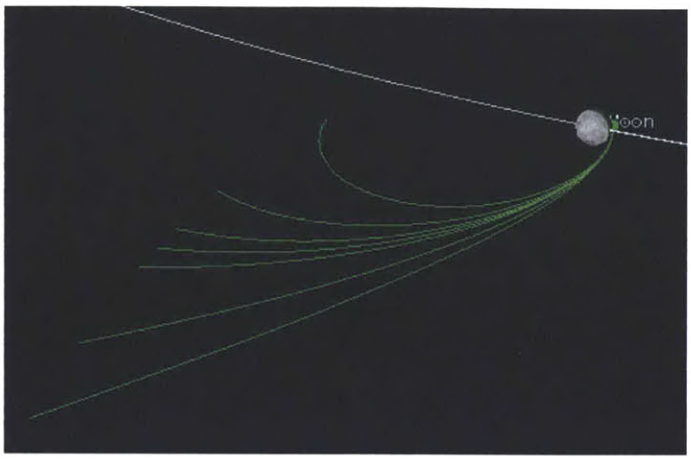

Figure 4-16: Search of the design space using back propagation from desired terminal state.

this trajectory.

Table 4.6: Lunar Swing-by Trajectory Data

Item	**Value**
ΔV (km/sec)	1.903
Total mission time (days)	124.972
Total thrusting time (days)	69.821
Terminal flight path angle (deg)	-19.645
Propellant used (g, I_{sp} = 2500 sec)	373

The low-thrust spiral is nearly identical to that in the direct impact trajectory, and the propellant consumption is slightly lower. The primary trade is flight time; proper phasing after the swing-by requires $\sim$1.5 lunar periods.

It is important to run the simulation for both scenarios; it is a possibility that the direct impact can be used as a contingency plan for the lunar swing-by should issues arise during flight. After each trajectory is designed, a table is produced that lists the spacecraft position and velocity at a uniform time interval. This path is what the spacecraft follows.

4.5.2 Guidance

The guidance routine computes the burns required to keep the spacecraft on the proper trajectory. An on-board targeting function designed to autonomously re-

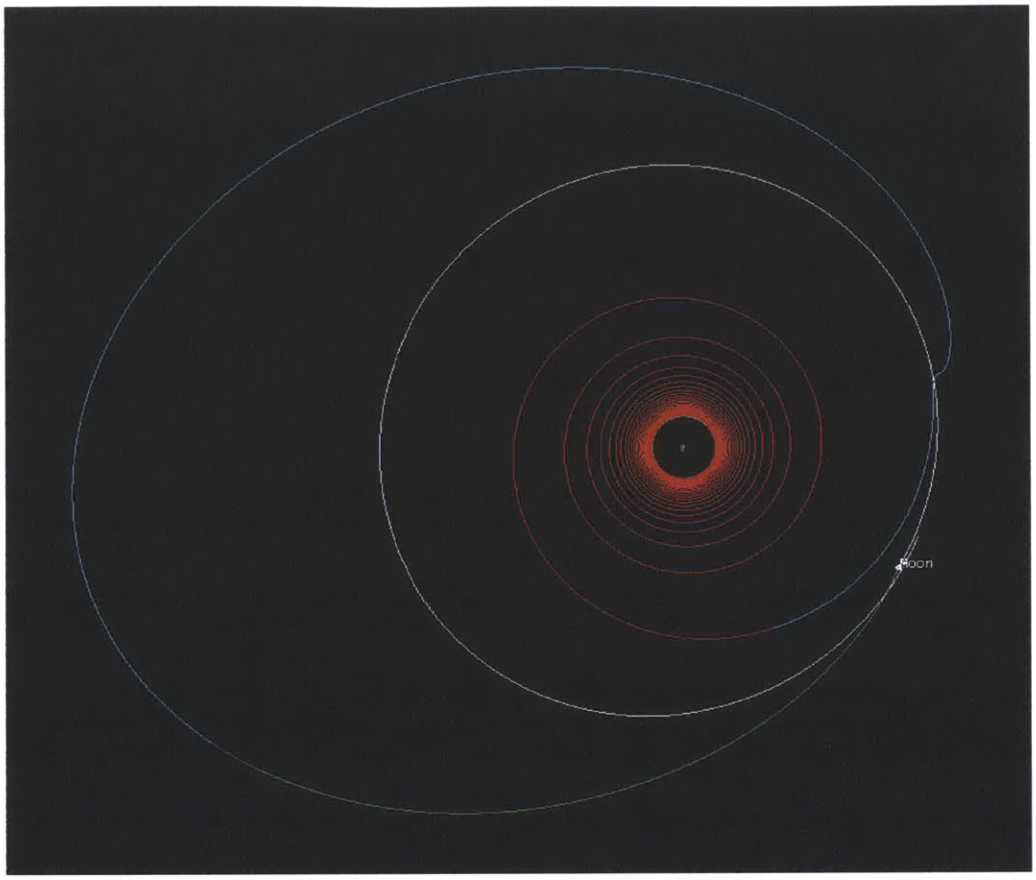

Figure 4-17: Employing lunar swing-by to gain energy. The orbital inclination is also changed, which assists in setting up the final approach. Red and purple represent maneuvers while all other colors represent coasting.

compute the trajectory would potentially supersede the "a priori" nominal trajectory previously designed.

Guidance Parameters

As discussed in Chapter 3, the various parameters must be set properly. This requires a series of tests to determine reasonable trade-offs. First, the simulation was run for short segments at GEO assuming 2-body conditions to ascertain the accuracy required to assure the spacecraft remains on course. Table 4.7 shows the position and velocity requirements. When sun, moon, and J_2 perturbations were incorporated, it was generally found that long-term trajectory following was successful should these requirements be met.

Table 4.7: Required Accuracy

Item	Requirement
Position error at t_{n+1}	<1 m/sec
Velocity error at t_{n+1}	<0.001 m/sec

The update rate for the controls is 0.2 Hz, meaning the solution is re-computed every 5 seconds. Lower rates result in excessive divergence from the desired state while higher rates do not greatly improve accuracy. The prediction horizon is 10 minutes (spacing between trajectory data points); this aligns with the requirement that $t_{n-1} - t_n \ll period$. Larger spacing demands more computational resources (particularly when performing the pseudoinversion) while smaller spacing requires more memory to hold the data points, and 10 minutes is a reasonable compromise. The control solution is held (no re-computes) when the prediction horizon falls below 2.5 minutes as the solutions tend to become erratic when the spacecraft nears its objective. This parameter more than the others affects terminal accuracy.

Figure 4-18 shows the course of the spacecraft during a nominal segment of its flight at geostationary altitude in the relative coordinate frame. It begins at the origin and moves to the right toward its objective, the small circle. The blue lines denote the desired trajectories (course prescribed by the re-computed burns). The spacecraft is not able to follow each new path perfectly because of its slow response, but it ultimately ends up very near its objective.

4.5.3 Navigation

Perfect navigation is assumed in the simulation, meaning the state estimate is equivalent to the actual state. This does not limit the overall architecture as sensor models and a navigation routine can be built into the spacecraft model. It is designed to include this functionality.

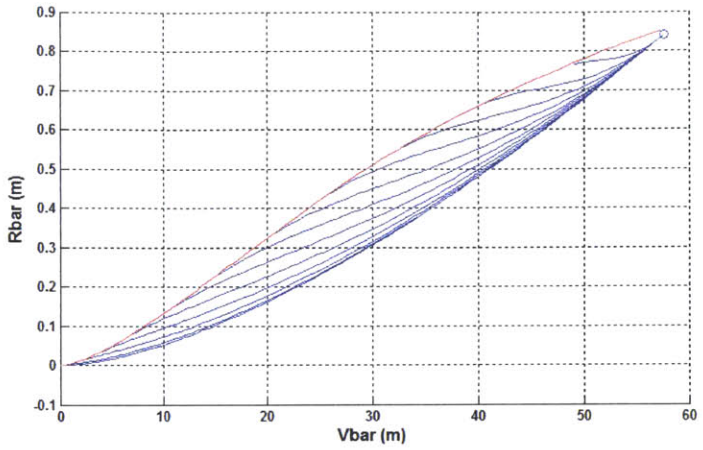

Figure 4-18: The spacecraft trajectory is denoted by the red line while the desired trajectories are shown in blue. The re-computed trajectories are shown at 50-second intervals to display the functionality of the guidance routine as the spacecraft nears its destination (the blue circle).

Sensors

Attitude and rate measurements must be made continuously. Precision pointing knowledge requires at least one star tracker. Sun sensors are desirable but not essential as the solar arrays can provide a rough approximation of the sun angle. An IMU measures attitude rates, and the signals are processed to yield a rotational state estimate. This can be combined with the main engine current measurements (which can be translated into thrust) to provide position and velocity estimates.

Translational State Estimation

The spacecraft state estimate diverges from the actual state over time, so its position and velocity must be determined from the ground. The differences between the actual and intended flight path, the residuals, are computed using Doppler shift ranging and uplinked to the spacecraft. A miniaturized X-band transponder is the hardware required on the spacecraft end to do so, and the technology is in development [21].

4.5.4 Control

The control system is responsible for computing the thrust magnitude for the main engine. It is determined using the control solution u, which represents the instantaneous ΔV required for that 5-second segment of flight. First, compute the magnitude of the maneuver.

$$u = \begin{bmatrix} u_x \\ u_y \\ u_z \end{bmatrix} \qquad |u| = \sqrt{u_x^2 + u_y^2 + u_z^2} \tag{4.1}$$

Next, re-arrange the rocket equation to solve for the spacecraft mass after the maneuver.

$$\frac{m_i}{e^{\frac{\Delta V}{I_{sp} g_0}}} = m_f \tag{4.2}$$

Compute the required constant mass flow rate to achieve the difference.

$$\frac{m_i - m_f}{t} = \dot{m} \tag{4.3}$$

Finally, calculate the thrust required to achieve this mass flow rate assuming a constant exhaust velocity.

$$T = \dot{m}c \tag{4.4}$$

The main engine is then commanded to fire with this thrust.

Simultaneously, the ADCS is commanded to align the +X axis of the body frame with the direction of the maneuver u. This cannot be accomplished instantaneously of course, but the change from the previous vector is small enough such that there are no significant errors induced. It is not perfect, but this is after all an approximation of continuous thrusting.

Control Parameters

It is assumed that each ADCS thruster fires with a constant thrust of 20 μN and achieves this thrust instantaneously. The actual latency is on the order of 3-5 ms, but this does not make a notable difference. Electrospray thrusters have minimal start-up transients; current levels typically rise over a sub-millisecond time scale. Overshoot is nearly non-existent at lower power levels (intended operating regime) and is well understood for higher levels. It is not necessary to model these behaviors in detail at this point [20].

4.6 Results and Analysis

Thoroughly demonstrating the reliability of the GC algorithm and the ability of iEPS to perform this mission requires examination of each phase. Of particular emphasis is the behavior of the spacecraft and the quantity of consumables expended to execute the commands.

4.6.1 De-tumble and Sun-tracking

After separation from the deployment module, the ADCS is activated. The spacecraft fires its thrusters to null the rates, and when they are sufficiently low, it slews to face the sun and charge its batteries. Figure 4-19 shows the Euler angles and angular rates during the de-tumble phase.

The only limiting factor for de-tumble time is battery life; the power balance must be positive before energy levels drop too far. The ADCS exhibits favorable performance on-par with expectations.

4.6.2 Check-out Phase

The check-out phase begins with a transition from sun pointing to nadir pointing, which requires a slew and hold. Figure 4-20 shows this maneuver, which is an essential capability.

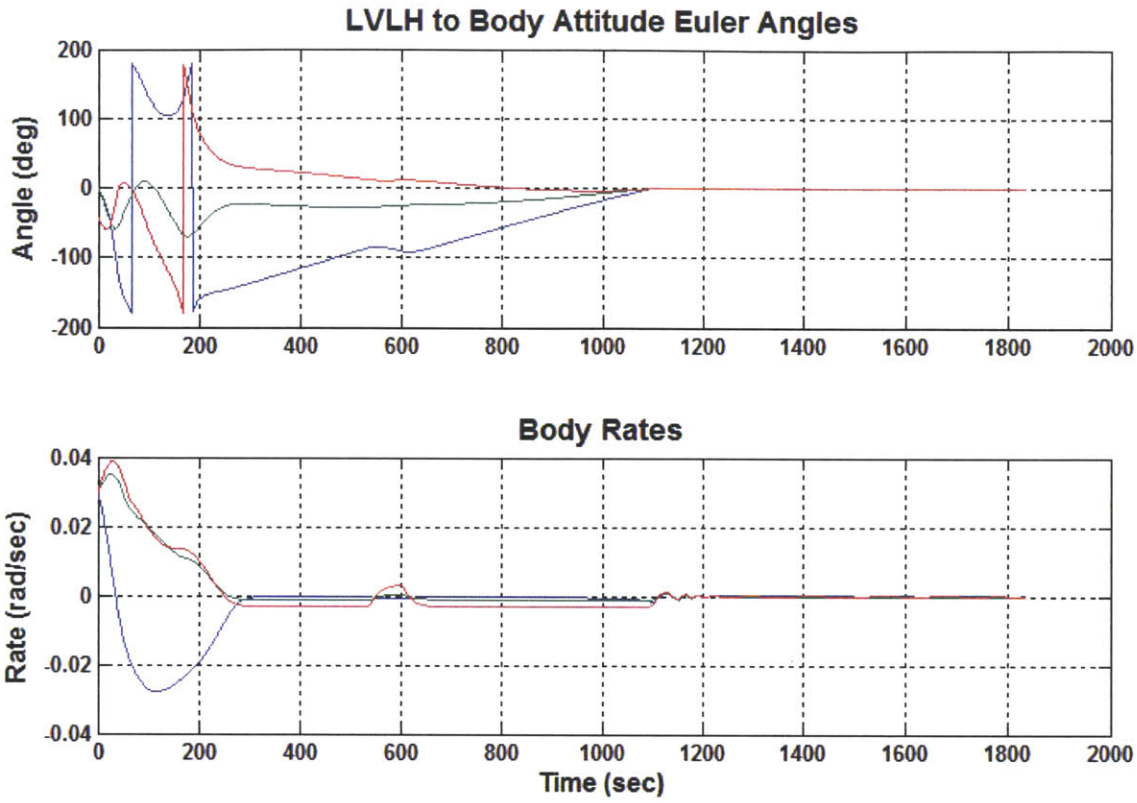

Figure 4-19: Euler angles and angular rates during the de-tumble phase.

The ADCS performs the maneuver favorably and holds the commanded attitude precisely. After this is verified on the ground, the other subsystems are powered up and diagnostic tests begin. Perhaps the most crucial is firing the main engine and determining whether or not there is any thrust misalignment or asymmetry; if the error is serious enough, a mitigation strategy must be devised and implemented. It is advisable to budget several days for this process to allow ample time to perform such tests.

4.6.3 Transit Phase

The GC algorithm commands the spacecraft during this phase, following the trajectory until its termination at impact. The overarching goal is to land within the 2 km ellipse described in the mission requirements, but it is important to determine the propellant consumption required to do so. Both the direct ascent and lunar swing-by

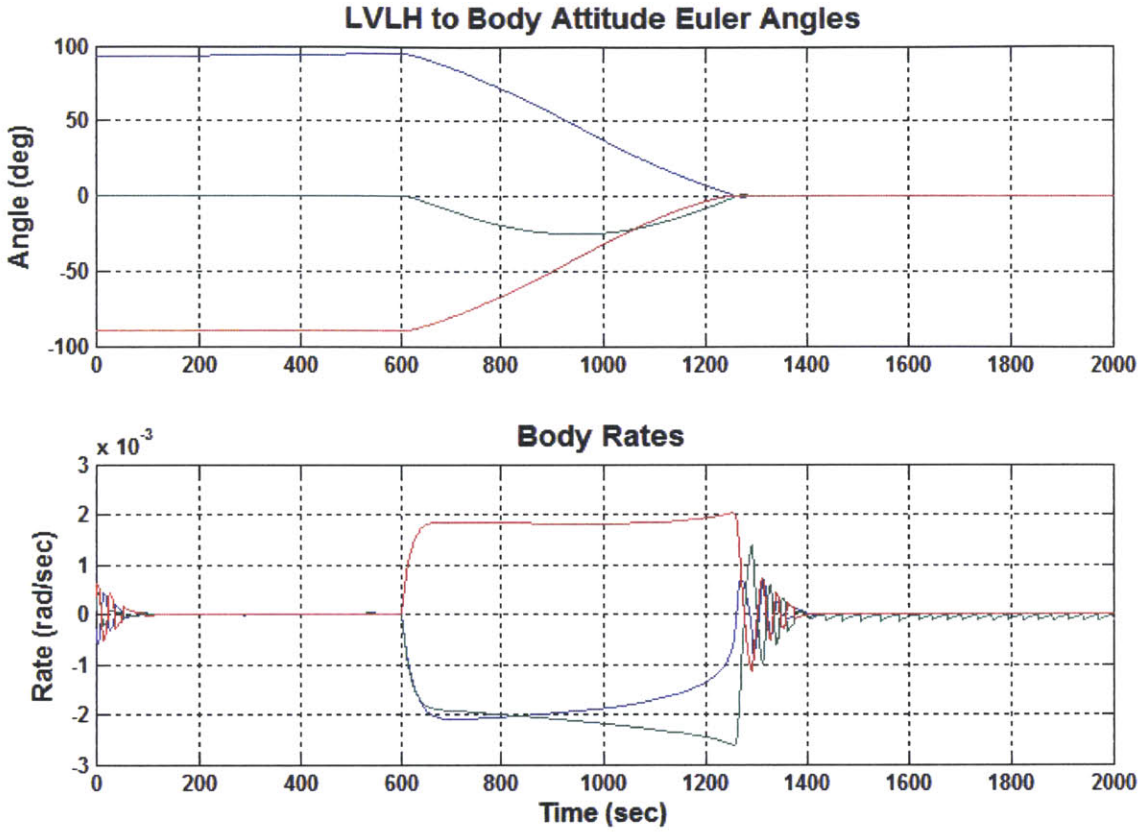

Figure 4-20: Slew and hold maneuver.

cases are simulated.

Direct Ascent

The direct ascent is an excellent first test case as it is relatively simple. There are few transitions, and little time is spent within the lunar sphere of influence. Figure 4-21 shows the trajectory with several key points labeled.

Lunar Impactor exhibits stable flight throughout the course of its journey. The LVLH to body Euler angles are graphed along with the body rates and the magnitude of deviation from the reference trajectory in Figure 4-22. The purpose for plotting the LVLH to body angles is to examine the roll, pitch, and yaw of the spacecraft relative to its nadir-pointing alignment, which is the default during all coasting phases. This gives an intuitive representation of stability and orientation in flight, which is useful for quickly evaluating the best location for antennae and other hardware.

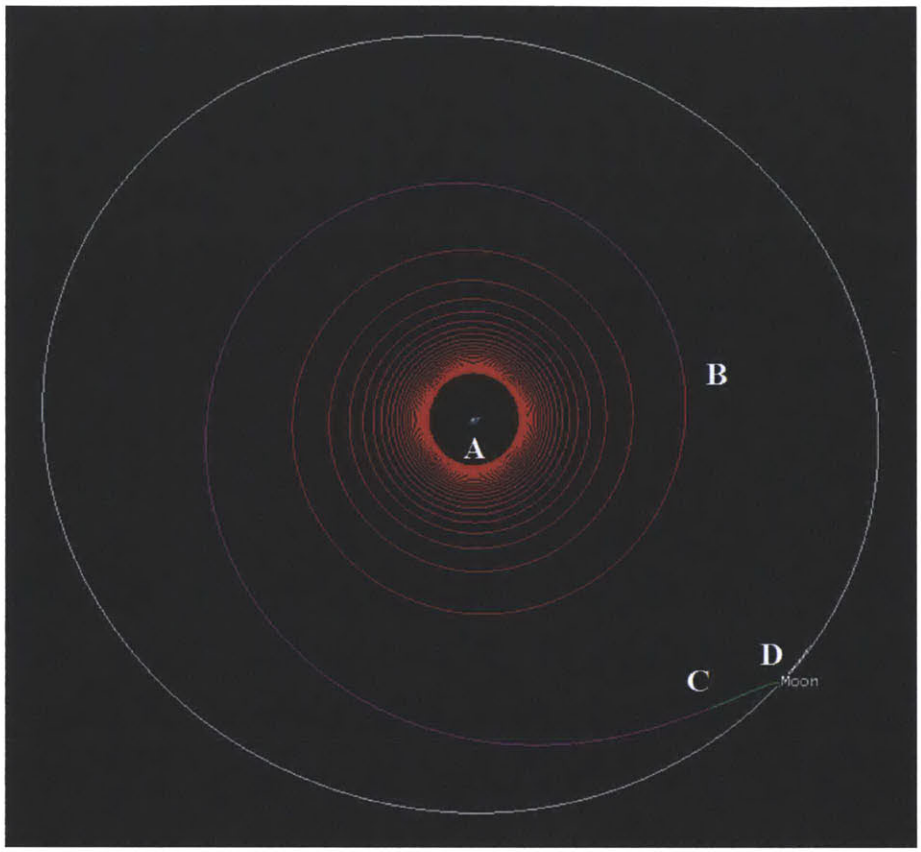

Figure 4-21: The labeled points correspond with those in the subsequent figures. A: Start B: Transition to different thrust vector (correction maneuver) C: Begin final coast D: Lunar impact.

Flight is very stable and smooth for the duration of the primary maneuver (point A to B), which is designed such that the spacecraft continuously thrusts along its velocity vector. As expected, the pitch angle slowly increases as the orbit becomes larger and more eccentric. The slow oscillations which decrease in frequency are due to lunar gravity; as the orbital period increases, the changes occur less frequently. Point B marks the transition to a 12 day maneuver designed to inject the spacecraft on its final trajectory, and the increase in rates due to the slew maneuver is evident in the second plot. The LVLH-relative roll and pitch angles change as the maneuver progresses. At point C, the main engines cut out and the spacecraft assumes a nadir-pointing orientation. The rates increase again with this slew maneuver. The spacecraft coasts the final day until it reaches its impact point, and the ADCS thrusters perform all commanded translations in addition to maintaining pointing. This results in a very

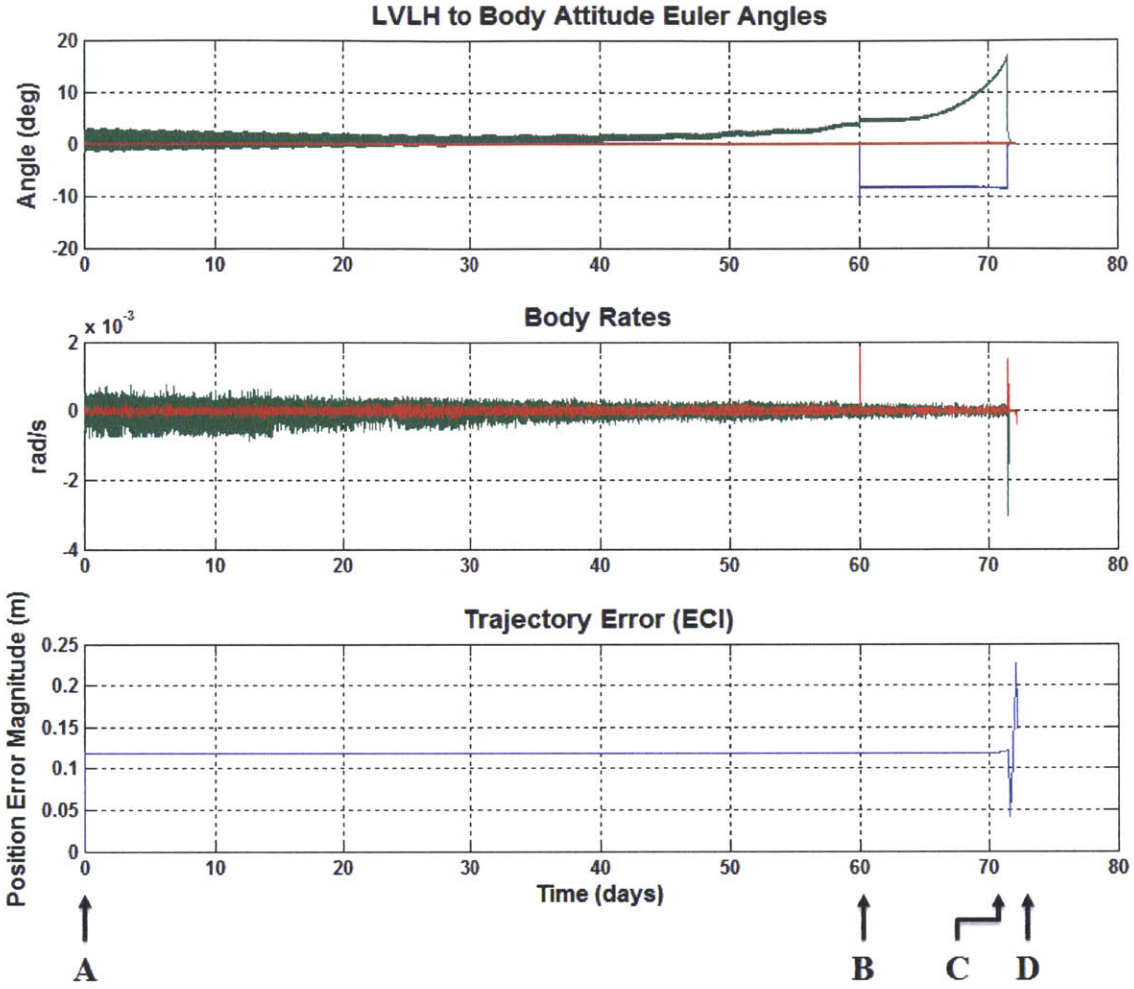

Figure 4-22: Results from the direct impact trajectory simulation. Blue represents roll (body X-axis), green represents pitch (Y-axis), and red represents yaw (Z-axis).

favorable terminal accuracy well within the requirements. The final 100 minutes of data are plotted in Figure 4-23 to show the behavior leading up to impact.

The angles and angular rates remain nominal, and the only feature of consequence is the decrease in trajectory error. This is due to an intentional decrease in the step size (5 sec to 0.2 sec) for the numerical integrator that predicts the state at X_{n+1} without thrusting. This is desirable within the lunar sphere of influence to accurately model motion.

Next, the fuel expenditures to perform these maneuvers and maintain pointing must be quantified. Figure 4-24 shows the cumulative total consumed by the ADCS

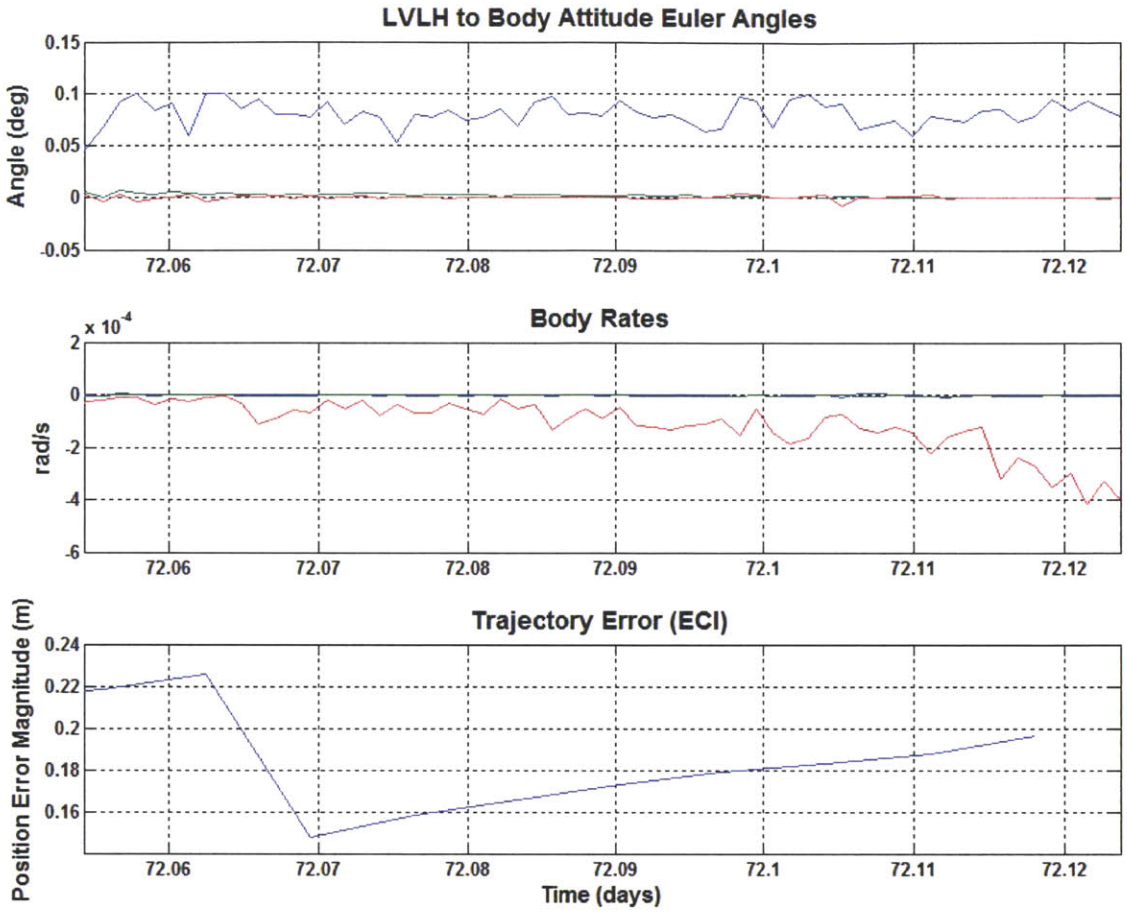

Figure 4-23: Last 100 minutes of direct impact trajectory simulation. Blue represents roll (body X-axis), green represents pitch (Y-axis), and red represents yaw (Z-axis).

thrusters as well as the main engine, which is logged in the simulation.

The 20 ADCS thrusters consume a total of 7 grams of propellant (~0.35 g/thruster), which is very favorable. The small spike at the end reflects the increase in translational corrections required near the moon, which makes sense considering the por fidelity of the lunar gravity model. The iEPS v2 tank stores ~1 gram, which would be more than sufficient to meet requirements and provide a large safety margin. The main engine consumes approximately 400 grams; this figure is important for sizing the propellant tank.

Quantifying the start/stop cycles for the ADCS thrusters is valuable for PPU designers as it gives a rough idea of the demand placed on the electronic components. Estimates for cycles per second come from examination of the thruster on-times during

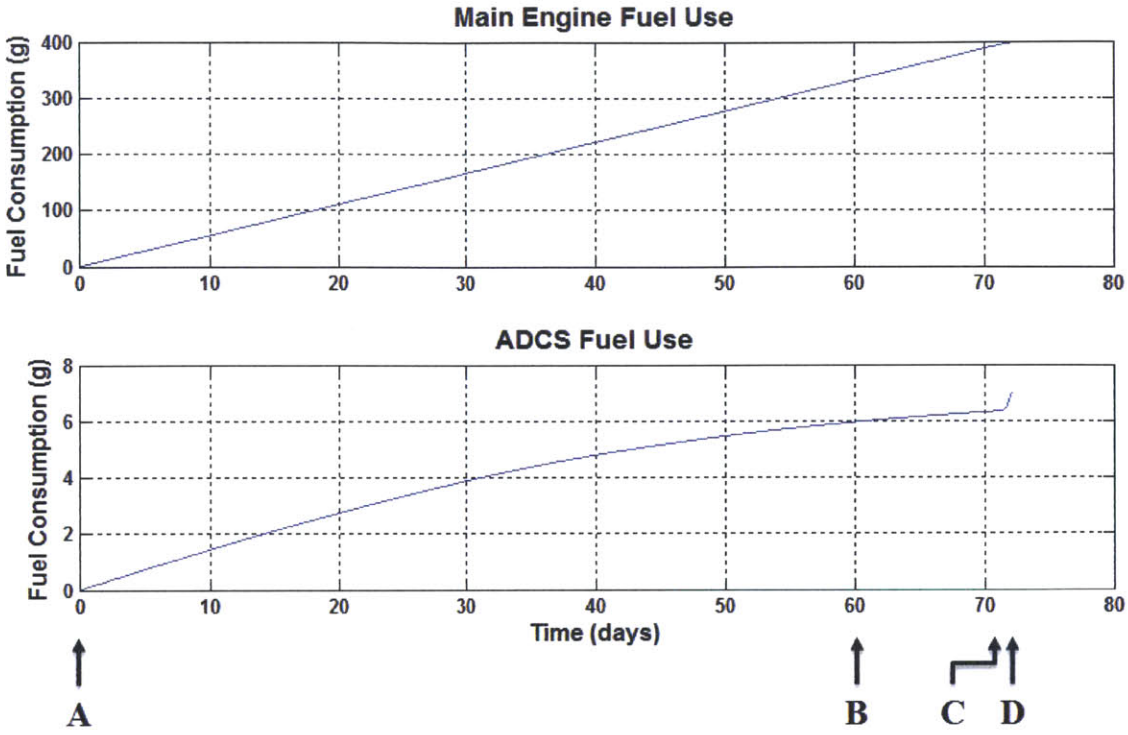

Figure 4-24: Results from the direct impact simulation; the values represent total fuel used.

nominal flight. The total is ~280,000 cycles; this is only an order-of-magnitude approximation.

Lunar Swing-by

The lunar swing-by trajectory is a more rigorous test for the algorithm. The mission is longer, the incidence angle is much lower, and there are more transitions. It is important to ensure favorable performance since this may be the only feasible way to ensure the impact angle requirements are met. Figure 4-25 shows the trajectory with key points labeled.

Lunar Impactor exhibits stable flight throughout transit and successfully reaches its target. The data in Figure 4-26 yields important insights into trajectory following with a lunar swing-by and conducting shorter mid-course correction burns.

The primary burn from point A to B looks nearly identical to that in the direct ascent trajectory as it is designed with the same parameters. The pitch angle slowly

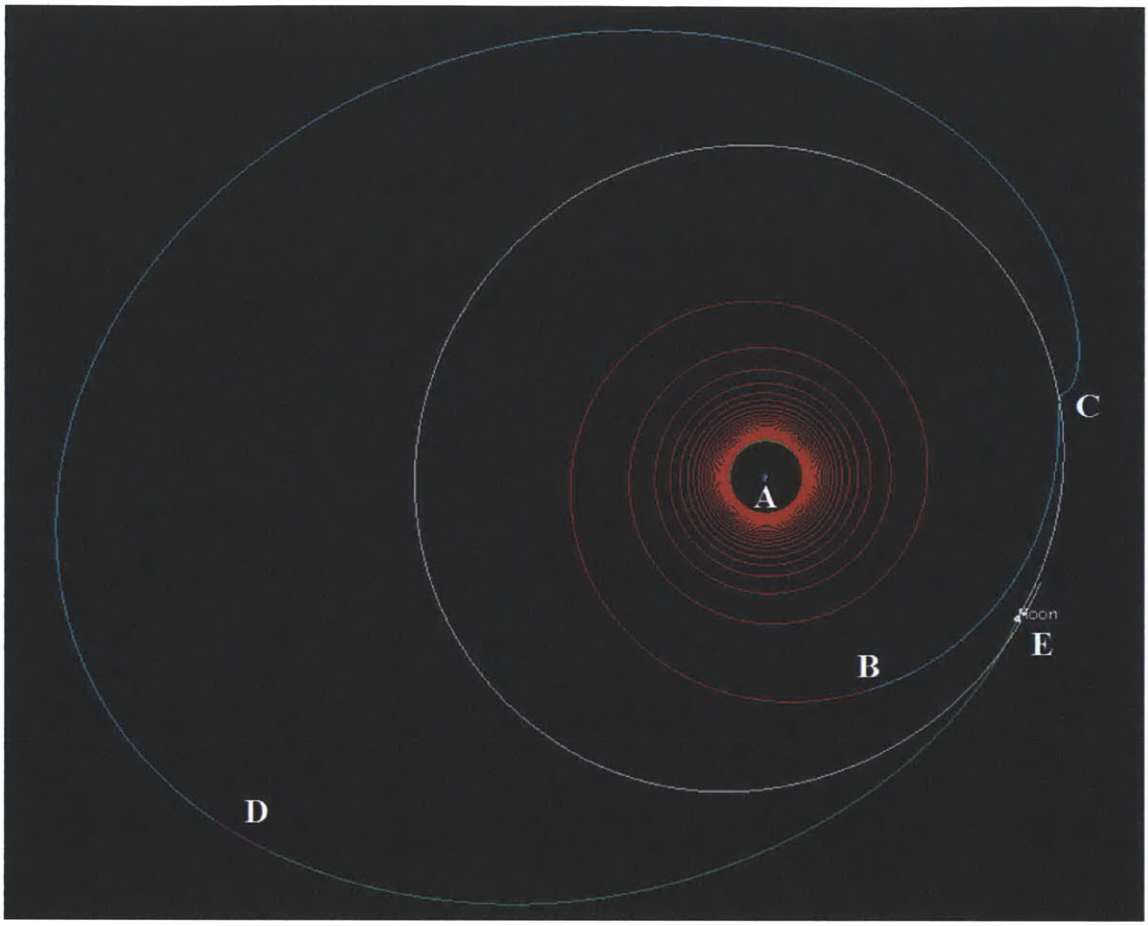

Figure 4-25: The labeled points correspond with those in the preceding figures. A: Start B: Begin coast C: Lunar swing-by D: Correction burn E: Lunar impact.

increases as the eccentricity of the orbit grows, and deviation from the intended trajectory remains below 0.1 m. At point B, the main engine cuts out; the spacecraft then assumes a nadir-pointing orientation. The ADCS thrusters keep it on course during the lengthy coast period.

Point C is the perilune, the closest Lunar Impactor gets to the moon during the swing-by, and there is a noticeable spike in position error (over 2 orders of magnitude greater than nominal levels). This is attributed to inaccuracy in the prediction of the final state without thrusting X_{n+1}; the numerical integrator step size is too large to provide an accurate enough solution at this distance from the moon. This is the same parameter adjusted in the terminal segment of the direct impact trajectory, and the reason is the same. Changing this value based on range from forcing bodies is an

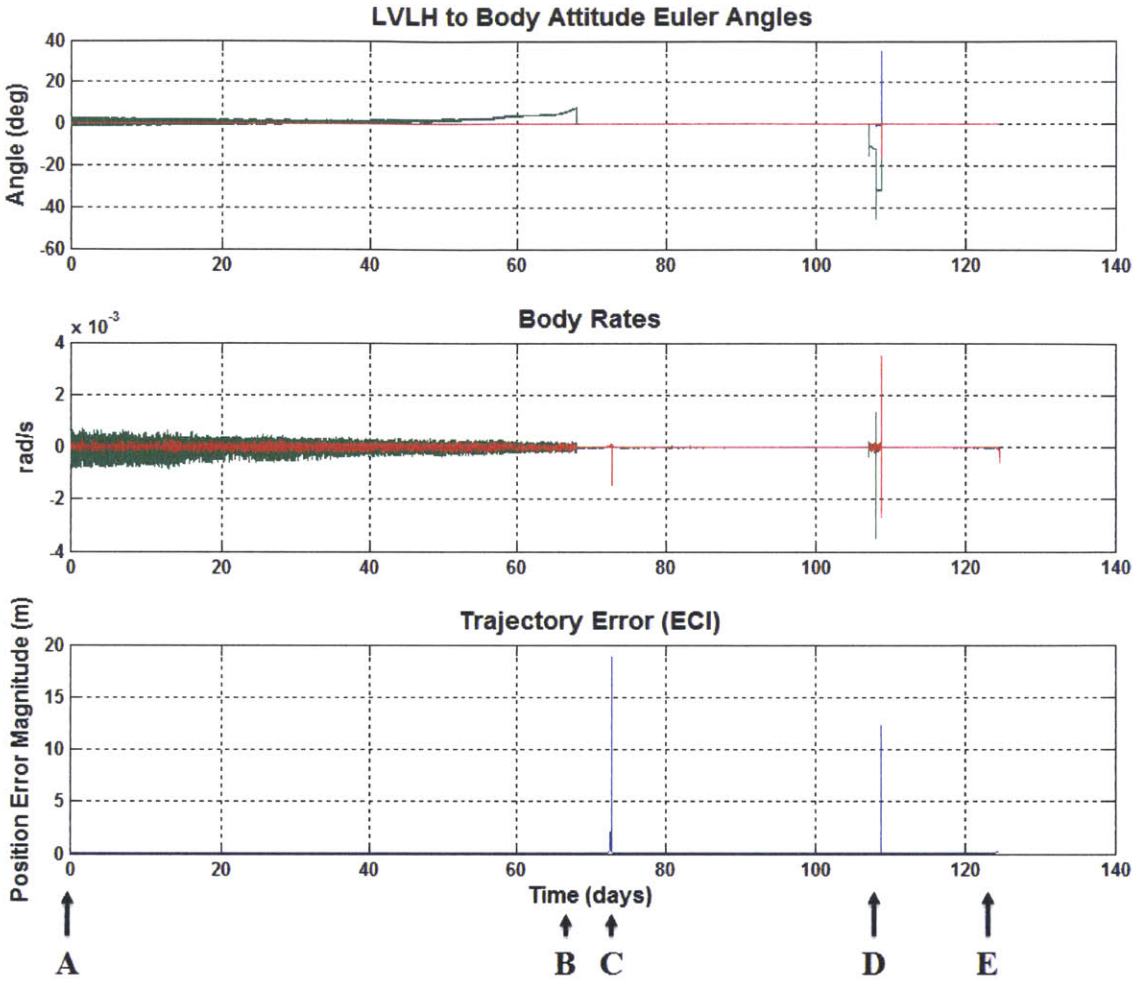

Figure 4-26: Results from lunar swing-by simulation. Blue represents roll (body X-axis), green represents pitch (Y-axis), and red represents yaw (Z-axis).

advisable update for future development of the algorithm. This deviation also shows the ability of the spacecraft to get back on track; the error is reduced to nominal levels.

Point D marks the beginning of two "short" correction burns (totaling approximately 1.6 days). The Euler angle plot shows the change in LVLH-relative attitude during the maneuvers, and the body rate plot shows the spikes marking the slew maneuvers required to transition to each new orientation. At the end of the second maneuver, the spacecraft deviates from its intended course. The errors are corrected as before, but their presence highlights another concern. The spacecraft does not

slew to the required maneuver attitude before the burn begins. Thrust magnitude and orientation are commanded simultaneously, and if there is a pointing discrepancy, it takes time to slew (100-300 seconds for large changes). This is not an issue during the course of maneuvers as the changes are so small; however, deviations can occur during transitions. The fix is straightforward; estimate the maneuver in advance and align the spacecraft with the initial thrust vector before firing commences.

Point E marks the final descent and impact. The final 100 minutes of data are plotted in Figure 4-27 to show the behavior in greater detail. The drop in error is due to the same adjustment in the step size of the numerical integrator detailed in the previous section. Prudent selection of this parameter allows for accurate trajectory following all the way to the lunar surface. The final error lies well within the requirements.

ADCS fuel expenditures are greater for this profile as expected, and Figure 4-28 shows the total consumption. Main engine expenditure is slightly less than that for the direct impact trajectory because of the lunar swing-by, but the ADCS thrusters consume more. The periods of rapid increase in total consumption for the ADCS thrusters align precisely with the spikes in trajectory error; additional fuel is required to get back on course.

The start/stop cycle estimates are based on the same assumptions detailed before. The total for the lunar swing-by trajectory is ~300,000 cycles.

Higher Order Perturbations

It is important to investigate whether or not the spacecraft can follow a trajectory designed using different assumptions, particularly which perturbations are included. Solar radiation pressure (SRP) is the most notable force not modeled in LunarSim. To answer this question, the direct impact trajectory was re-designed including SRP and high-fidelity gravity models. Table 4.8 lists the important parameters.

The key is determining whether or not the plant model used in LunarSim is detailed enough. Figure 4-29 shows the results from this test, and the only difference from the original direct impact fly-out is the reduced terminal accuracy. This makes

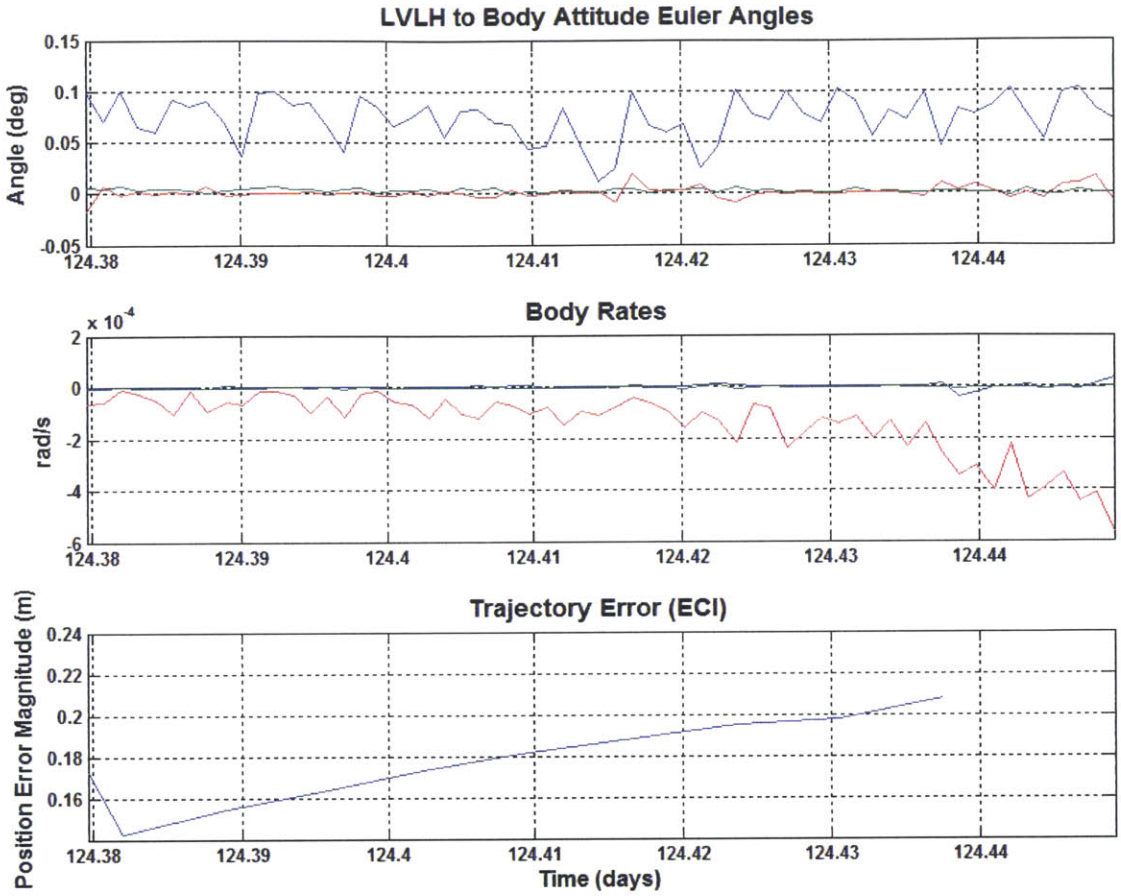

Figure 4-27: Last 100 minutes of lunar swing-by simulation. Blue represents roll (body X-axis), green represents pitch (Y-axis), and red represents yaw (Z-axis).

sense as the gravitational field of the moon is relatively uneven; the plant model cannot predict motion close to the moon as accurately.

Fuel consumption for the ADCS thrusters is only slightly higher (~0.1-0.2 g) as shown in Figure 4-30.

What these results convey is that the plant model is accurate enough for cis-lunar flight and impact trajectories. Increasing the fidelity of the lunar gravity model increases terminal accuracy, but this improvement may not be necessary. This must be evaluated further once the navigation routine is incorporated into the simulation.

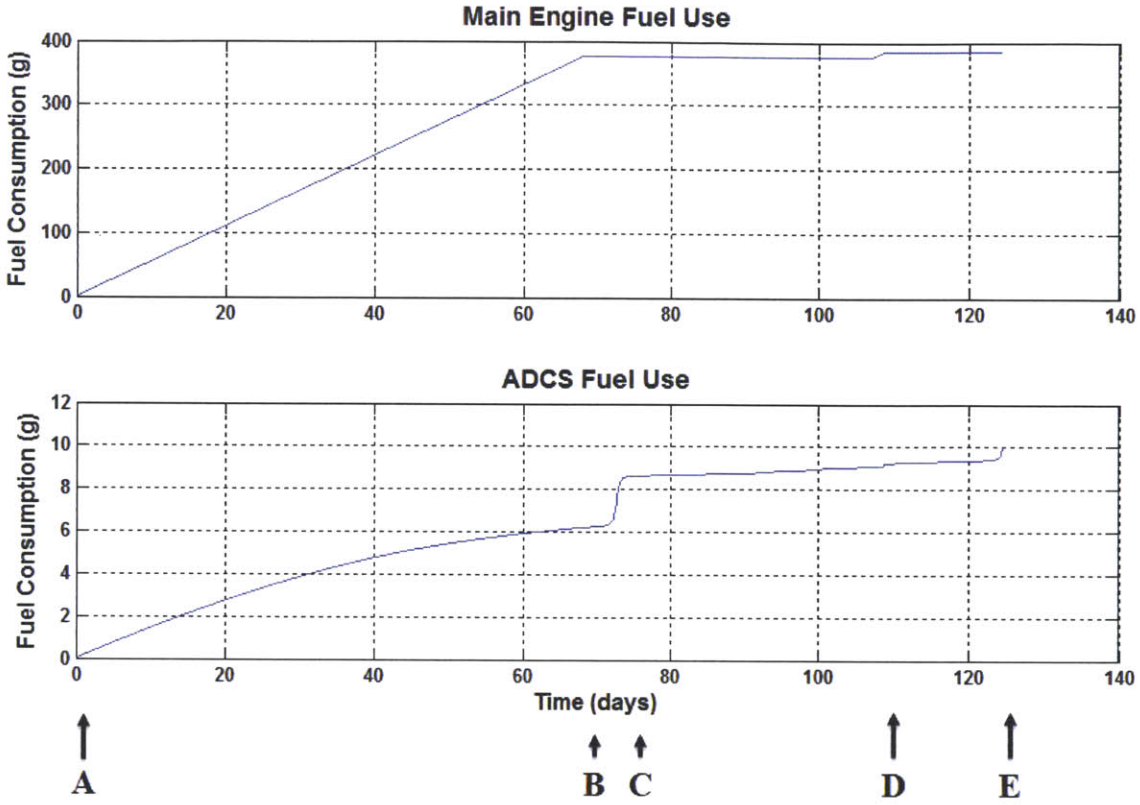

Figure 4-28: Results from the lunar swing-by simulation; the values represent total fuel used.

4.6.4 Science Phase

The science phase is very short; data collection and transmission from the region of interest lasts only seconds. The most critcal requirements at this point are to maintain attitude knowledge and a sufficient link margin. Pointing knowledge of$\sim$1-5 deg is required to build the map of the magnetic field with the data collected.

Figures 4-23 and 4-27 show the spacecraft behavior during the science phase for each trajectory. The ADCS thrusters are the only actuators firing, and it is desirable in the final seconds to cease all operation. This minimizes the chance of the thruster plume or the PPU interfering with the scientific instruments.

Table 4.8: Trajectory Design

Item	Description
Numerical integrator	RK7/8 variable step size
Cis-lunar space	8×8 earth gravity model; sun and moon point mass; spherical SRP
Lunar sphere of influence (SoI)	48×48 lunar gravity model; sun and earth point mass; spherical SRP
Targeting routine	Astrogator differential corrector

4.6.5 Extension to Other Missions

This simulation and algorithm can be adapted to a number of other nanosatellite missions. It can be used for maneuvering in LEO missions as long as high-fidelity gravity and drag models are used (some of these capabilities exist in the simulation as-is). Drag compensation, proximity operations, and orbital transfers can be performed with the right setup.

With a few changes, this simulation can be used for interplanetary missions. Computation of the maneuvers in the heliocentric LVLH frame (beyond Earth's sphere of influence) is more practical, and the parameters must be tailored for this phase. Developing this second mode is the next logical step in expanding the capabilities of this simulation.

4.7 Concluding Remarks

Overall, the guidance algorithm functions as intended, and this is demonstrated through simulation. It enables a spacecraft equipped with an iEPS main engine and ADCS actuators to follow a low-thrust trajectory with termination at lunar impact. The miss distance is well within the requirements. Full analysis of terminal accuracy pends construction of a targeter as well as a navigation routine, but the GC system is fully functional.

Although assumptions are made, it is clear that iEPS is capable of performing this mission should it have a sufficient lifetime. The thrusters are suitable for ADCS actuators, even with performance similar to that demonstrated in the lab. Sufficient

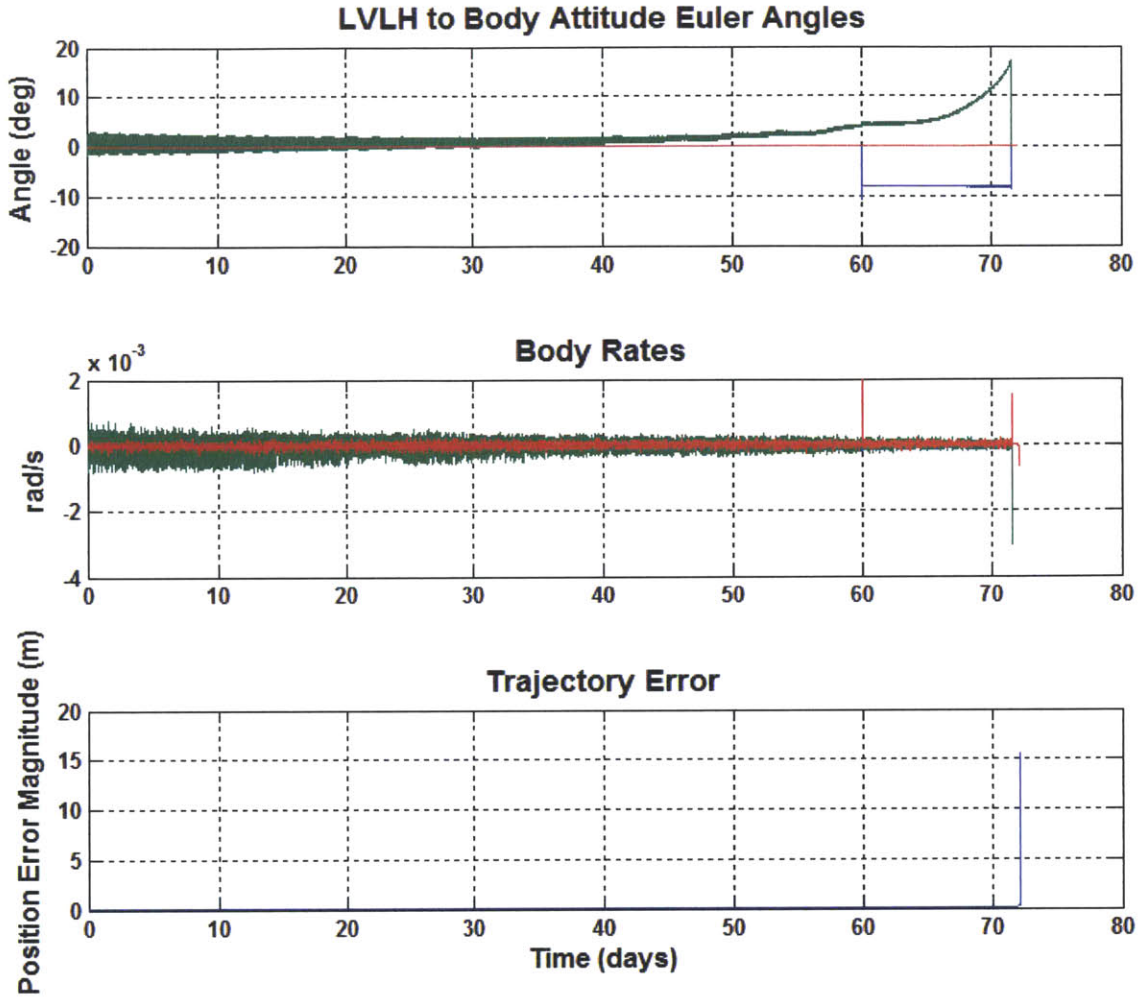

Figure 4-29: Results from following direct impact trajectory designed assuming high-fidelity force models.

refinement and testing promise a system capable of performing this mission.

4.7.1 Concerns

Thruster alignment is the greatest concern. Since the main engine delivers approximately 80 times more thrust than any individual ADCS thruster, small misalignments can cause unwanted torques for which compensation may not be possible. One feasible strategy to mitigate this issue is to segment the main engine into multiple independently controlled panels, which allows some measure of control over the thrust vector. Before implementing this strategy, further analysis is warranted.

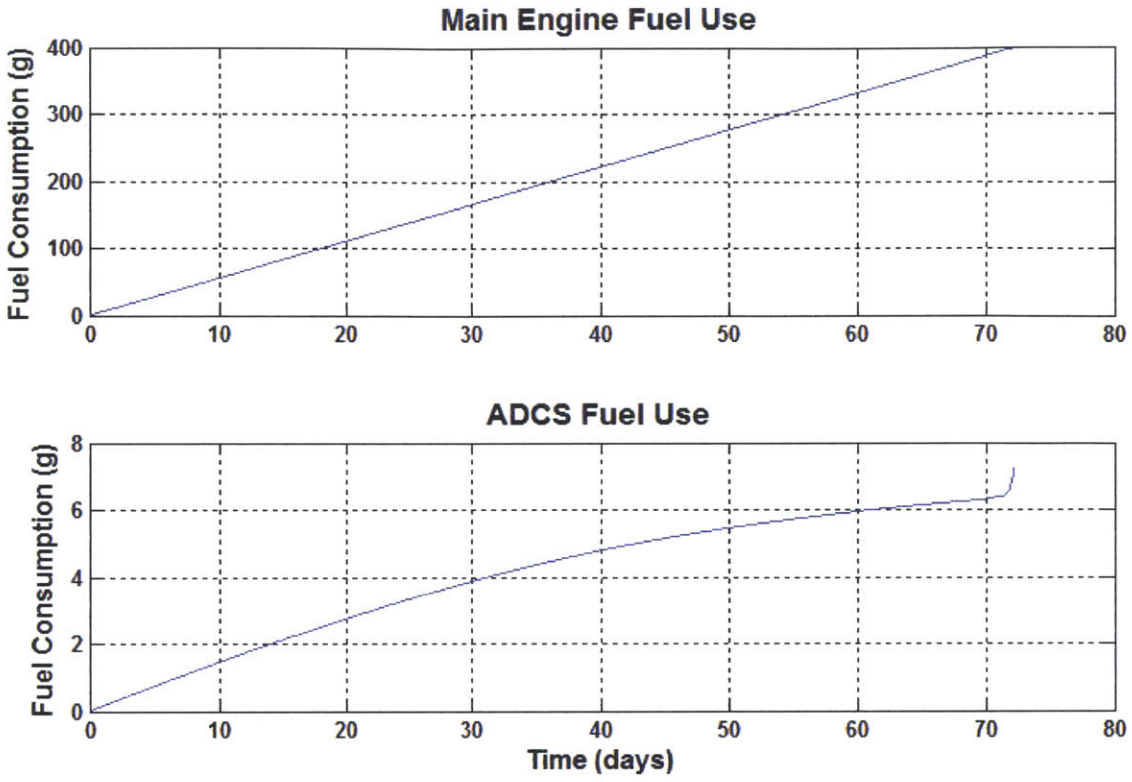

Figure 4-30: Total propellant consumption as a function of mission time.

Beam impingement on the solar arrays must also be addressed. With the current configuration, some of the ADCS thruster plumes will hit the array. Induced torques and degradation of the panels must be analyzed.

A key concern is the spacecraft deviating from its intended course. If this occurs, the targeter must be able to re-compute the trajectory to the destination, but more importantly, operators must be able to diagnose the issue with the ADCS or propulsion systems should they be the culprit. Telemetry is critical, particularly the current drawn by each thruster, which can indicate degradation or complete failure. It is prudent to ensure the controllers can account for lost capability.

One of the primary limitations of nanosatellites is the lack of radiation-hardened components available commercially. This makes the prospect of flying through the radiation belts very unfavorable. Starting from GEO is plausible should critical components be hardened, shielded, or redundant. Higher orbits are even more favorable as this reduces transit time, but these launches are rare.

These spacecraft will not be nearly as cheap as LEO CubeSats, and cost estimation must be realistic. Development issues are sure to appear as they do with every new project, and the budget and schedule must account for slip. The avionics and sensors are weak points; the star tracker, IMUs, flight computer, and power electronics must be reliable and well-tested.

Chapter 5

Interplanetary Missions

Humanity's natural desire to explore and understand the universe is nowhere more clear than in the audacious interplanetary voyages conducted by the major space agencies. They are tremendously challenging from an engineering perspective, but years of painstaking research have yielded the technology and techniques to properly execute them. Unmanned spacecraft have visited protoplanets, comets, asteroids, and all of the planets, and manned missions to Mars and beyond are a major topic [2]. The scientific return alone has been astounding, and the opportunities for future exploration, colonization, and commercial endeavors are nearly limitless.

5.1 NEO Surveyor

The methodology and design of Lunar Impactor can be extended to interplanetary missions as well. A relatively brief exposition of an endeavor in the early stages of development showcases the value of such applications.

The near-earth object (NEO) Surveyor mission is designed to provide a low-cost alternative to the flagship asteroid exploration missions currently in flight or development. This is particularly relevant as NASA's Exploration Mission 2 will be sent to a captured asteroid in lunar orbit; evaluating potential targets before sending the capture vehicle is advisable. Since iEPS is capable of delivering substantial ΔV with proper sizing, it can be used to achieve escape velocity and perform aggressive

maneuvers to arrive at these bodies.

5.1.1 Background

Near-earth asteroids are a great starting target; they offer a wealth of scientific data as they are remnants from the agglomeration of the inner planets [11]. Their low gravity makes a large capture maneuver unnecessary, which is advantageous for a spacecraft equipped with a low-thrust propulsion system. Furthermore, many NEOs reside in orbits very similar to that of the Earth, meaning that costly heliocentric maneuvering is kept to a minimum. Any data returned to earth, even images and perhaps readings from a small sensor, would be tremendously valuable.

Science Objectives

Although the primary goal is to demonstrate the feasibility of a NEO mission with a CubeSat, there are scientific objectives. The spacecraft is to host a $\sim$0.5U payload which includes a 3-axis magnetometer.

Primary Science Objectives

1. Return imagery of the NEO.
2. Return magnetometer measurements as well as data from TBD instruments.

Imagery can be analyzed to determine the composition and rotation rate of the NEO. Magnetometer measurements would be tremendously valuable as the magnetic properties of asteroids are poorly understood. There is concern that these bodies could act like large permanent magnets, which could have catastrophic consequences for nearby exploration spacecraft. Preliminary characterization would be very valuable.

Destination

Selecting a NEO with an orbit similar to the earth is prudent for the first mission; the candidates selected for consideration are 1991 VG, 2013 LE7, and 2008 HU4.

Table 5.1: 1991 VG Orbital Elements

Element	1991 VG (01 Jan 2016)	Earth (01 Jan 2016)
a (AU)	1.027	1.000
e	0.049	0.016
i (deg)	1.45	0.002
Ω (deg)	73.980	224.056
ω (deg)	24.560	237.745
M (deg)	169.524	357.963

Examining their close approach times and orbital elements, the most suitable object is 1991 VG. Table 5.1 lists its heliocentric orbital elements.

The primary advantage of 1991 VG is that the ΔV requirement is low compared with most other NEOs. Escaping earths gravitational influence constitutes the majority of the thrusting. Furthermore, it is a small object, which is advantageous because the gravitational force at the surface is lower than the thrust of a single iEPS module.

5.1.2 Mission Requirements

This mission is significantly different from previous extraterrestrial voyages. The mass and volume constraints are far more stringent, and the initial conditions are not at all the same. Because budget is a key consideration, the spacecraft is assumed to be a ride-share payload on a launch to GEO. This is much preferred to geostationary transfer orbit (GTO) because the spacecraft is not designed to take radiation doses from multiple passes through the Van Allen belts. Table 5.2 lists key assumptions made in the preliminary analysis, which assesses whether or not the propulsion system can be designed to achieve the objectives.

5.2 Mission Architecture

The objective of this mission is to use a 6U CubeSat with iEPS to intercept and study a NEO. Because iEPS has yet to be flown on an interplanetary mission, it is critical to keep it as simple and cost-effective as possible. Figure 5-1 shows the high-level architecture.

Table 5.2: NEO Surveyor Assumptions and Design Considerations

Power	Input power	- Solar (articulated gallium arsenide arrays providing constant power) - Two different scenarios simulated: 40 W and 80 W total power to the thruster PPU
	Number of thrusters	- There are enough thruster modules to utilize the power delivered as well as flight spares for redundancy - 50-60 μN per thruster (thrust density is expected to increase 2-4 times as development progresses)
	Efficiency	- Propulsive efficiency $\sim$0.85 - Overall efficiency (including power conversion) of $\sim$0.7
	PPU	- Use upgraded PETA PPU for main thruster assembly
Propulsion	ΔV	- Spacecraft starts from GEO, escapes earth SoI, navigates to asteroid, and performs scientific mission; $\sim$3-5 km/sec
	I_{sp}	- Ion electrospray thrusters operate in fully ionic regime to provide high specific impulse - 2500-3000 sec used in simulations
	Propellant	- EMI-BF_4 (1.24 g/cc)
	Thrust	- Thrust computed using Equation 1.9
	Longevity	- Thrusters are designed to operate nominally for at least as long as the total expected thrusting time
	Operations	- Capable of continuous firing - Unlimited re-starting
Configuration	Spacecraft size and volume	- Spacecraft form factor is a 6U CubeSat (3$\times$2$\times$1) - 8 kg dry mass - 9.5 kg initial wet mass
	Tank size and volume	- 10-20% margin of usable propellant in the main tanks - Tank size/volume based on density of EMI-BF_4

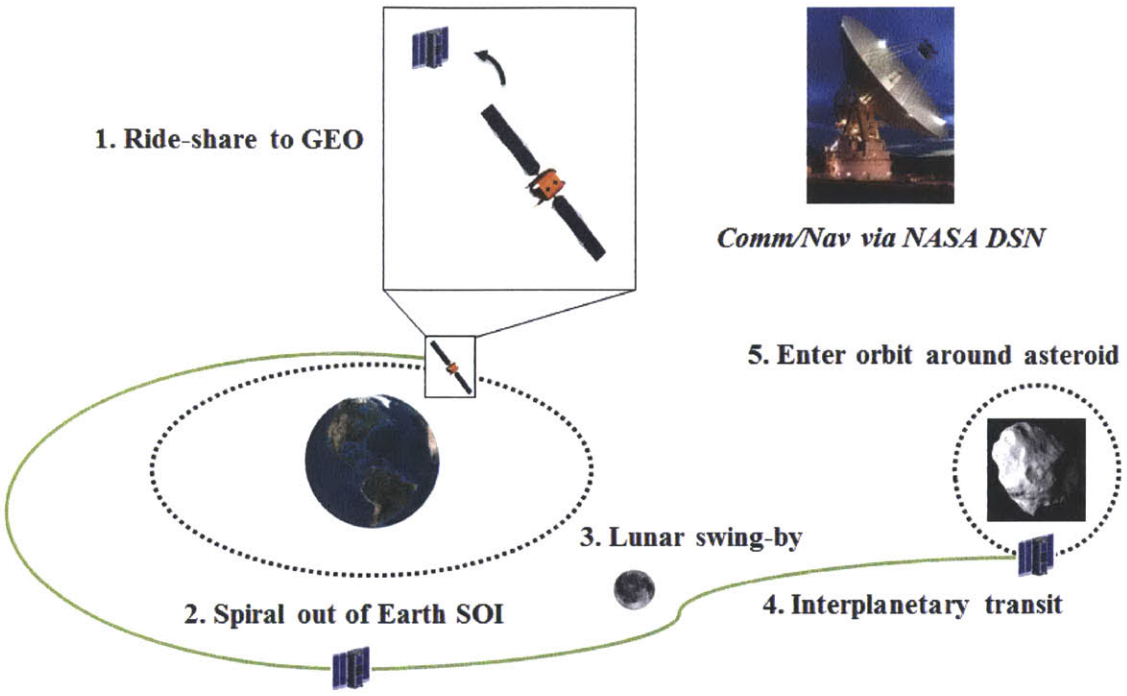

Figure 5-1: NEO Surveyor mission architecture.

The plan calls for delivering the spacecraft to GEO, where it is released from a deployment module and begins a low-thrust ascent. Once it escapes the gravitational influence of earth, it performs additional maneuvers as required to navigate to the object of choice. The lunar swing-by is optional of course, but it can be used as an assist.

5.2.1 Concept of Operations

The concept of operations describes how the spacecraft is employed to achieve the scientific objectives. It closely resembles that of Lunar Impactor and is not laid out in full detail.

Science Operations

The science phase consists of imaging the whole surface of the NEO (shown in Figure 5-2) as well as data collection by the payload. It is expected to last approximately

two months and consist of proximity operations around the asteroid. The survey plan depends on the rotation rate of the asteroid, but the spacecraft is to circumnavigate it at least once.

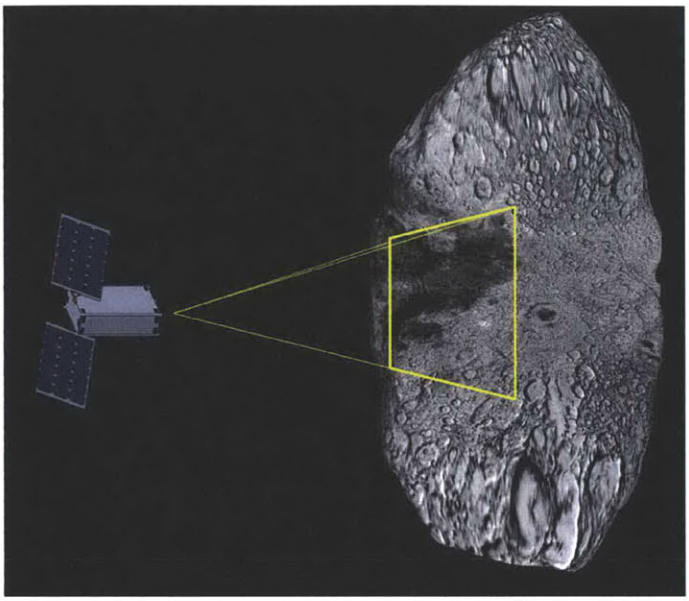

Figure 5-2: Capturing images of the NEO with the spacecraft.

ADCS

The ADCS must precisely point the spacecraft; like Lunar Impactor, the main engine is body-fixed. The key difference is the incorporation of a 3-axis reaction wheel assembly. The duration of this mission as well as the less constrained form factor make it a prudent addition.

Propulsion

The main engine must fire as commanded to follow the trajectory. It is segmented into four individually controlled cells, allowing it to apply torque about two axes and compensate for thrust asymmetry or misalignment. Testing this functionality during check-out is required. The transit phase demands the most of the propulsion subsystem, and the main engine must fire for thousands of hours. Ground operators must be able to identify and compensate for any failures or degradation.

5.3 Spacecraft Architecture

The requirements are the starting point for the spacecraft architecture. The CubeSat form factor aligns very well with the goals of this mission and greatly assists in designing platforms for similar voyages.

5.3.1 Instrumentation

The payload has yet to be defined, but the spacecraft design calls for at least one camera, which is to be used for optical navigation and scientific imagery. High resolution is not required as the spacecraft is to fly very close (tens of meters) to the asteroid. Radiation-hardened complementary metal-oxide semiconductor (CMOS) image sensors are widely available and can be integrated easily. A product like the UI-1641LE shown in Figure 5-3 is sufficient as it captures 1.3 megapixel images and can record video at 25 Hz.

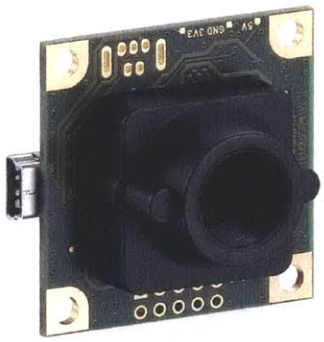

Figure 5-3: UI-1641LE camera by iDS. Dimensions: 36.0 mm × 36.0 mm × 20.2 mm.

There are a growing number of instruments available for CubeSats, including infrared spectrometers, which can be used to collect valuable information about the composition of 1991 VG.

5.3.2 Communication

The communications subsystem must receive commands and data sent from the ground and be able to transmit scientific data and telemetry back to earth. The link margin must be sufficient for the desired data rate, which is driven by available antenna time and data volume. The NASA DSN is the provider of choice and can also be used for Doppler shift ranging, which allows operators to track the spacecraft.

A high-gain antenna (HGA) is absolutely necessary for sending back imagery at a reasonable rate. A high gain reflectarray antenna like that designed for the Integrated Solar Array and Reflectarray Antenna (ISARA) mission is a tenable option; a flat reflector that doubles as a solar array collimates the beam [12]. The reflectarray elements are simply copper patches etched on a printed circuit board (PCB), allowing for compact storage and relatively simple manufacturing. Total gain for the antenna to be used in the ISARA mission, pictured in Figure 5-4, is approximately 35 dB for the Ka-band. If adapted for the X-band, the gain is lower but can still enable data rates in the kilobit per second range.

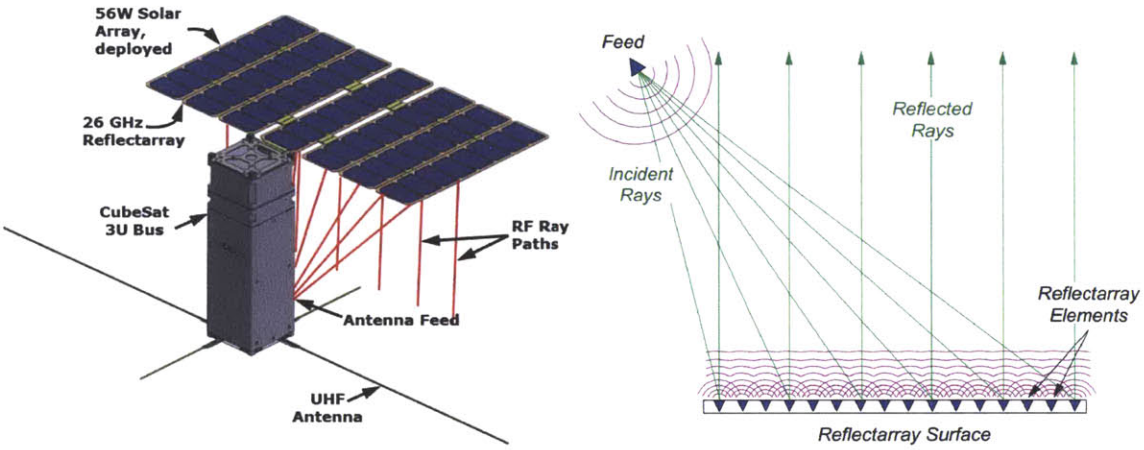

Figure 5-4: ISARA antenna configuration (left) and reflectarray configuration (right).

Another option is an inflatable HGA similar to that under development at MIT [17]. It is designed specifically for CubeSats, stowing into a small volume and deploying using gas generated by sublimating powder. As with ISARA, it is still under development, but full scale tests have shown gains ~20 dB in the S-band are achiev-

able with a 1 m antenna. Figure 5-5 shows an image of a prototype mounted in an anechoic chamber.

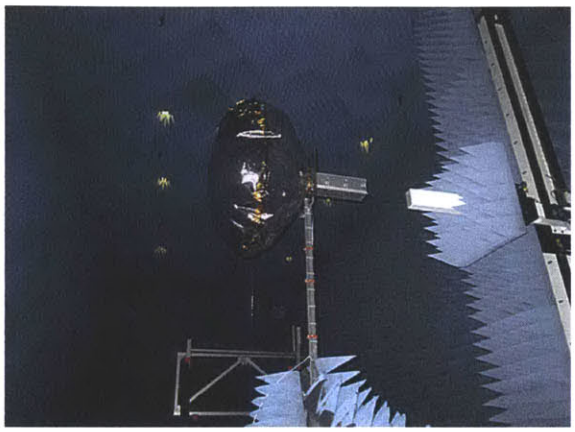

Figure 5-5: Prototype of high-gain inflatable CubeSat antenna designed for X-band communications.

If the HGA fails, it is still possible to achieve limited mission success. Basic telemetry, tracking, and command functions can theoretically be performed using a low-gain antenna (LGA) like the Galileo mission to Jupiter, which suffered from a HGA failure [33]. The communication techniques developed as a result of this failure allow for tracking and data transfer from antennas not designed for use at such ranges. It may be difficult to send back images, but at least the spacecraft can reach its destination.

5.3.3 Physical Configuration

The layout is largely driven by the 6U form factor. Although the propulsion system is extraordinarily compact for the performance it delivers, it occupies ~1.5-2U. The transponder, RWA, power processing unit, flight processor, solar array (SA), payload, and other components must all fit within this envelope.

Propulsion System

The propellant mass and volume dictate tank sizing and the thrust required dictates the number of thruster pairs. Each thruster pair occupies 3.38 cm^2, meaning 36

pairs can easily fit on the bottom face of a 6U CubeSat. This allows for a compact arrangement of the tank and electronics. Figure 5-6 shows a CAD drawing of the propulsion subsystem including a rough sketch of the PPU.

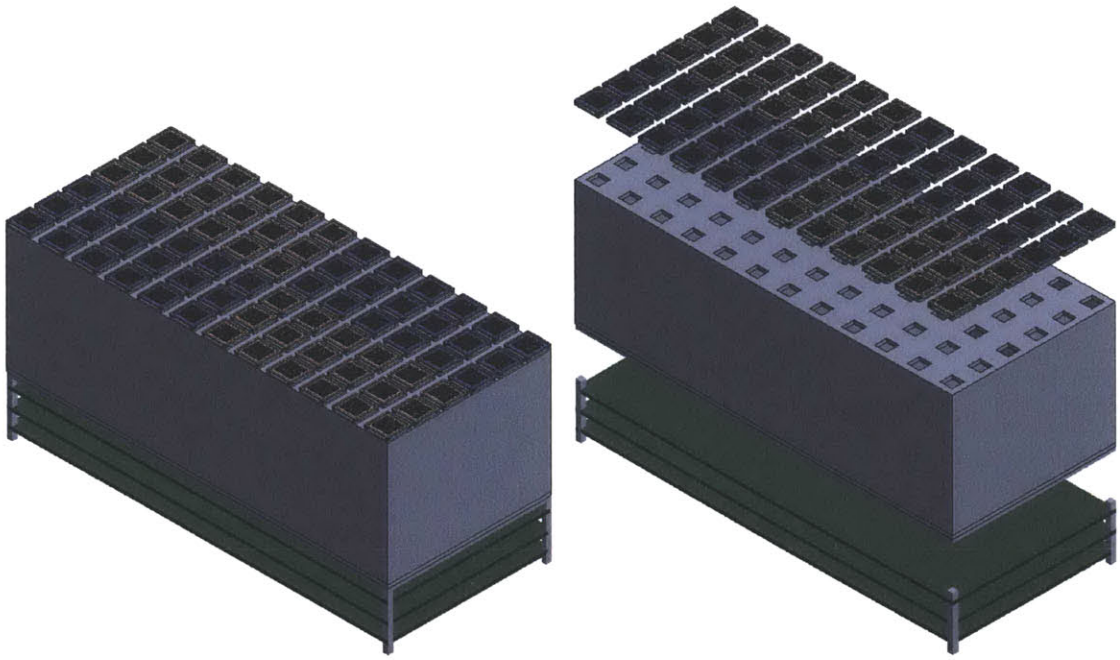

Figure 5-6: CAD drawing of propulsion subsystem for NEO Surveyor.

The thrusters are configured in pairs and are fed from 24 separate propellant tanks. Each pair requires one head firing positive ions and one firing negative ions, meaning the polarity of adjacent tanks is opposite. Figure 5-7 shows a cut-away drawing illustrating these features.

The walls of each tank are lined with porous material that allows propellant to flow to the back of the thruster, where the electrical contact is made. The same porous glass constituting the emitter tips extends downward from the back of the thruster through an opening to the tank. This construction minimizes the negative effects of propellant slosh.

The thrusters are arranged in quadrants; each is independently controlled. This allows for variation of thrust (simply by changing the input voltage), meaning the engine can apply torque in two axes. This is desirable because it can provide compensation for asymmetries or misalignments.

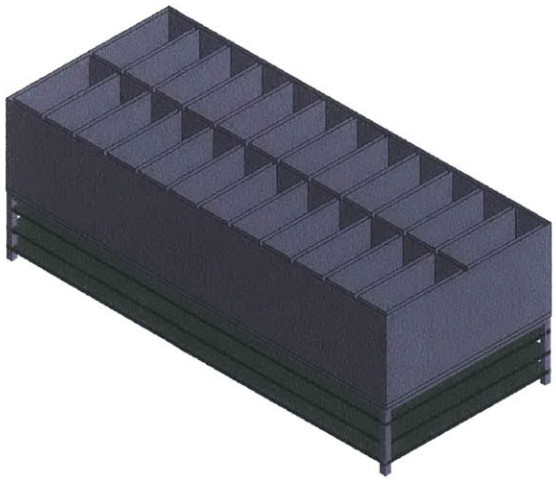

Figure 5-7: Cut-away drawing showing propellant tank structure.

Integrated Configuration

The propulsion system is a large driver of the overall spacecraft configuration. The main engine must be positioned such that the thrust vector passes through the center of mass; otherwise, unwanted torque is induced. The base of the bus is a desirable location, and this is shown in Figure 5-8.

The attitude control system thrusters are positioned to maximize the moment arm. They are included for momentum wheel de-saturation as well as redundancy; in the case of a partial or total RWA failure, they can provide 3-axis pointing control. Figure 5-9 shows their configuration.

Figure 5-10 shows the propulsion system mounted in the CubeSat bus. Even with the PPU, the whole system occupies less than 2U.

5.4 Trajectory Design, Guidance, Navigation, and Control

GNC is a challenge for any interplanetary mission, but NEO Surveyor presents unique difficulties because of its small size and low power generation capabilities. With proper engineering, it is possible to execute the mission.

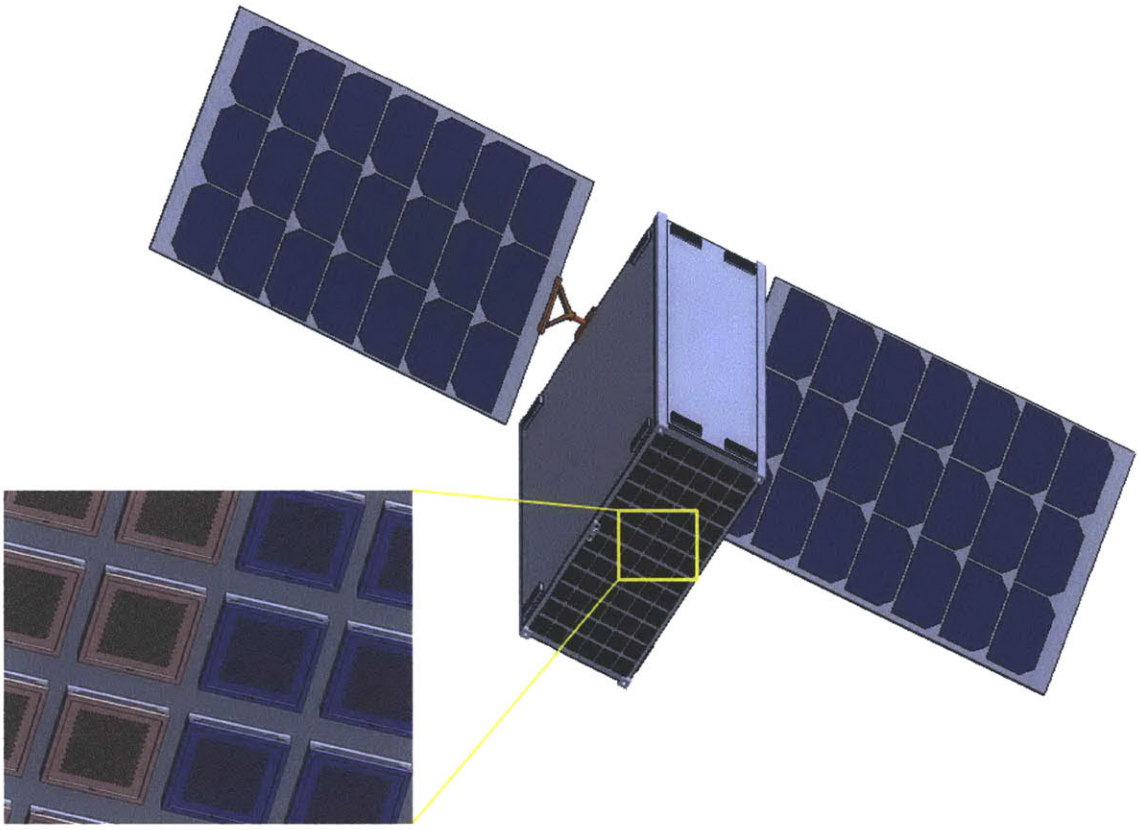

Figure 5-8: Drawing of the propulsion subsystem integrated with a 6U CubeSat.

5.4.1 TrajectoryDesign

Modeling the trajectory is a critical first step in determining the propulsion system requirements. The relevant assumptions are listed in Table 5.3. The timing of the simulation is based on the closest approach of 1991 VG to Earth, which occurs in August of 2017. Launch is delayed to September of 2017, however, to allow for better phasing.

Two trajectories are designed: in the first it is assumed that 40 W of power is available for the propulsion system and in the second it is assumed that 80 W is available. The relevant quantities are listed in Table 5.4.

The trajectories provide a good estimate of the required ΔV and thrusting time required to reach 1991 VG. They are not optimized, meaning that this is a conservative estimate. The earth escape portion of the 40 W and 80 W cases is shown in Figure 5-11.

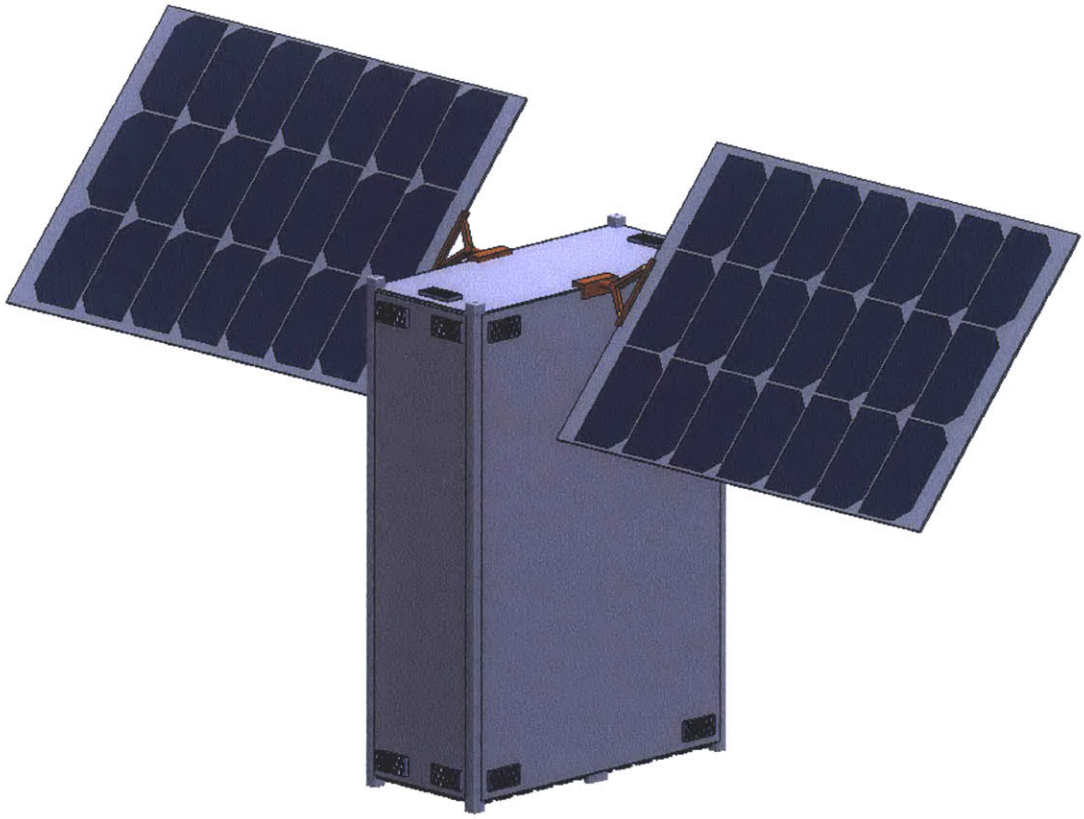

Figure 5-9: CAD drawing of NEO Surveyor.

As expected, the ascent time is approximately half as long as that for the 80 W spacecraft. The majority of the propellant is expended escaping the gravitational influence of the Earth and inserting the spacecraft into the correct interplanetary trajectory. Increasing power shortens the mission duration as well as the thrusting hours. More arrays are required, but this is not an issue because they are so compact. Thrust density is expected to increase as research continues, meaning the number of arrays required will decrease.

Once the spacecraft escapes the earth's sphere of influence, it coasts until it nears the line of nodes for the asteroid orbit, and it performs a plane change burn. This is followed by two additional corrective maneuvers and another coast period. Figure 5-12 shows the interplanetary portion of the trajectory for the 40 W case; that for the 80 W case is nearly identical as the earth escape conditions are designed to match.

The total flight time is substantially longer than the thrusting time because there

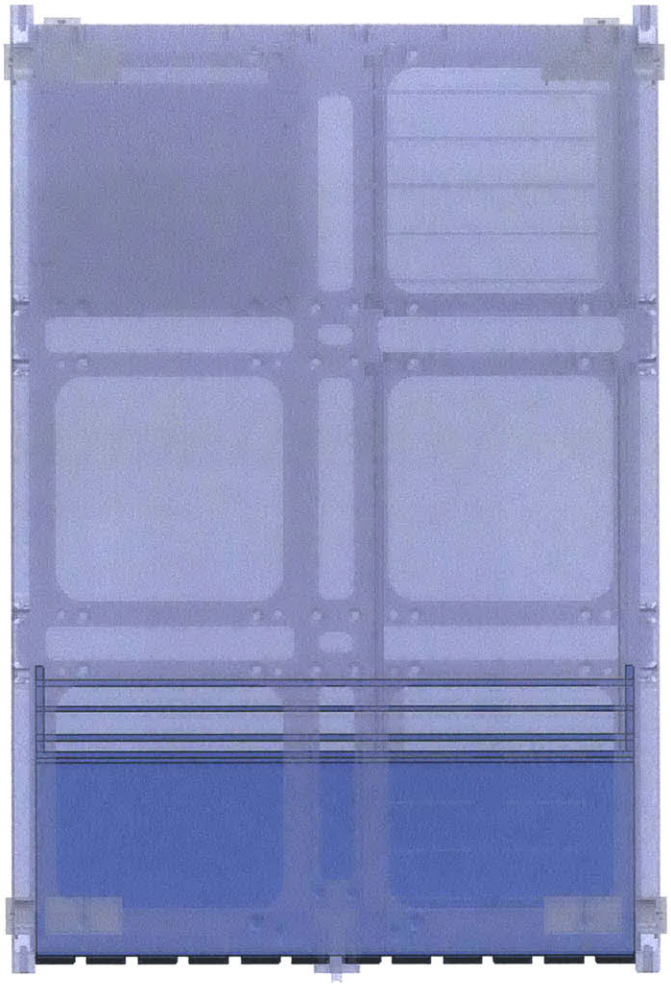

Figure 5-10: Cut-away drawing showing the physical size and configuration of the propulsion subsystem.

are large coasting segments built into the trajectories. These are included for phasing but are not necessary if more aggressive transfers are desired. The trade-off is time and propellant; direct transfers are shorter but consume more fuel. Furthermore, longer flight time means higher radiation exposure, which is an issue for a lightly shielded spacecraft.

Another promising strategy is using a lunar swing-by to lessen the propulsive requirements for the transfer. This is particularly helpful in accomplishing the inclination change necessary to get to 1991 VG. The 40 W case is used as the baseline for a new trajectory designed using backward propagation.

The spacecraft starts at GEO, spiraling out along the equatorial plane until near-

Table 5.3: NEO Surveyor Trajectory Design

Item	**Description**
Numerical integrator	RK7/8 variable step size
Gravity model	Cis-lunar: 8×8 earth gravity; sun and moon point mass Heliocentric: sun and all planets point mass
1991 VG ephemerides	NASA Horizons tool
Targeting routine	Astrogator differential corrector

Table 5.4: NEO Surveyor Propulsion System Performance

Metric	**40 W to PPU**	**80 W to PPU**
Thrust (mN)	2.283	4.566
Time of flight (days)	440	381
Thrusting time (days)	157	78.5
ΔV (km/sec)	3.487	3.502
Propellant mass (g) with I_{sp} = 2500 sec	1259	1264
Tank volume (cc) with I_{sp} = 2500 sec	1015	1019
Propellant mass (g) with I_{sp} = 3000 sec	1061	1065
Tank volume (cc) with I_{sp} = 3000 sec	856	859
Number of thruster modules (78.6 μN pairs)	36	72

ing the lunar sphere of influence. The main thruster array is deactivated, and it executes a lunar swing-by to change its inclination and orbital energy. The spacecraft continues coasting until it nears perigee; another burn is performed to escape the gravitational influence of the earth. Figure 5-13 shows these segments.

After a long coasting segment, the spacecraft performs another burn, which is followed immediately by a plane change maneuver that brings it to the NEO. It arrives precisely at the asteroid. Table 5.5 lists the important properties of this trajectory. The flight time is the most noticeable improvement, decreasing 80 days.

This trajectory is an excellent option for a spacecraft equipped with iEPS. There are no high-rate slew maneuvers, burns are long and continuous at the same thrust levels, and lengthy coast periods allow for additional corrective maneuvers.

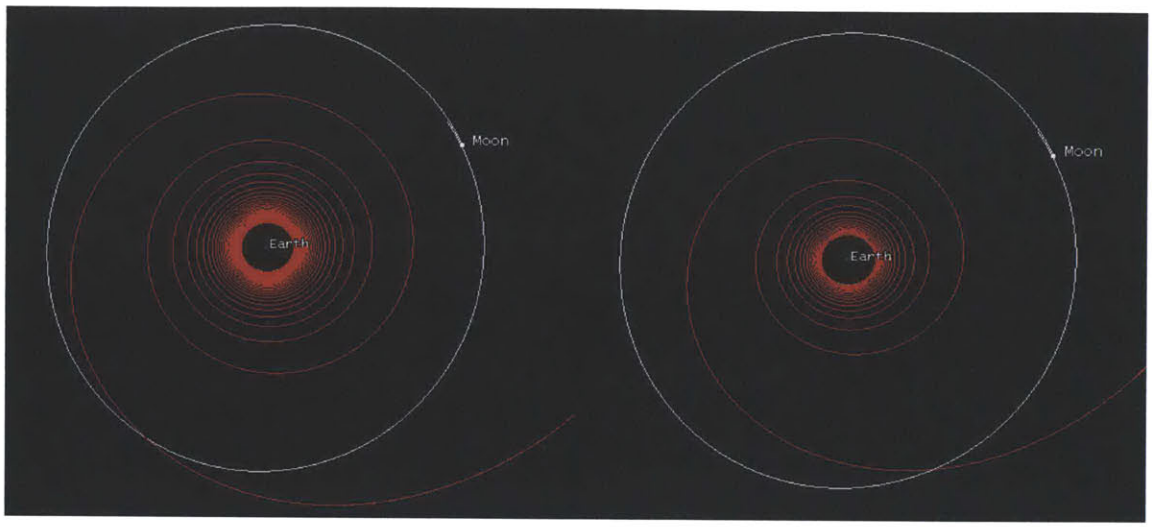

Figure 5-11: Earth-escape portion of trajectory for 40 W case (left) and 80 W case (right).

Table 5.5: NEO Surveyor Propulsion System Performance

Metric	**40 W to PPU**
Thrust (mN)	2.283
Time of flight (days)	361
Thrusting time (days)	156.39
ΔV (km/sec)	3.478
Propellant mass (g) with I_{sp} = 2500 sec	1257
Tank volume (cc) with I_{sp} = 2500 sec	1014
Propellant mass (g) with I_{sp} = 3000 sec	1059
Tank volume (cc) with I_{sp} = 3000 sec	855
Number of thruster modules (78.6 μN pairs)	36

5.4.2 Guidance

NEO Surveyor can employ the same guidance strategy used for Lunar Impactor. The primary difference is the addition of heliocentric trajectory following as well as the ability to conduct proximity operations around the asteroid.

5.4.3 Navigation

Attitude and rate measurements must be made continuously, and periodic updates of position and velocity are required. More measurements are required early in flight, particularly during thrusting, to ensure the spacecraft does not deviate too far from

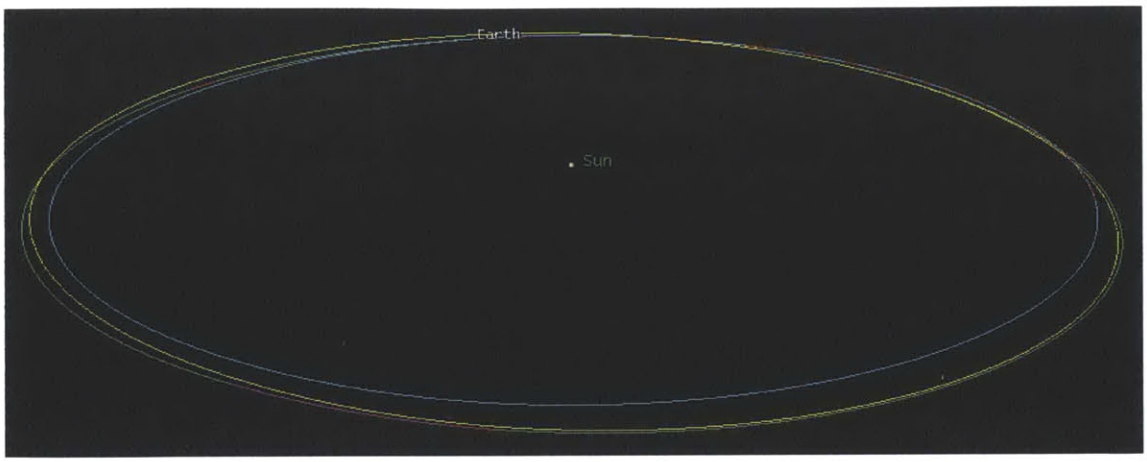

Figure 5-12: Interplanetary portion of trajectory for 40 W case (blue represents earth orbit, yellow represents 1991 VG, green represents coast segments, other colors represent thrust arcs.)

its intended course.

Sensors

Precision pointing knowledge requires a star tracker. Sun sensors are desirable but not essential as the solar arrays can provide a rough approximation of the sun angle. An IMU measures attitude rates, and the signals are processed to yield a rotational state estimate. This can be combined with the main engine current measurements (which can be translated into thrust) to provide position and velocity estimates.

Translational State Estimate

The spacecraft state estimate diverges from the actual state over time, so its position and velocity must be determined from the ground. The differences between the actual and intended flight path, the residuals, are computed using Doppler shift ranging and uplinked to the spacecraft. The approximate frequency and duration of communication periods are summarized in Table 5.6.

The main restriction is the availability of the DSN, particularly the 70 m antennas (preferred for imagery downlink). The schedule is already very full with operational missions; NEO Surveyor must work with what is available.

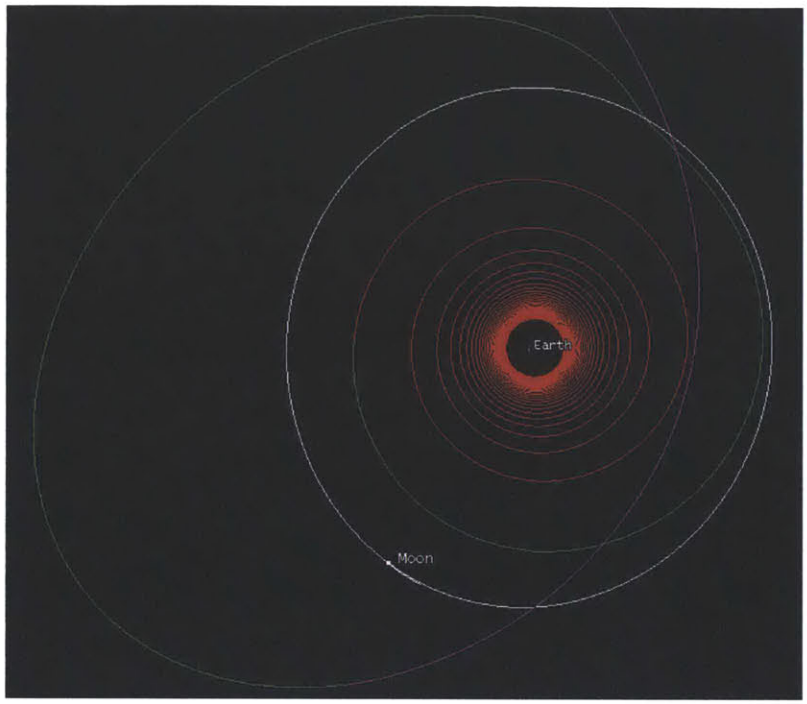

Figure 5-13: Upward spiral, lunar swing-by, and earth escape.

Table 5.6: NEO Surveyor Propulsion System Performance

Phase	**Frequency and Duration (34 m antenna)**
Transit; thrusting	2-3 hours 2-3 times per day
Transit; coasting	2-3 hours 2-3 times per week
Science; approach	Near continuous depending on availability
Science; operations	2-3 hours 2-3 times per day

5.4.4 Control

The control system must execute the guidance commands using the actuators. Precise pointing is essential for communications and maneuvering. As mentioned before, the primary ADCS actuator is a 3-axis RWA. A set of thrusters is included to perform momentum de-saturation and to provide a back-up system in case the RWA fails. In addition, the main engine can produce torque in two axes.

5.5 Results and Analysis

Using LunarSim as-is to simulate portions of NEO Surveyor trajectories offers valuable insight into ADCS and propulsion system performance. The two spacecraft are very similar structurally, and the results are not anticipated to differ substantially when the spacecraft model is updated. The algorithm functions well far beyond earth and keeps the spacecraft on course to 1991 VG.

5.5.1 Transit Phase

The spiral up from GEO and lunar swing-by is nearly identical to that of Lunar Impactor, so focus is directed immediately to the burns that must occur far outside earth's sphere of influence. The final 20 days of maneuvering required to bring NEO Surveyor to 1991 VG are examined, and Figure 5-14 shows the relevant segment of the trajectory in the heliocentric inertial frame.

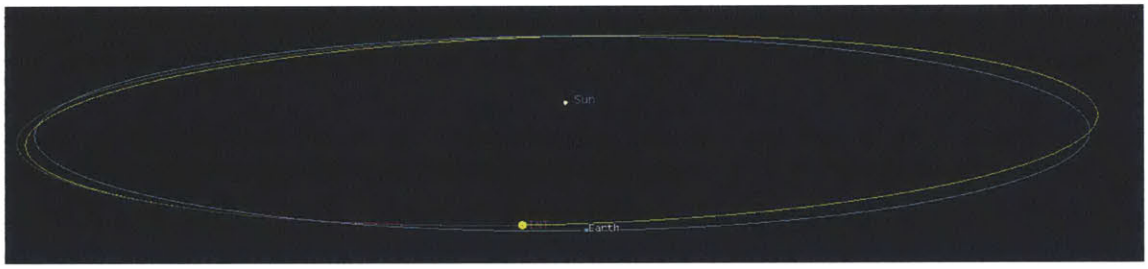

Figure 5-14: Last 20 days of maneuvering required to rendezvous with 1991 VG.

The thrust arc shown in purple lasts 20 days and brings the spacecraft within 100 meters of the asteroid, which is represented by the yellow ellipse. Figure 5-15 shows the view along the orbit normal.

The spacecraft is over 13 million kilometers from Earth when it reaches 1991 VG, and the results show successful trajectory following and reasonable spacecraft behavior. Figure 5-16 displays the position error and fuel consumption.

Deviation from the intended flight path is minimal and remains at levels typical of trajectories in cis-lunar space. While not properly reflecting fuel consumption for NEO Surveyor, the simulation shows steady profiles indicative of stable, controlled

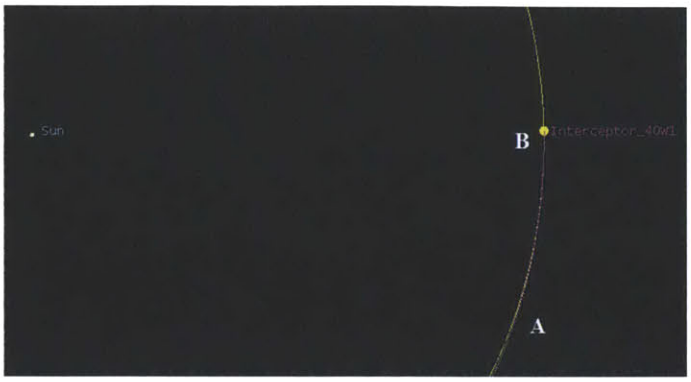

Figure 5-15: Last 20 days of maneuvering represented by purple arc; NEO orbit shown in yellow. HCI frame.

flight.

5.5.2 Science Phase

The science phase consists of all data collection in the vicinity of the asteroid. The primary goal is to return detailed imagery of the entire surface, which can be used to determine its body rates and composition.

Another fascinating prospect is landing on the asteroid should the rotation rates be sufficiently low. The gravity at the surface is weak enough that the thrusters can be used to take off after making contact. As always, sample return is an exciting prospect, but carrying along some sort of earth re-entry mechanism may be prohibitive to the mission. An alternative is using the remaining propellant on board to send the spacecraft back on a path requiring a zero ΔV earth capture. Although it would be stranded in a high earth orbit, it would be easier to retrieve the spacecraft with a sample than to conduct a complete sample return mission. The only additional cost would be a simple containment mechanism and extra propellant. This may be an excellent mission for a follow-on program.

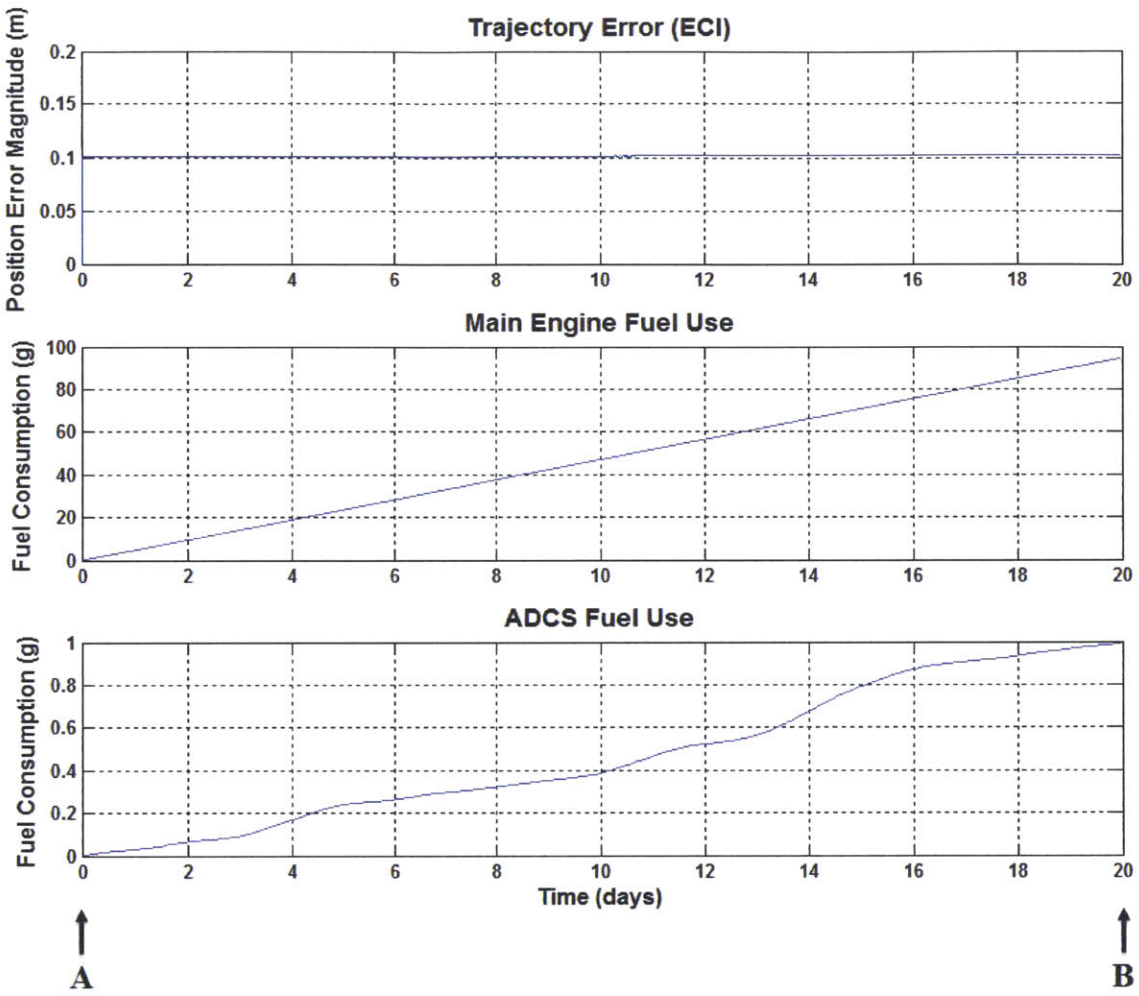

Figure 5-16: Deviation from desired trajectory and fuel consumption.

5.6 Concluding Remarks

This mission is feasible should the necessary advances in ion electrospray propulsion technology be made. The simplicity of the system enables it to be scaled down enough to fit in a 6U CubeSat, but it still provides the maneuvering capability and performance of heritage electric thrusters. Ongoing developments in every other aspect of nanosatellite design, technology, and operations promise to make this ambitious mission feasible in the near term.

The propellant mass and volume are very reasonable; the tanks occupy less than 2U. The PPU, thruster arrays, and other propulsion system components are compact,

leaving sufficient room for other subsystems as well as the scientific payload. The GC algorithm is capable of following the trajectory, and LunarSim can be re-worked to incorporate a model of NEO Surveyor for added detail.

Additionally, if this bus can be designed as a standardized interplanetary platform, cost can be reduced by economy of scale. Much of the hardware and software is already available because of the CubeSat standard, and further development can extend these benefits beyond LEO. This platform has extensive commercial applications including scouting asteroids and other objects for resource utilization.

5.6.1 Concerns

Thruster alignment is a key concern as errors cause unwanted torque. The ADCS alone can be used to compensate for it, but this requires additional propellant for momentum de-saturation. The main engine is segmented to help mitigate this issue and provide greater in-flight flexibility. Beam impingement on the solar arrays must also be addressed. In certain configurations, some of the ADCS thruster plumes intersect with the solar array. Induced torques and degradation of the panels must be analyzed before finalizing the design.

One of the primary limitations of nanosatellites is the lack of radiation-hardened components available commercially. This makes the prospect of flying through the radiation belts unfavorable and traversing vast expanses of interplanetary space risky. Starting from GEO is plausible should critical components be hardened, shielded, or redundant. The benefit of using such inexpensive spacecraft is the possibility of launching multiple identical copies at once; even with a 50% failure probability, a formation of four spacecraft stands a 94% chance of arriving with at least one intact. This is assuming the systems are truly independent, but the point is that reliability through numbers rather than rigorous engineering can be far less expensive.

These spacecraft will not be nearly as cheap as earth-orbiting CubeSats, and cost estimation must be realistic. Development issues are sure to appear as they do with every new project, and the budget and schedule must account for slip. The avionics and sensors are weak points; the star tracker, IMUs, flight computer, RWA, and power

electronics must be reliable and well-tested.

Chapter 6

Conclusion

Lunar and interplanetary vehicles are crafted much like fine pieces of art; they are unique, expensive, and serve a particular purpose very well. Designers are effectively buying reliability, which means extensive testing, preferential use of high Technology Readiness Level (TRL) technologies, costly insurance, and dealing with the realities of a flat launch market. There is little overall architecting, and each spacecraft is developed as the need arises. While this suffices for early ventures beyond earth, it is not a prudent model for long-term expansion and development. Even a cursory examination of microeconomics yields the assertion that economies of scale, cost advantages obtained through the size and scope of an operation, are a key necessity for any large enterprise [13]. Just as skillful architecting of microprocessors yields low-cost, high capability, and flexible products, proper focus on key aspects of spacecraft design leads to tremendous benefits.

Mankind is reaching a crossroads in space exploration where a fundamental change in overall strategy must occur before the full benefits of space travel are realized. Missions cannot be considered as stand-alone ventures; the whole exploration architecture has to be considered. This is not nearly as simple as stamping out ten thousand identical spacecraft and hoping they will fit most requirements, but practical steps in that direction include the following:

1. Exploit key technologies that drastically simplify and cheapen subsystems that

usually carry large price tags. Scalability (while retaining or exceeding performance) is essential! The technology must provide reasonable capability for a multitude of different designs.

2. Settle on standards for various mission classes where able. This leads to reduction in launch costs and an increase in launch opportunities. Using commercial off-the-shelf (COTS) components where able can further reduce spacecraft bus price.

3. Consider achieving reliability through numbers and redundancy rather than extraordinary reliability. For many missions, this costs less.

4. Address what needs to be done with the ground segment and other players to accommodate a larger number of missions and higher data volume. This increase is expected no matter what plan is carried out.

5. Adjust thought processes to focus on overall strategy rather than the year-to-year budget. Yes, this will very likely cost a lot by the time everything is said and done, but the benefits may be well worth it.

The ultimate objective is to provide solutions that easily scale to the requirements in terms of reliability, cost, and return. This architecture for lunar and interplanetary exploration provides such an option for the low end of the spectrum. The detailed simulations of the Lunar Impactor mission show that iEPS can be used for main propulsion and ADCS actuation. Trajectory following using model predictive control is a viable GNC strategy and can be adapted for a variety of missions, including NEO Surveyor.

6.1 Future Work

A great deal of research and development remains before these ideas become reality, but concerted effort can enable them in the next several years. The following suggestions provide a framework for continuing these endeavors.

6.1.1 GC Algorithm

There is room for improvement with the guidance and control algorithm. The controls are not optimized, meaning the main engine may expend more propellant than necessary to reach the destination. Building a cost function that incorporates both the main engine and ADCS thrusters would allow for computation of the fuel-optimal flight path, which is particularly important for long voyages.

The force applied by each ADCS thruster can be modulated easily, but this is not leveraged in an advantageous way. Using maximum output during higher rate maneuvers would reduce slew time while minimal actuation is ideal for fine correction (reduces mechanical wear and overshoot). Employing this capability promises to save fuel and increase performance.

In future iterations of the algorithm, it would be prudent to compute the controls in an inertial frame. Because a rotating frame is used, fictitious forces are present, and they are not properly considered. Since the prediction horizon and the rotation rate of the frame is small, it does not compromise the functionality of the algorithm, but it is advisable to address this issue.

Short prediction horizons are avoided by holding the last segment of controls, but another way to deal with this issue is to pick up the next trajectory point X_{n+2} before reaching X_{n+1}. This makes it more difficult to determine the accuracy with which it arrives at each, but it is likely to be more robust. Testing this postulation is a logical measure.

A reliable navigation algorithm must be developed to complement the guidance and control logic. The spacecraft must be able to interpret sensor measurements to estimate its state. This is perhaps the most important component required to determine whether or not the terminal accuracy requirements can be met.

The guidance algorithm must be able to re-plan the entire trajectory after receiving residuals from ranging measurements, which necessitates a targeter if this process is to be autonomous. New trajectories can be computed and uploaded from the ground, but this places additional demand on the communications subsystem.

Autonomy is desirable for a mission in which uplink time is limited and expensive.

6.1.2 Lunar Impactor

Testing with a wider variety of lunar trajectories is advisable; the possibility of maneuvering into a selenocentric orbit and lowering it until the perilune intersects a magnetic anomaly is particularly appealing. This requires more propulsive capability and a high fidelity lunar gravity model, but it may yield more data. Exploring the use of weak stability boundary (WSB) transfers to enter into lunar orbit is another possibility.

6.1.3 NEO Surveyor

Building a model of NEO Surveyor and running it through the same series of tests as Lunar Impactor is an excellent place to begin. The controller must be re-worked to include a RWA as well as the segmented main engine. Running simulations on trajectories to other destinations like Mars would help refine the GC algorithm further and test its flexibility. An easily adaptable platform and architecture is a key goal, so it makes sense to evaluate many different missions.

6.1.4 Further Exploration

Exploring applicability beyond nanosatellites is prudent. Ion electrospray propulsion systems can be scaled up easily; this is a simple matter of including more thruster modules, larger propellant tanks, and more capable PPUs. Such systems can provide propulsive capability for much larger spacecraft and replace traditional electric engines.

Bibliography

[1] Mars Reconnaissance Orbiter. http://www.nasa.gov/missionpages/MRO. Accessed: 2014-04-09.

[2] NASA Planetary Science. http://science.nasa.gov. Accessed: 2014-04-09.

[3] Dawn Mission. http://www.nasa.gov/missionpages/dawn. Accessed: 2014-04-09.

[4] NASA Awards Launch Contract For Goes-R And Goes-S Missions. http://www.nasa.gov/home/hqnews/2012/apr/HQC12-016GOES-RGOES-SLaunch.html. Accessed: 2014-04-10.

[5] MIT Open Courseware. http://ocw.mit.edu/courses/aeronautics-and-astronautics/16-522-space-propulsion-spring-2004/lecture-notes/lecture1a.pdf. Accessed: 2014-04-09.

[6] NSTAR. http://www.grc.nasa.gov. Accessed: 2014-04-09.

[7] BHT 200. http://www.busek.com. Accessed: 2014-04-09.

[8] Pulsed Plasma Thrusters. http://www.grc.nasa.gov. Accessed: 2014-04-09.

[9] CubeSat Design Specification Rev. 12. http://www.cubesat.org. Accessed: 2014-04-09.

[10] Deep Space Network. http://www2.jpl.nasa.gov/basics/bsf18-1.php. Accessed: 2014-04-10.

[11] Near Earth Object Program. http://neo.jpl.nasa.gov. Accessed: 2014-04-10.

[12] Integrated Solar Array and Reflectarray Antenna. http://www.nasa.gov/directorates/spacetech/smallspacecraft/isaraproject. Accessed: 2014-04-10.

[13] MIT Open Courseware. http://ocw.mit.edu/courses/sloan-school-of-management/15-010-economic-analysis-for-business-decisions-fall-2004/recitations/proandpostcon.pdf. Accessed: 2014-04-09.

[14] Apollo 15 preliminary science report. Technical Report SP-289, NASA, Wash. D.C., 1972.

[15] Apollo 16 preliminary science report. Technical Report SP-315, NASA, Wash. D.C., 1972.

[16] Space transporation costs: Trends in price per pound to orbit 1990-2000. Technical report, Futron Corporation, Bethesda, Maryland, 2002.

[17] A. Babuscia. Commcube 1 and 2: A cubesat series of missions to enhance communication capabilities for a cubesat. In *Proc. IEEE Aerospace Conference*, 2013.

[18] C. Coffman, D. Courtney, F. Hicks, S. Jamil, H. Li, and P. Lozano. Progress toward a variable specific impulse electrospray propulsion system. Technical report, American Institute of Aeronautics and Astronautics, 2011.

[19] D. Courtney and P. Lozano. Electrochemical micromachining on porous nickel for arrays of electrospray ion emitters. *Journal of Microelectromechanical Systems*, 22(2):471–482, 2012.

[20] Daniel Courtney. *Ionic Liquid Ion Source Emitter Arrays Fabricated on Bulk Porous Substrates for Spacecraft Propulsion.* PhD thesis, MIT, 2011.

[21] Courtney Duncan. Low mass radio science transponder. In *Proc. Interplanetary CubeSat Workshop*, 2012.

[22] J. B. Fenn, M. Mann, C. K. Meng, S. F. Wong, and C. M. Whitehouse. Electrospray ionization for mass spectrometry of large biomolecules. *Science*, 246(4926):6471, 1989.

[23] I. Garrick-Bethell. Lunar magnetic field measurements with a cubesat. Technical report, Department of Earth and Planetary Sciences, University of California, Santa Cruz, 2013.

[24] D. Hemingway and I. Garrick-Bethell. Magnetic field direction and lunar swirl morphology: Insights from airy and reiner gamma. *J. Geophys. Res.*, 117(E10012), 2012.

[25] R. S. Legge and P. Lozano. Electrospray propulsion based on emitters microfabricated in porous metals. *Journal of Propulsion and Power*, 27(2):485–495, 2011.

[26] L. Y. Liu, S. B. Jiang, and T. L. Yeh. The magneto-resistive magnetometer of bcu on the tatiana-2 satellite. *Terrestrial, Atmospheric, and Oceanic Sciences*, 23(3):70–79, 2012.

[27] P. Lozano. Ionic liquid ion sources: Suppression of electrochemical reactions using voltage alternation. *Journal of Colloid and Interface Science*, 280(1):149–154, 2004.

[28] F. Martel, P. Lozano, and L. Perna, editors. *Miniature Ion Electrospray Thrusters and Performance Test on CubeSats*, Small Satellite Conference, Technical Session VI, 2012. MIT and ESPACE.

[29] M. Martinez-Sanchez and J. E. Pollard. Spacecraft electric propulsion an overview. *AIAA Journal of Propulsion and Power*, 14(5):688–699, 1998.

[30] M. Purucker and J. Nichols. Global spherical harmonic models of the internal magnetic field of the moon based on sequential and coestimation approaches. *J. Geophys. Res.*, 115(E12007), 2010.

[31] J. E. Riedel and M. Aung. Guidance, navigation, and control technology assessment for future planetary science missions. Technical report, NASA Strategic Missions and Advanced Concepts Office, 2013.

[32] C. Rossi. Vehicle health monitoring using stochastic constraint suspension. Master's thesis, MIT, 2012.

[33] J. I. Stratman and L. J. Deutsch. *The Three Galileos: The Man, the Spacecraft, the Telescope*, volume 220. Springer Netherlands, Oxford, 1998. 107-113.

[34] M. Tajmar, A. Genovese, and W. Steiger. Indium field-effect electric propulsion microthruster experimental charactization. *AIAA Journal of Propulsion and Power*, 20(2):211, 2004.

[35] G. I. Taylor. Disintegration of water drops in an electric field. *Proceedings of the Royal Society of London*, 280(1382):383397, 1964.